Nilton Alejandro Cuellar Loyola

Robust topology optimization using a non-intrusive stochastic spectral approach

TESE DE DOUTORADO

DEPARTAMENTO DE ENGENHARIA MECÂNICA
Programa de Pós-graduação em Engenharia Mecânica

Rio de Janeiro
October 2018

Pontifícia Universidade Católica
do Rio de Janeiro

Nilton Alejandro Cuellar Loyola

Robust topology optimization using a non-intrusive stochastic spectral approach

Tese de Doutorado

Thesis presented to the Programa de Pós–graduação em Engenharia Mecânica of PUC–Rio in partial fulfillment of the requirements for the degree of Doutor em Ciência – Engenharia Mecânica.

Advisor : Prof. Ivan Fábio Mota de Menezes
Co–Advisor: Prof. Anderson Pereira

Rio de Janeiro
October 2018

Pontifícia Universidade Católica
do Rio de Janeiro

Nilton Alejandro Cuellar Loyola

Robust topology optimization using a non-intrusive stochastic spectral approach

Thesis presented to the Programa de Pós–graduação em Engenharia Mecânica of PUC–Rio in partial fulfillment of the requirements for the degree of Doutor em Ciência – Engenharia Mecânica. Approved by the undersigned Examination Committee.

Prof. Ivan Fábio Mota de Menezes
Advisor
Departamento de Engenharia Mecânica — PUC–Rio

Prof. Anderson Pereira
Co–Advisor
Departamento de Engenharia Mecânica — PUC–Rio

Prof. Carlos Alberto de Almeida
Departamento de Engenharia Mecânica — PUC-Rio

Prof. Fernando Alves Rochinha
Programa de Engenharia Mecânica – UFRJ

Prof. Americo Barbosa da Cunha Junior
Instituto de Matemática e Estatística – UERJ

Prof. Rodrigo Bird Burgos
Departamento de Estruturas e Formações – UERJ

Prof. Márcio da Silveira Carvalho
Vice Dean of Graduate Studies
Centro Técnico Científico — PUC–Rio

Rio de Janeiro — October 26th, 2018

Nilton Alejandro Cuellar Loyola

Nilton Cuellar graduated as Mechatronic Engineer in 2008 from the UNI (Lima, Peru). He is specialized in Robotics, Control Systems and in Project Management. Obtained his Master's degree from the PUC–Rio (2012) and a MBA degree from the same institution in 2014. He worked in various research institutes as Tecgraf, Coppe, and currently work at TechnipFMC developing projects in subsea robotics.

Bibliographic data

Cuellar Loyola, Nilton Alejandro

Robust topology optimization using a non-intrusive stochastic spectral approach / Nilton Alejandro Cuellar Loyola ; advisor: Ivan Fábio Mota de Menezes; co–advisor: Anderson Pereira. — 2018.
140 f.; 30 cm

Tese (doutorado) – Pontifícia Universidade Católica do Rio de Janeiro, Departamento de Engenharia Mecânica, 2018.
Inclui bibliografia

1. Engenharia Mecânica – Teses. 2. Otimização topológica robusta. 3. Quantificação de incertezas. 4. Métodos estocásticos espectrais. 5. Caos polinomial generalizado. 6. Expansão de Karhunen-Loève. I. Menezes, Ivan Fábio Mota de. II. Pereira, Anderson. III. Pontifícia Universidade Católica do Rio de Janeiro. Departamento de Engenharia Mecânica. IV. Título.

CDD: 621

Acknowledgments

First I would like to thank and expressing my greatest gratitude to the most important people in my life, my father Alejandro, my mother Ana, my sibling Rosa and Julio and my wife Pâmela because they are always encouraging and giving me support to achieve my goals.

A especial and huge thank to my advisors Ivan Menezes and Anderson Pereira for the constant support, the everyday kindness and the incentive for the realisation of this work. I learned a lot with them!.

To my colleagues of the PUC–Rio, Luiz Fernando, Bruno Cayres, Americo Cunha, Ronald Padilla, Renato Gutierrez and Arturo. To these friends I express my gratitude for the nice moments lived together.

I thank the members of the jury, for having accepted to participate in the evaluation of my thesis, and for the valuable comments made on the day of the thesis defense. These comments were very relevant, and helped to improve the final version of the manuscript.

This study was financed in part by the Coordenação de Aperfeiçoamento de Pessoal de Nível Superior - Brasil (CAPES)- Finance code 001.

To the people of the Mechanical departament for the constant help.

Abstract

Cuellar Loyola, Nilton Alejandro; Menezes, Ivan Fábio Mota de; Pereira, Anderson. **Robust topology optimization using a non-intrusive stochastic spectral approach**. Rio de Janeiro, 2018. 140p. Tese de Doutorado — Departamento de Engenharia Mecânica, Pontifícia Universidade Católica do Rio de Janeiro.

This work presents some applications of stochastic spectral methods for structural topology optimization in the presence of uncertainties. This procedure, known as robust topology optimization, minimizes a combination of the mean and standard deviation of the objective function. For this purpose, a non-intrusive polynomial chaos expansion is integrated into a topology optimization algorithm to calculate the first two statistical moments of the mechanical model response. In order to address variabilities in the structural response, the uncertainties are considered in the loading and the material properties. In this proposed probabilistic formulation, uncertainties are represented as a set of random variables (e.g., magnitudes and directions of the loads) or as random fields (e.g., distributed loads and material properties). A non-Gaussian homogenous random field with a specified marginal distribution and covariance function is used to represent the material uncertainties because it ensures their physical admissibility. Nonlinear "memoryless" transformation of a homogeneous Gaussian field is used for obtaining non-Gaussian fields. The Karhunen-Loève expansion is employed to provide a representation of the Gaussian field in terms of countable uncorrelated random variables. The sparse grid quadrature is considered for reducing the computational cost when computing the coefficients of the polynomial chaos expansion. Moreover, an efficient prediction (i.e., with a low computational cost) of the structural response under uncertainties is presented. Accuracy and applicability of the proposed methodology are demonstrated by means of several topology optimization examples of 2D continuum structures. The obtained results are in excellent agreement with the solutions obtained using the Monte Carlo method. Finally, conclusions are inferred and possible extensions of this work are proposed.

Keywords

Robust topology optimization; Uncertainty quantification; Stochastic spectral methods; Generalized polynomial chaos; Karhunen-Loève expansion.

Resumo

Cuellar Loyola, Nilton Alejandro; Menezes, Ivan Fábio Mota de; Pereira, Anderson. **Otimização topológica robusta usando uma abordagem espectral estocástica não intrusiva**. Rio de Janeiro, 2018. 140p. Tese de Doutorado — Departamento de Engenharia Mecânica, Pontifícia Universidade Católica do Rio de Janeiro.

Este trabalho apresenta aplicações de métodos espectrais estocásticos para otimização topológica de estruturas na presença de incertezas. Esse procedimento, conhecido como otimização topológica robusta, minimiza uma combinação entre a média e o desvio padrão da função objetivo. Para tanto, uma expansão de caos polinomial não intrusiva é integrada a um algoritmo de otimização topológica para se calcular os dois primeiros momentos estatísticos da resposta do modelo mecânico. A fim de abordar as variabilidades na resposta estrutural, as incertezas são consideradas no carregamento e nas propriedades do material. Na formulação probabilística proposta, as incertezas são representadas como um conjunto de variáveis aleatórias (por exemplo, magnitudes e direções das cargas) ou como campos aleatórios (por exemplo, cargas distribuídas e propriedades do material). Um campo aleatório homogêneo não Gaussiano com uma função de distribuição marginal e covariância especificada é usado para representar as incertezas nas propriedades dos materiais, pois garante a sua admissibilidade física. A transformação não-linear "sem memória" de um campo Gaussiano homogêneo é usada para obter campos não Gaussianos. A expansão de Karhunen-Loève é empregada para fornecer uma representação do campo Gaussiano em termos de um número finito de variáveis aleatórias independentes. A quadratura de grade esparsa é empregada para reduzir o custo computacional no cálculo dos coeficientes da expansão do caos polinomial. Além disso, é mostrada uma previsão eficiente (isto é, com um baixo custo computacional) da resposta estrutural sob incertezas. A precisão e a aplicabilidade da metodologia proposta são demonstradas por meio de vários exemplos de otimização topológica de estruturas contínuas 2D. Os resultados obtidos estão em excelente concordância com as soluções obtidas pelo método de Monte Carlo. Finalmente, conclusões são apresentadas e possíveis extensões deste trabalho são propostas.

Palavras–chave

Otimização topológica robusta; Quantificação de incertezas; Métodos estocásticos espectrais; Caos polinomial generalizado; Expansão de Karhunen-Loève.

Contents

List of Figures

List of Tables

Nomenclature

List of abbreviations

FEM	finite element method
gPC	generalized polynomial chaos
KL	Karhunen Loève
LHS	latin hypercube sampling
MCS	monte carlo simulation
OUU	optimization under uncertainty
PCE	polynomial chaos expansion
QoI	quantities of interest
RBDO	reliability based design optimization
RDO	robust design optimization
RTO	robust topology optimization
SO	structural optimization
TO	topology optimization
UQ	uncertainty quantification

List of symbols

$\boldsymbol{\epsilon}$	tensors of strain
$\boldsymbol{\mathcal{C}}^0$	the elasticity tensor
$\boldsymbol{\sigma}$	the tensors of stress
$\boldsymbol{X}$	random vector
δ_X	skewness of the random variable X
δ_{ij}	Kronecker delta
$\hat{\Gamma}_p$	the space of polynomials degree p
κ_X	kurtisis of the random variable X
λ_i	the eigenvalues
$\mathbb{E}[\cdot]$	mean value
$\mathbb{N}$	natural number set
$\mathbb{R}$	real number set

$\mathbf{C}$	the covariance matrix
$\mathbf{F}$	force vector
$\mathbf{K}$	stiffness matrix
$\mathbf{K}_e^0$	the element stiffness matrix
$\mathbf{R}$	the correlation matrix
$\mathbf{u}$	displacement vector
$\mathcal{D}_X$	real number sub-set
$\mathcal{M}$	mathematical model representation
$\mathfrak{F}$	$\sigma-$field
$\mathrm{Var}(\cdot)$	variance value
Ω	sample space
ω	event
ϕ_i	the eigenfunctions
Ψ_j	polynomial basis functions
$\rho(\mathbf{x})$	density map
$\rho_{X,Y}$	the correlation coefficient of the random variables X, Y
σ_X	standard deviation of the random variable X
c	continuum structure compliance
$Cov[X, Y]$	the covariance of the random variables X, Y
CV_X	coefficient of variation of the random variable X
F_X	cumulative distribution function
f_X	probability density function
H	gaussian random field
I_p	Wiener-Askey basis polynomial
P	probability measure
p_X	probability mass function
$Q_l^{(1)} f$	family of quadrature rules
u_i	deterministic coefficient of PCE
X	random variable
Z	non-gaussian random field
L_2	square integrable L2-functions

1
Introduction

The field of stochastic computations in the context of understanding the impact of uncertainty sources on numerical modeling and simulation results, is relatively new. It has become the main tool in many fields for understanding complex systems and predict physical events with greater accuracy. Thanks to the evolution of computers, simulation techniques have become essential tools for engineers because they can minimize the need for costly physical experiments specially during early design stages. Nevertheless, to get a good performance we must be careful to design models that produce useful and reliable information regarding the system being studied.

In this chapter it is presented the motivation for the development of this thesis, followed by the issues of scientific and technological interest associated to the subject, the problem statement, the methodology for achieving the objectives and contributions and finally the scope of the thesis.

1.1
Motivation and related works

Nowadays there exists an increasing variety of engineering systems that require more critical and complex designs. For this reason, several engineers integrate uncertainties into their simulations to find critical values in the initial stage of design. Therefore, this new process will allow one to design mechanical systems statistically with better performance, because the probability of failure of the mechanical systems due to uncertainties will be minimized. Thus, with this perspective of design, there is a need to develop more robust and accurate approaches to effectively represent uncertainties in the computer models.

There are several real-world engineering problems for which the requirements are related to finding optimal solutions. We can frequently find these applications in the design of mechanical structures or other particular problems

in the field of engineering. For instance, new systematic and computational tools have been developed for designing high-performance structures with a minimal cost. Numerous computational optimization methods have become available to solve problems highly constrained and with multiples objectives.

Due to new requirements of design associated with the most modern engineering applications, mechanical systems with very complex geometrical configurations are becoming increasingly common. In this context, some of the most promising design approaches are based on topology optimization (TO), which seeks to find the best layout for a system, by optimizing the material distribution in a predefined design domain [9, 12]. The growing popularity of TO solutions is demonstrated by their wide range of application in various fields such as structural mechanics [13–18], composite and multi-materials [19, 20], nanotechnology [21], fluid mechanics [22, 23], fluid-structure interaction [24], medicine [25], etc.

The main goal of an optimization is to find an optimum solution with a high degree of precision. Generally, classical algorithms consider deterministic models to solve the problem. For this reason, that solution is not robust to the perturbations leading to a final design whose performance might degrade significantly. In this scenario, a better methodology would be used to get an optimal design with a minimum level of sensitivity to variability on the system parameters. This methodology for finding such optimal is known, in the field of engineering, as robust optimization or robust design.

Since various optimization models, where their objective and constraint functions are highly sensitive because involve uncertainties within the model, the optimization under uncertainties (OUU) becomes an issue transposing the concepts of robustness and reliability into the conventional optimization context.

In the last few years, a variety of approaches have been developed to solve the OUU problems [26]. We can find in several works (see for example [27–30]), that the OUU problems may be subdivided into two main fields, namely: Robust design optimization (RDO) and Reliability-based optimization (RBDO). There are other approaches to OUU, such as: stochastic programming (robust stochastic programming, recourse models and probabilistic models), fuzzy programming (flexible and possibilistic programming), and stochastic dynamic programming whose applications are mainly applied to linear problems [31], and are not in the scope of this work.

RDO and RBDO are effective tools to incorporate uncertainties in the design: while RDO minimizes the loss quality of the product, RBDO achieves the target confidence of product reliability. When we consider Robustness in

the problem of RBDO simultaneously, a new formulation called Reliability-Based Robust Optimization (RBRDO) was proposed in various papers [32–36], to generate reliable and robust solutions.

Another powerful approach in OUU is the use of global approximations, i.e., meta-models, surrogate models or emulators, since they are used as temporary substitution for the true objective and constraint functions by means of a mathematical expression that is much cheaper to evaluate. There are many techniques to generate surrogate models, such as, Kriging, Artificial Neural Networks, Support Vector Machine (SVM), Polynomial Response Surface Models, among others [37, 38]. The Surrogate-based analysis and optimization (SBAO) approach has been shown to be an effective tool for optimization problems. An overview of SBAO can be found in [39, 40], where some of the most popular methods in OUU problems were covered.

The application of surrogate models in optimization can be found in many publications (see, for example, [41–43]). Also, to reduce the numerical effort related to the described robustness analyses, surrogate techniques are used to replace the actual numerical analysis codes by simple formulations together with RDO [44–46] and RBDO [47–49].

The need for robust design and analysis of uncertainties in topological optimization applications naturally induce the search for computationally efficient frameworks for TO. For this purpose, TO literature started to take uncertainty quantification (UQ) into account over the last decade, as can be seen in several papers addressing the two issues [50–63].

Some of these works are based on classical techniques for stochastic computation like Monte Carlo (MC) method [57, 61] or series expansion [52, 56, 58, 60, 62] which, despite of being very simple in conceptual terms, are limited by the high computational cost, the former, or very small range of applicability, the latter. These limitations open space for spectral-based approaches [50, 51, 54, 55, 59, 63], that use state-of-the-art tools for representing and propagating uncertainties in computational models, like Karhunen-Loève (KL) and generalized polynomial chaos (gPC) expansions. They add robustness to the topology optimization model to become a robust model of Topology Optimization (RTO) (see, for example, [64–69])

A recent work by Keshavarzzadeh et. al [51] presents a non-intrusive gPC strategy to propagate uncertainties in topology optimization problems. They use non-intrusive polynomial chaos expansion to evaluate low-order statistics of compliance and volume and the uncertainties are considered in the applied loads and also in the geometry of the problems. However, few works in TO under uncertainty that use stochastic spectral method for quantifying

uncertainties can be found in the technical literature.

Finally, another important point that should also be considered, is related with the frameworks that are available for quantification of uncertainties and Topology Optimization. UQLab is a general purpose UQ framework developed at ETH Zurich (Switzerland) and is implemented in protected file of Matlab known as a P-file [70]. Dakota is other software open-source under GNU LGPL and written in C++. The Dakota project delivers both state-of-the-art research and robust, usable software for optimization and UQ developed at Sandia National Laboratories [71]. OpenTurn is other framework open-source under GNU LGPL and written in Python initiative to Treat Uncertainties, Risks'N Statistics [72]. Top3d is programs that solves topology optimization in 3D written in Matlab code [73]. ToPy is a lightweight topology optimization framework for Python that can solve compliance (stiffness), mechanism synthesis [74]. `PolyTop` is an efficient Matlab code for structural topology optimization that includes a general finite element routine based on isoparametric polygonal elements [75].

After an extensive literature review, we can view that there are very few works and softwares implemented for the treating in topology optimization in presence of uncertainties. This motive the study and development of an efficient computational algorithm, capable of performing a minimum number of simulations to achieve a robust optimal solution.

1.2 Problem statement

The use of deterministic models to approximate physical systems may cause some structural failure due to the several uncertainties that are not often considered within the mathematical models and may be found for example in structural mechanical systems, i.e. in their material properties, geometric shapes, distributed loads, manufacturing processes, among others. Another system where such uncertainties arise are in robotic control whose applications have been important in surgery or in the control of unmanned space vehicles whose mass and moments of inertia might change over time. We can also notice the source of uncertainties in the evaluation of forces of turbulence that a plane interacts during its flight or those turbulent vortices that an offshore platform supports daily.

Therefore, when the levels of uncertainty sources are very high, we must use stochastic approaches to develop mathematical models to describe the real physics. For example, the consideration of the uncertainties in the material properties of mechanical structures has attracted significant interest in the

engineering community owing to the need for quantitatively characterizing and reducing the variability in the analysis and optimal design of such structures.

Additionally, there are criteria and methodologies for modeling uncertainties, such that, represent the phenomena with greater accuracy. Returning to the previous example, sometimes structural analysis assumes that the uncertainties in the material properties are concentrated at discrete points in space as a variation across samples, represented as single-valued random variables that are mostly used for concentrated loads, stiffness of joint and supports, etc. However, most properties of mechanical structures are distributed in space and not concentrated at a point; such as, distributed loads, Young's modulus, and geometric properties that vary over the length, area, or volume.

In recent years, several approaches have been developed to quantify and propagate uncertainties whose main goal is to address the impact of such errors and subsequently to provide more reliable predictions for this class of problems. In order to accomplish this goal, it is required the numerical solution of numerous high-order nonlinear algebraic and differential equations.

Many different approaches have been considered in the past to include uncertainty in the modeling or in the design process. Most of these approaches are based on applications or extensions of the Monte Carlo method. The crude Monte Carlo method is a widely used and very powerful technique to propagate the input randomness onto the system response or specific quantities of interest in problems without limitations concerning the structure of the uncertainty or the properties of the probability distribution. On the other hand, this method has a major disadvantage of being extremely expensive in terms of computational cost, and also to present a very slow convergence rate, despite of being flexible and of easy implementation. Therefore, this method is sometimes avoided for large real-time applications.

In order to overcome the lack of exploitation of possible regularities that the solution must present with respect to the input variables, several methods have recently been developed, such as, Stochastic Galerkin, Polynomial Chaos expansion, Probabilistic Collocation, Karhunen-Loève expansion, among others. These approaches are known as stochastic spectral methods and their applications to problems of uncertainty propagation and quantification in model-based computations are an open and relevant research topic.

There exist many commercial software and tools to quantify robustness and to achieve optimal design that are now available to the engineers, such as: modeFRONTIER, OptiY, LS-Opt, optiSlang for Ansys and COSSAN-X. However, only a few of them are mainly concentrated on quantifying reliability and robustness of a given solution, rather than performing the optimization

under uncertainty.

Therefore, the optimization models often need broader measures of objective and constraint functions and their respective sensitivities, several statistical measures such as: expected value, standard deviation, and probability of failure can provide such information. Since these statistical measures usually cannot be integrated analytically within the optimization model due to their nonlinearity, they must be approximated numerically. Then, both the objective function and implicit constraints will require the execution of an uncertainty quantification procedure to evaluate the output response. Each evaluation of the response is carried out by calculating the nonlinear model which, in turn, is a very expensive computationally task.

In order to deal with this problem, we should develop an efficient algorithm to reduce the number of simulations and to manage the uncertainties in the optimization procedure. In this case, procedures to quantify and propagate uncertainties such as the Stochastic Spectral approach will be study for the conception of the solution.

1.3 Objectives and Methodology

Being motivated by the importance of finding robust designs in mechanical structures, the main objectives of this thesis are:

- Describe all the basic ingredients necessary for the understanding of stochastic methods to quantify uncertainties;
- Implement the most common stochastic spectral methods: the Polynomial Chaos and Karhunen-Loève expansion;
- Investigate and compare the efficiency of the non-intrusive Polynomial Chaos expansion with other techniques, e.g. the Monte Carlo simulation method;
- Investigate non-Gaussian random field in order to represent the spatial variabilities of uncertainty material;
- Develop in a systematic and coherent way numerical strategies to optimize mechanical structures in the presence of uncertainties based on polynomial chaos expansion, which it is called Robust Topology Optimization;
- Compare the efficiency and assess the performance of the numerical algorithms developed with some examples available in the literature;

In order to accomplish the goals of this proposal, a deep literature review is necessary to learn the concepts and techniques of the different approaches that will be used to solve our problem. The proposed methodology will be divided into four main parts:

First, we must realize study the details about quantification and propagation of uncertainties, whose approach demands previous knowledge on functional calculus, approximation theory, numerical integration, probability theory, stochastic process and stochastic spectral methods. Thus, we will be able to model the uncertainties mathematically and propagate them efficiently through the appropriate choice of different techniques found in the literature. We need to perform a detailed comparison between Monte Carlo Simulation and the most advanced methods, such as, polynomial chaos expansion and or stochastic collocation to solve benchmark uncertainty quantification problems.

Second, we continue with the study about convexity and the different optimization algorithms known as Unconstrained and Constrained optimization, such as: Dichotomy, Nelder Mead, Steep Descent, Method of Penalties, Newton Raphson, Lagrange Method, among others. To compare each algorithm, we should consider three criteria: Efficiency, Robustness and Accuracy. These different elements are usually a trade-off. The responsibility in choosing the algorithm will be an important step of the work, because it often determines the quality and speed of the problem resolution.

Third, it will be studied all theoretical principles for modeling continuum structures, starting from basic concepts to the design of mathematical equations that describe its physical behavior. Next, we will formulate the basic equations to achieve optimal designs using the topology optimization methodology. This step involves other methods of optimization, such as: Optimality Criteria, Sequential Quadratic Programming and Method of Moving Asymptotes, together with the evaluation of the finite element method. Therefore, we need to develop a finite element code with the capability to be coupled with the topology optimization modulus.

Finally, we began to formulate the optimization problem in the presence of uncertainties. The various approaches developed in the literature will be the starting point to find the best alternatives and thus to achieve the optimal robust design. The results of the proposed methodology will be compared with the ones available in the technical literature.

1.4 Research Contribution

This doctoral thesis presents as main contributions:

- Nilton Cuellar, Anderson Pereira, Ivan F Menezes (2015). Robust Topology Optimization under Uncertain Loads: A Spectral Stochastic Approach. CILAMCE2015.

- Nilton Cuellar, Anderson Pereira, Ivan F Menezes and Americo Cunha (2018). Nonintrusive polynomial chaos expansion for topology optimization using polygonal meshes. Journal of the Brazilian Society of Mechanical Sciences and Engineering (Accepted).
- Nilton Cuellar, Anderson Pereira, Ivan F Menezes and Americo Cunha (2018). An Accurate Representation of Material Uncertainty using non-Gaussian Random Field applied in Topology Optimization. (To be submitted).
- All developed Matlab® code during the thesis(the Polynomial Chaos expansion, the Karhunen-Lo'eve expansion, two-dimensional non-Gaussian random field and the computational algorithm for solving the Robust Topology Optimization (RTO) problem) will be made available after being published.

1.5 Outline of the thesis

This thesis is divided into seven chapters being the first one a brief introduction which seeks to give an ambience of the work to be developed. The remainder of this thesis is organized as follows:

In chapter 2, it is introduced the definition of Uncertainty Quantification (UQ) that is concerned with understanding and calculating the uncertainties inherent in such system and by which are characterized and propagates to a given quantity of interest. A more precise characterization is based on the identification of the types of uncertainties (aleatory and epistemic), while uncertainty propagation is often associates to the effects with each of the system's inputs on the system's outputs. In addition, in this chapter it is investigated how the analysis UQ can reduce the impact caused by the uncertainties and subsequently to provide more reliable prediction for practical problems. Several classes of methods have been developed to represent and propagate uncertainties, in this thesis a special focus is given to well-known probabilistic methods, which are also described in this chapter. It also shown as uncertainties are represented as random variables or random fields which are generated from a probability density function through of a random sampling method.

In chapter 3, it is presented in detail the underlying theory and implementation of stochastic spectral methods of a specific class random model output. Generally, these spectral methods consist in representing the random model response through of a series expansion composed of selected functionals basis suitable on a particular space and a set of deterministic coefficients in

order to satisfy the response as well as possible. Thus, this series expansion once available can be immediately used to determine the statistical measures of random model output. We focus our attention in two stochastic spectral methods: the Karhunen-Loeve and Polynomial expansion where the main concepts, rate convergence and approximation error are briefly analyzed. The Karhunen-Loeve expansion of a second-order random process or field, is based on the spectral decomposition of its autocorrelation function and are extended to discretize them in an optimal way and be computationally implementable. The mathematical formulation and basic steps for the construction of the PC expansion are examined for the case de different types of random variables and through of non-intrusive way, the deterministic coefficients are estimated. This chapter also provide some practical examples for the well understanding of both methods.

In chapter 4, we provide a brief overview about the structural optimization which is a class of optimization problem where the evaluation of an objective function or constraints require the use of structural analyses. Due to increasing demands for performance improvement together with reduced weight and costs several strategies and methods such as size, shape and topology optimization were developed for achieving such objectives. Our attention is focused in the Topology optimization problem which consists to find the best distribution of material in a domain previously defined to obtain a structure with an optimal format for a given set of loads. It also introduces fundamental concepts about optimization under uncertainties which is referred as a branch of optimization problem when uncertainties are involved in the parameters or model. Therefore, this thesis does a review the main approaches and the state-of-art in computation which it is key for understanding and for the implementation of algorithm proposed.

The next chapters are devoted to the author's contribution in the field of robust design optimization for mechanical structures.

In chapter 5, we present the robust topology optimization (RTO), which is mathematically formulated for simultaneously addresses optimization and robustness analysis. This strategy combines deterministic topology optimization algorithm with stochastic spectral methods for a non-intrusive propagation of uncertainties which are associated with loads that can be in either concentrated or uniformly distributed and structural stiffness, such as, material properties or structure geometry. The use of spectral methods in turn leads to significant computational reducing when compared with Monte Carlo simulation which involve multiple assessments and inversions of the global stiffness matrix. Also, an efficient sensitivity analysis is developed and integrated to

solve the robust topology optimization problem.

In chapter 6, it is provided a detailed treatment of elementary numerical examples of applications using the proposed RTO methodology. The analysis is focused on the optimization of 2D mechanical structures where our discussion covers the setup of the deterministic and stochastic problems, the representation of uncertainties, the spatial discretization of random fields and addresses various numerical results which show the performance and efficiency of the computational algorithm.

Finally, in chapter 7 are presented the conclusions of the thesis with some remarks and suggestions for possible future works.

2
Uncertainty Quantification

Uncertainty Quantification (UQ) is a inter-disciplinary area and lies at the intersection of branches of physics and applied mathematics. UQ is concerned with of quantitative characterization, management and reduction of uncertainties to evaluate the likelihood of a certain outcomes in a given quantity of interest. When real-world phenomena need to be studied through of mathematical and computer models, UQ describe a framework to estimate and predict the impact caused for those uncertainties onto the physics system response.

UQ addresses two main aspect to develop and analyze the solution through of numerical methods. i.e., forward problems with uncertain inputs (propagating of uncertainties in model inputs to model outputs) and inverse problems (where unknown model inputs are to be estimated from possibly noisy observations of model outputs) being the latter one will not be considered in this work.

In this chapter it is presented briefly an overview of fundametal concepts corncerning to the types of uncertainties, the probabilistic modeling, definitiond of random variables and random fields. Finally it discusses and illustres some approaches for quantifying uncertaties with conventional methods.

2.1
Definition and basic concepts

The need to make prediction of physical reality is increasing as the computational science has been revolutionizing but we must know how good the predictions are. Thus the process of prediction taken on a special meaning and attention. The systematic treatment of model and data uncertainties and their propagation through a computational model to produce predictions of quantities of interest with quantified uncertainty but What are the target

outputs? What are the principal quantities of interest, or QoI's?

Quantities of Interest (QoI), specific objectives that can be expressed as the target outputs of a model (mathematically, they are often defined by functionals of the solutions and provide focus on the goal of scientific computation). Before asking whether a model is or is not invalid, we must specify the quantities we wish to predict, and the situations or scenarios in which they are to be predicted [1].

It is also important to understand the distinctions between a computational model, a simulation or analysis, and a mathematical model, which are an important part of this prediction process. A mathematical model is an approximate representation of the behaviour and essential aspects of a real physical system that is based on theoretical hypotheses and empirical observations thus it presents the knowledge of the system in a usable form. A computational model uses numerical techniques to disrcete and produce an approximate solution of a mathematical model. Therefore, a mathematical model and a computational model are tools which are used to perform an analysis or simulation.

However, mathematical models generally involve parameters that must be tuned so that the model best represents the particular system and computational model must use good numerical techniques that can simulate the continuous behavior of a system inside a computer code. On the other hand, the experimental observations themselves are often fraught with errors and uncertainties owing to imperfections in the instruments or the difficulty or impossibility of acquiring observational data relevant to the problem at hand.

The imperfect mathematical model of reality with the unknown or incomplete information on model parameters, with incomplete observational data or observations delivered by imperfect devices or instruments, and the corruption of the model itself through the discretization process necessary for computation, all lead to imperfect paths to knowledge [1], depicted symbolically in Figure 2.1.

In the scheme of the imperfect path of knowlegde (Figure 2.1), we also include the UQ to obtain the computational predicition from an engineering perspective which is the main focus of this study.

2.1.1 Error and Uncertainties

Traditionally, in the area of measurement, the error is defined as the difference between the value true and the measured value, and uncertainties as the variation of measured value that would be obtained if the measurement

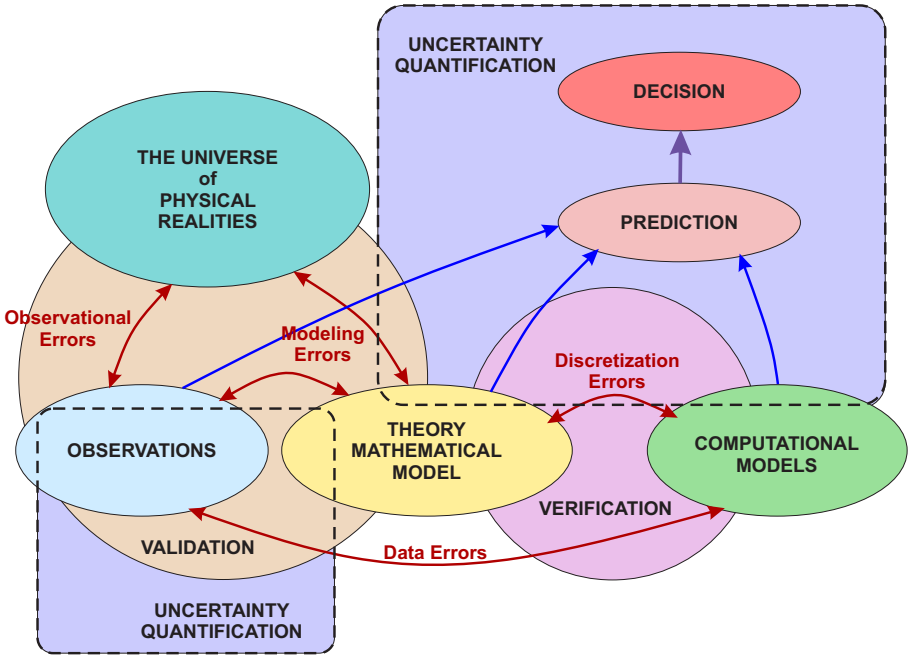

Figure 2.1: The Imperfect Paths to Knowledge. (Adapted from [1])

were infinitely repeated (in this case it is assumed as a distribution).

The acuracy of the measurement result, is characterized by measurement uncertainty (or simply uncertainty), which defines an distribution or interval around of the measured value. Figure 2.2, show the relation the accuracy (bias) and the uncertainty also referred to as random error.

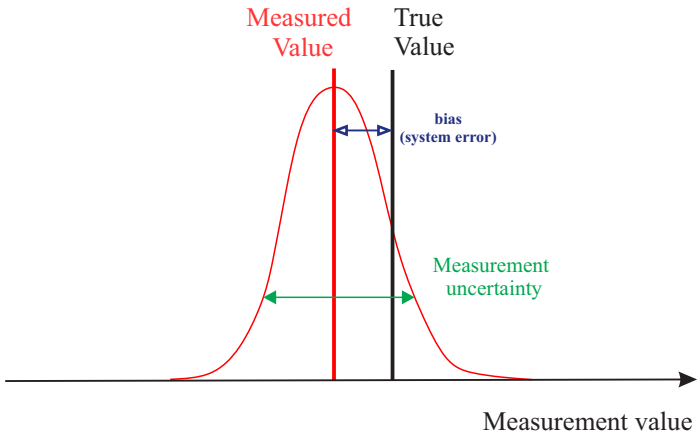

Figure 2.2: Interrelations between the concepts true value, measured value, error and uncertainty.

The American Institute of Aeronautics and Astronautics (AIAA) Guide for the Verification and Validation of CFD Simulations [76] defines errors as recognisable deficiencies of the models or the algorithms employed and uncertainties as a potential deficiency that is due to lack of knowledge. From these two definitions imply that error is deterministic in nature and uncertainty is stochastic or non-deterministic in nature.

According to Gianluca Iaccarino [77], the latter definition does not emphasize a distintion between the mathematics and the physics, i.e., the errors must be defined as the translation of a mathematical formulation into a computational numerical algorithm and uncertainties as the choice of the physical models and to the specification of the input physical parameters required for performing the analysis.

In most cases the errors will be allowed to remain in a computational model if they are estimated to be within reasonable limits and whose effect on the results is deemed negligible. These error are known as acknowledged errors, e.g. (round-off error, discretization error, limited convergence error of certain iterative numerical algorithm). On the other hand, when the errors are not recognizable and have no set procedures for finding them. Moreover they migth continue within the code or computational model. These error are known as unacknowledged errors, e.g. (computer programming errors or usage errors, including mistakes and blunders).

Therefore, it is important to distinguish between, "uncertainty" and "error" to understand and evaluate contribution in modeling and simulation and how they should be represented and propagated through the mathematical model.

For example, Figure 2.3, show a mathematical model for the friction force (blue line) and data points were taken experimentally (red points), boths associated with velocity (see [78]). This classical model known as Coulomb friction model is used to estimate the true friction force, which is formulated as:

$$F = \begin{cases} F_c \,\mathrm{sign}(v) & \text{if } \; v \neq 0, \\ F_{app} & \text{if } \; v = 0 \;\; \text{and} \;\; |F_{app}| < F_c. \end{cases} \tag{2-1}$$

where F is the friction force, v the velovity and F_{app} the applied force on the body. F_c is the Coulomb sliding friction force defined as $F_c = \mu N$ being μ is the coefficient of friction and N the normal load in the contact.

It also can be seen from Figure 2.3, that the Coulomb model does not represent perfectly the experimental results, which generates an error. This may be due the several uncertainties that are integrated to the model and we represented them through a distribution (blue dashed line).

2.1.2 Aleatory and Epistemic Uncertainties

Uncertainty analysis are being adopted due to the need of obtaining more rigour safety factors, to asses the safe lifetime and quantify the risk

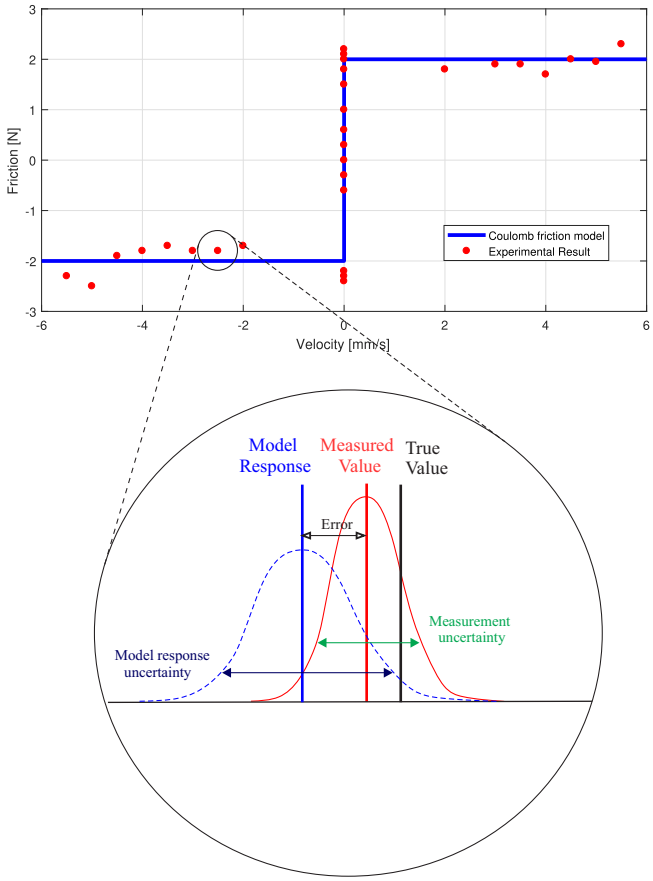

Figure 2.3: Example of matematical model for the friction force.

involved. Thus, the degree of conservatism in traditioanl enginering design can be diminished.

Through this analysis we can determine what procediment might be used when uncertainties are found. For example, uncertainties in the mathematical modeling can be reduced with a additional knowledge available. On the other hand, uncertainties that are related with the physical or intrinsic nature can not. Then, a correct clasification of the uncertainties will help to represent the behavior of the model that want to approximate.

Although, the entire spectrum of uncertainties is also not known (Figure 2.4), the sources of uncertainties must be appropriately accounted for to guarantee that the components or systems will continue to perform satisfactory despite fluctuations. Otherwise, different representations of uncertainty may yield different interpretations for the given system.

Therefore, due to this limitation a more precise categorization is based on the distiction according to their fundamental essence. Generally, uncertainties

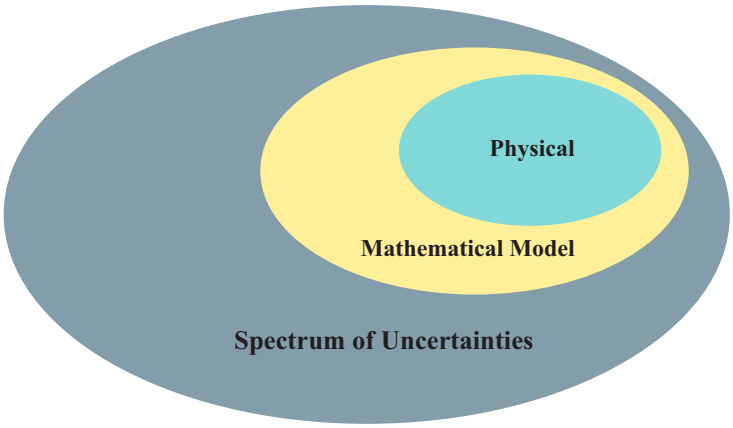

Figure 2.4: Entire spectrum of uncertainties (Adapted from [2]).

can be classified in two categories: as either aleatory or epistemic.

Aleatory uncertainty is also called variability, stochastic uncertainty or inherent uncertaintiy. It is related with physical phenomena, which are random by nature and are not strictly due to a lack of knowledge. Therefore it cannot be reduced. For example:

- Determination of material properties or operating conditions of a physical system.
- Determination of the pressure field in a fully developed turbulent boundary layer.
- Determination of the wind speed for a wind turbine plant to produce electric power.

Epistemic uncertaint is a potential deficiency due to a lack of knowledge, imprecision (vagueness), measurement error and ignorance. It should be noted that epistemic uncertainty can be reduced by further studies. For example:

- It can arise from assumptions introduced in the derivation of the mathematical model or from simplications as surrogates etc.
- The lack of knowledge in the mechanical description of a boundary condition in a structure.
- The geometrical tolerances induced by the manufacturing process in a structure.

Figure 2.5, summarizes with a pratical example the two types of uncertainties tha can be identified in a Industrial manipulator robot. These uncertainties will be adressed with differents theories for being characterized.

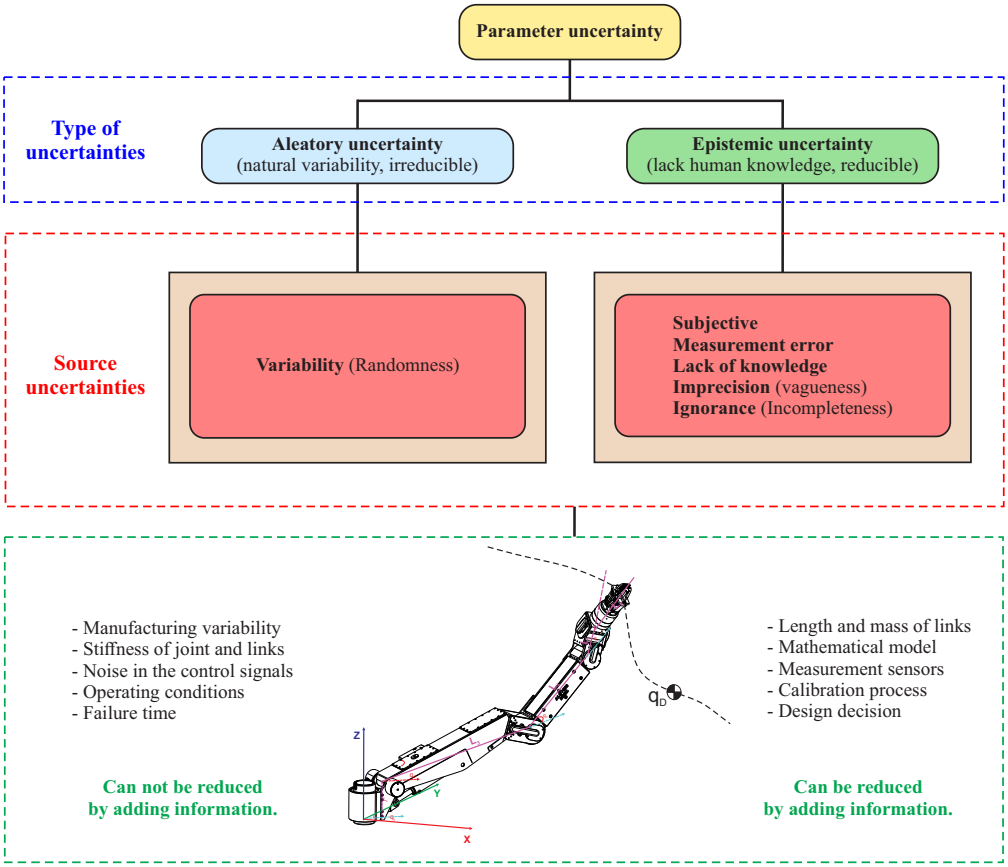

Figure 2.5: Classification of uncertainties: Aleatory and Epistemic.

2.1.3 Sources of Uncertainties

Uncertainty arises from different sources in various forms and must be identified. Thus, the uncertainties should be classified as aleatory, epistemic, or mixed uncertainites and through of a appropriate mathematical representation they are charaterized. Variability, vagueness, ambiguity and confusion are some factors that introduce uncertainties in the simulations and must be treated in different ways.

When physical systems need to be studied, a useful tool for this is through of mathematical models but in reality the parameters and model are not known exactly because they contain uncertainties. Then, model and parameter uncertainties are the two main sources of uncertainty able to affect the analysis of physical systems.

Model uncertainty starts from the fact that conceptual models are based on simple mathematical equations which represent reality but cannot completely characterize the complex physical systems of any given phenomenon, usually represents a superposition of errors [79]; [80]. The parametric uncertainty related to the inputs arises from the inability to define exact values for

certain parameters of the mathematical model [81].

In this study, only parametric uncertainties are addressed due that this type of uncertainty has the most significant effect on the model response and needs to be quantified accurately in order for the UQ analysis to be reliable. Two approaches are found in the literature for the development of parametric uncertainty analysis: Probabilistic and non-probabilistic approach.

The Probabilistic aproach uses probability theory to model the physical system uncertainties as random quantities such as random variables, process random or random fields. Consequently, the model response becomes aleatory and is calculated using a stochastic solver.

The non-probabilistic approach uses possibility theory to model the physical system uncertainties when has one value but we don't know what it is due to lack of information. Fuzzy, Interval, Evidence and Information-gap theory are some of the theories used for this analysis. This approach is less suitable for problems in high stochastic dimension. Usually it is applied only when the probabilistic approach can not be used [82].

Figure 2.6, illustrates five uncertainty handling theories: Probabilistic, Fuzzy, Interval, Evidence and Information-gap theory.

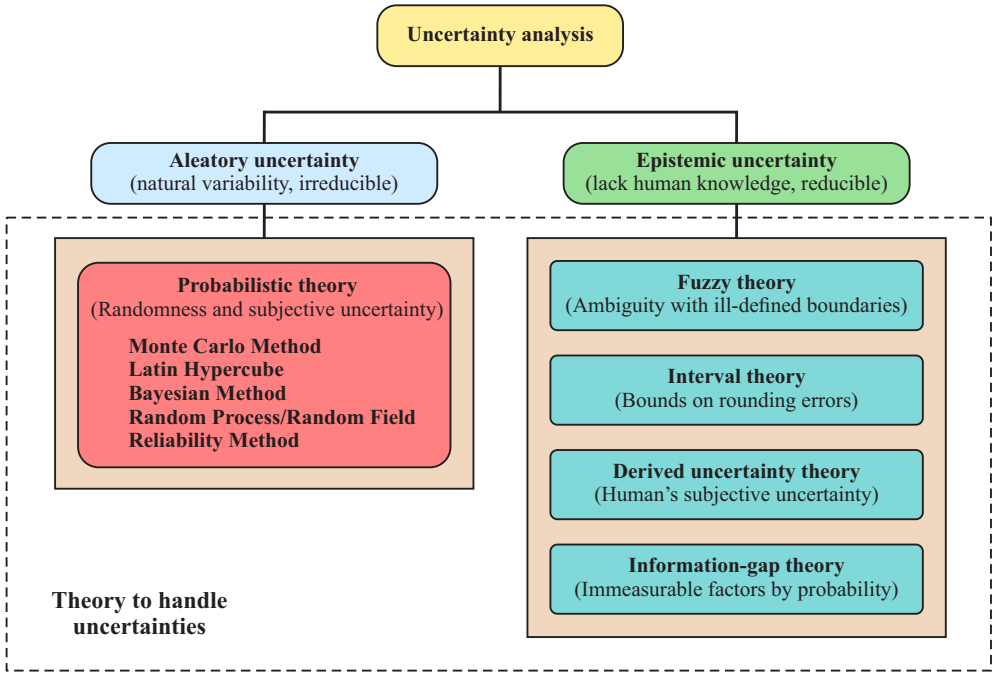

Figure 2.6: Uncertainty Analysis Categories.

Thus, the parametric probabilistic approach is an appropriate method to describe aleatory uncertainties. In addition, a consistent estimate of the pior probability distribution of the parameters can be carried out in several ways;

- The probability distributions are assigned by assumption to the parameters taking into account experience and wisdom
- Through of extensive measurements of the parameters or when a significant amount of experimental data is available, the probability distributions are fitted using several statistical techniques.
- Through of statistical inference, the probability distributions are reconstructed using measurements of the quantity of interest.
- When few or none experimental data is available, a tool from information theory can be used e.g. Maximum Entropy Principle.

Some uncertain parameters may have a time-space dependency and this leads to the necessity of employing random processes or random fields when they are indexed by a space variable.

2.1.4 Sensivity and Uncertainties analysis

In the this section was addressed the uncertainty analysis whose aims at identifying and describing the input and output uncertainty of in a given model, i.e., the probability distributions of the QoIs. It is understood that the stochastic dimension depends on the number of parametric uncertainty that will be represented in the model and as this number increases the computational cost as well. However, not all uncertainties need to be represented because their influence in some cases does not cause greater variability on the model output.

Sensitivity analysis describes the relation between the inputs and outputs of model, i.e., it allows to identify and predict how the variability in an output QoIs is connected to an input in the model and which input sources will dominate the response of the system.

Therefore, the sensitivity analysis is an important and useful tool for model refinement, once the most influential parameters have been identified, the remaining parameters can be considered without uncertainty, leading to a model with a lower stochastic dimensional input. This refined model can then be used for other more accurate and efficient analysis [77].

Sensitivity analysis is often based on the concept of sensitivity derivatives, the gradient of the output of interest with respect to input variables.

2.1.5 Verification and Validation

The American Institute for Aeronautics and Astronautics (AIAA) has developed the Guide for the Verification and Validation (V&V) of Computa-

tional Fluid Dynamics Simulations [76]: define Verification as the process of determining that a model implementation accurately represents the developer's conceptual description of the model and Validation as the process of determining the degree to which a model is an accurate representation of the real world for the intended uses of the model.

From this definition, we can characterize them in terms of two questions: Verification (are we solving the equations correctly?):

- Estimates the errors (due to discretization, iteration, and computer round off) in the computational model implementation of the mathematical model.
- Compares the several numerical methods used in the computational code to exact analytical results.

Validation (are we solving the correct equations?):

- Estimates the magnitude of the difference between the computational model response and physical phenomenon or quantity of interest.
- Statistical comparisons of model results with experimental results carefully obtained from the real system.

Finally, we also can represent a relation for V&V similar to the indicated for the error and uncertainty, i.e., verification makes a reference for a mathematical context while validating for a physical context.

Taking the last example of friction force model 2.3, we can show a possible notion of V&V. In the literature, the Coulomb model is not the only model used to represet the friction force, there are another models that can represent better the experimental results. Figure 2.7, present the Coulomb-Viscous and Static-Coulomb-Viscous friction model and whose equations are the following.

$$F = \begin{cases} F_c \operatorname{sign}(v) + F_v v & \text{if } \ v \neq 0, \\ F_{app} & \text{if } \ v = 0 \ \text{ and } \ |F_{app}| < F_c. \end{cases} \tag{2-2}$$

$$F = \begin{cases} F_{app} & \text{if } \ v = 0 \ \text{ and } \ |F_{app}| < F_c \\ F_c \operatorname{sign}(v) + F_v v & \text{if } \ v \neq 0, \\ F_s \operatorname{sign}(F_{app}) & \text{if } \ v = 0 \ \text{ and } \ |F_{app}| \geq F_c. \end{cases} \tag{2-3}$$

We can see that the latter model (b), has a minor error because it covers more points of the experimental result. The implementation of this mathematical model to a computatational code leads to a verification being this as a mathematical exercise. However, when looking for other models to

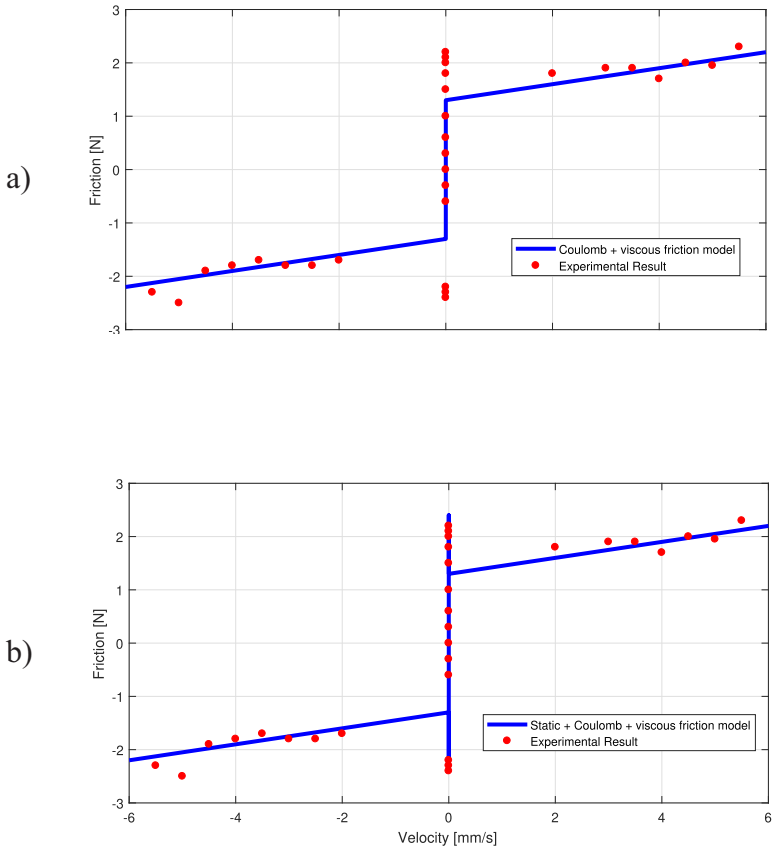

Figure 2.7: Coulomb-Viscous (a) and Static-Coulomb-Viscous (b) friction model.

have a better approximation we are doing a validation being this as a physical exercise.

Through of V&V, and comparing the simulation and experiment results a correct model can be found to reduce the error even more and so we would be so close to the real model. Figure 2.8 show the Stribeck friction model [83] and whose equation is as follow

$$F = \begin{cases} F_{app} & \text{if } v = 0 \text{ and } |F_{app}| < F_c \\ \left(F_c + (F_s - F_c)\, e^{-(|v|/v_s)^2}\right) \text{sign}(v) + F_v v & \text{if } v > 0, \\ F_s \,\text{sign}(F_{app}) & \text{if } v = 0 \text{ and } |F_{app}| \geq F_c. \end{cases} \tag{2-4}$$

The Stribeck friction model to reach a better agreement between simu-

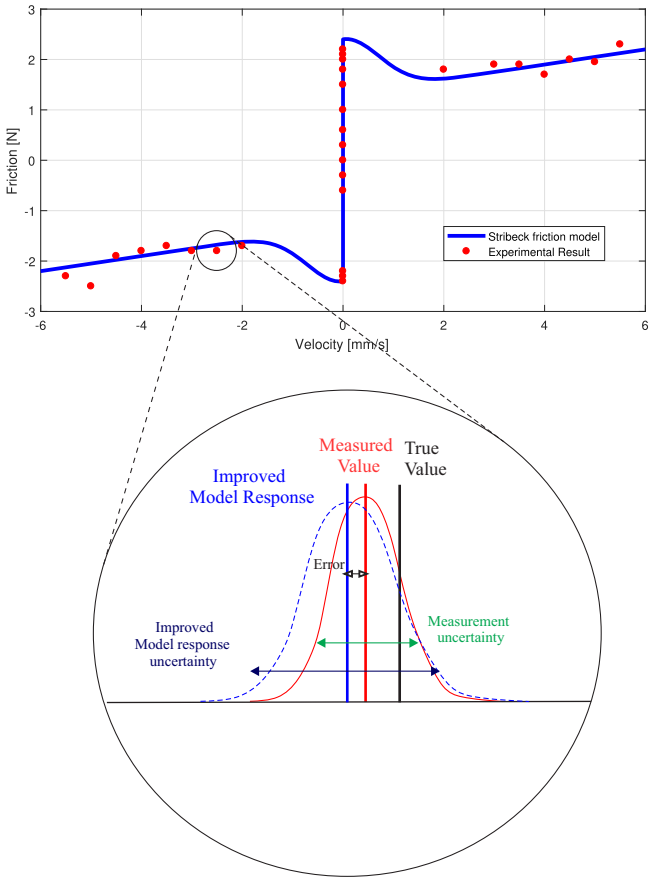

Figure 2.8: Stribeck friction model.

lation and experiment. From the figure 2.8, the reader can see the comparison between experimental results and the responses of the model, where we note that the improved model provides more plausible result.

Finally, the computational model is considered acceptable if the admissible range for the experimental value (represented by red line) is contained within the reliability envelope around the simulation (blue dashed line).

2.2 Preliminary definitions and notation

Consider the triplet $(\Omega, \mathfrak{F}, P)$, where Ω is called the sample space, $\mathfrak{F}$ a σ-field over Ω, and P denotes the probability measure.

The sample space Ω is a set which contains all possible outcomes (events) for a certain random experiment. An elementary event belonging to space Ω is denoted by ω. The sample space may contain a number of events that is finite or infinite (countable or uncountable).

Let $\mathfrak{F}$ be an non-empty collection of subsets of Ω, but not all of the outcomes are of interest so that, in a probabilistic context. We will only focus in a collection of relevant outcomes for a random experiment, which is called $\sigma-$field on Ω satisfying the following conditions:

- $\emptyset \in \mathfrak{F}$ and $\Omega \in \mathfrak{F}$
- If $A \in \mathfrak{F}$, then $A^c \in \mathfrak{F}$
- If $A_1, A_2, \ldots, \in \mathfrak{F}$, then

$$\bigcup_{i=1}^{\infty} A_i \in \mathfrak{F} \quad \text{and} \quad \bigcap_{i=1}^{\infty} A_i \in \mathfrak{F} \tag{2-5}$$

The probability measure is a function $P : \mathfrak{F} \mapsto [0, 1] \subset \mathbb{R}$ which indicates the level of expectation that a certain event in $\mathfrak{F}$ occurs.

- $0 \leq P(A) \leq 1, \forall A \in \mathfrak{F}$
- $P(\Omega) = 1$
- For $A_1, A_2, \ldots, \in \mathfrak{F}$ and $A_i \cap A_j = \emptyset, \forall i \neq j$

$$P\left(\bigcup_{i=1}^{\infty} A_i\right) = \sum_{i=1}^{\infty} P(A_i) \tag{2-6}$$

Note that $P(\emptyset) = 0$ (empty set have probability zero).

Throughout this thesis, random variables are denoted by upper case letters $X(\omega)$, while their realizations are denoted by the corresponding lower case letters, e.g. x. Moreover, bold upper and lower case letters are used to denote random vectors, e.g. $\boldsymbol{X} = \{X_1, \ldots, X_n\}$ and their realizations, e.g. $\boldsymbol{x} = \{x_1, \ldots, x_n\}$.

2.2.1 Random Variables

In many random experiments the outcome of the experiment are not necessarily numbers, but it is always of interest that has a numerical representation even if we do not know precisely what mechanism drives the experiments. Many problems are associated with random variable X, e.g. when tossing a coin we get two possible outcomes.

A real random variable X on the probability space $(\Omega, \mathfrak{F}, P)$, is a mapping $X : \Omega \mapsto \mathcal{D}_X \subset \mathbb{R}$. Then, X is a $\mathbb{R}$-valued random variable, where usually it is denoted a realization of X by $X(\Omega)$.

The image $X(\Omega)$ of Ω under X is a countable or non countable set $\mathcal{D}_X$, i.e., $X^{-1}(x) = \{\omega \in \Omega : X(\omega) = x\} \in \mathfrak{F}$ or $X^{-1}(x) = \{\omega \in \Omega : X(w) \leq x\} \in \mathfrak{F}$, for all $x \in \mathbb{R}$ respectively.

The cumulative distribution function, or simply distribution function, of a random variable X is defined by the collection of the probabilities

$$F_X(x) = P\left(X^{-1}(\langle -\infty, x])\right) = P(X \leq x) = P(\{\omega : X(\omega) \leq x\}) \qquad (2\text{-}7)$$

where F_X is the distribution function of X.

The distribution function is right-continuous and is monotone non-decreasing whit range $[0, 1]$. In addition,

$$\lim_{x \to +\infty} F_X(x) = 1, \quad \lim_{x \to -\infty} F_X(x) = 0$$

It yield the probability that X belongs to an interval $[a, b\rangle$, $[a, b]$ or $\langle a, b]$ for all $a\langle b$, That is,

$$\begin{aligned} P(\omega : a \leq X(\omega) < b) &= F_X(b) - F_X(a) + P(x = a) - P(x = b) \\ P(\omega : a \leq X(\omega) \leq b) &= F_X(b) - F_X(a) + P(x = a) \\ P(\omega : a < X(\omega) \leq b) &= F_X(b) - F_X(a) \end{aligned}$$

Moreover, we obtain the probability that X is equal to a number

$$P(X = x) = F_X(x) - \lim_{\epsilon \to 0} F_X(x - \epsilon)$$

For continuous random variable its distributions function does not have jumps i.e. F_X is absolutely continuous in $\mathbb{R}$; hence

$$P(X = x) = 0, \qquad \forall x \in \mathbb{R}$$

or, equivalently

$$\lim_{\epsilon \to 0} F_X(x + \epsilon) = F_X(x), \qquad \forall x; \qquad (2\text{-}8)$$

Therefore, there is a function f_X called the probability density function or density function, is defined as:

$$f_X(x) = \lim_{\epsilon \to 0, \epsilon > 0} P(x \leq X \leq x + \epsilon)/\epsilon \qquad (2\text{-}9)$$

Hence:

$$f_X(x) = \frac{d}{dx} F_X(x) \qquad (2\text{-}10)$$

so,

$$F_X(x) = \int_{-\infty}^{x} f_X(y) dy \qquad (2\text{-}11)$$

where f_X satisfy

$$f_X(x) \geq 0 \quad \forall x \in \mathbb{R}, \qquad \int_{-\infty}^{\infty} f_X(y) dy = 1$$

The mathematical expectation will be denoted by $\mathbb{E}[\cdot]$ The mean value (or expected value) of a random variable X is defined by

$$\mu_X \equiv \mathbb{E}[X] = \int_{\mathcal{D}_\mathcal{X}} x f_X(x) dx \tag{2-12}$$

For a real-valued function $g(x)$, the expectation of $g(X)$ is defined as

$$\mathbb{E}[g(X)] = \int_{\mathcal{D}_\mathcal{X}} g(x) f_X(x) dx \tag{2-13}$$

The m-th moment of a random variable X for $m \in \mathbb{N}$ is defined by

$$\mathbb{E}[X^m] = \int_{\mathcal{D}_\mathcal{X}} x^m f_X(x) dx \tag{2-14}$$

The variance, the standard deviation and the coefficient of variation of a random variable X, is defined as follows:

$$\begin{aligned} \mathrm{Var}(X) &= E\left[(X-\mu_X)^2\right] && (2\text{-}15)\\ \sigma_X &= \sqrt{\mathrm{Var}(X)} && (2\text{-}16)\\ \mathrm{CV}_X &= \frac{\sigma_X}{\mu_X},\ \mu_X \neq 0 && (2\text{-}17) \end{aligned}$$

The ratio between the standard deviation σ_X and the expected value μ_X of a random variable X is denoted the coefficient of variation CV_X. The coefficient of variation provides a useful descriptor for the variability of a random variable around its expected value.

The third and fourth order centered moment is called skewness δ_X and kurtosis κ_X repectively and they are denoted by

$$\begin{aligned} \delta_X &= \frac{1}{\sigma_X^3} E\left[(X-\mu_X)^3\right] && (2\text{-}18)\\ \kappa_X &= \frac{1}{\sigma_X^4} E\left[(X-\mu_X)^4\right] && (2\text{-}19) \end{aligned}$$

The covariance of two random variables X and Y is defined as:

$$\mathrm{Cov}[X,Y] = E\left[(X-\mu_X)(Y-\mu_Y)\right] \tag{2-20}$$

The correlation coefficient of two random variables is obtained by normalizing the covariance by the respective standard deviations:

$$\rho_{X,Y} = \frac{\mathrm{Cov}[X,Y]}{\sigma_X \sigma_Y} \tag{2-21}$$

2.2.2 Random Vectors

A real random vector $\boldsymbol{X}$ on the probability space $(\Omega, \mathfrak{F}, P)$, is a mapping $\boldsymbol{X} : \Omega \mapsto \mathcal{D}_{\boldsymbol{X}} \subset \mathbb{R}^n$, where n is the size of vector ($n > 1$). Then, $\boldsymbol{X}$ is a $\mathbb{R}^n$-valued random vector whose components are random variables, $\boldsymbol{X} \equiv \{X_1, \ldots, X_n\}$ and their realizations are denoted by $\boldsymbol{x} = \{x_1, \ldots, x_n\}$.

The joint distribution function of $\boldsymbol{X}$ is the direct extension of the definition of the random variable distribution function:

$$F_{\boldsymbol{X}}(\boldsymbol{x}) = P\left(\bigcap_{i=1}^{n} \{X_i \leq x_i\}\right), \quad \boldsymbol{x} = \{x_1, \ldots, x_n\} \in \mathbb{R}^n \tag{2-22}$$

The following properties of the joint distribution function of $\boldsymbol{x}$ are:

$$\begin{aligned} \lim_{x_i \to -\infty} F_{\boldsymbol{X}}(\boldsymbol{x}) &= 0, \qquad i = 1, \ldots, n; \\ x_i \;&\mapsto\; F_{\boldsymbol{X}}(\boldsymbol{x}), \quad \text{is increasing}, \quad i = 1, \ldots, n; \\ x_i \;&\mapsto\; F_{\boldsymbol{X}}(\boldsymbol{x}), \quad \text{is rigth-continuous}, \quad i = 1, \ldots, n; \end{aligned}$$

In addition,

$$\lim_{x_i \to +\infty} F_{\boldsymbol{X}}(\boldsymbol{x}) = F_{\boldsymbol{X}_{|i}}(\boldsymbol{x}_{|i}), \qquad i = 1, \ldots, n;$$

is the joint distribution of the $\mathbb{R}^{n-1}$-valued random vector

$$\boldsymbol{X}_{|i} = \{X_1, \ldots, X_{i-1}, X_{i+1}, \ldots, X_n\}$$

The probabilistic description of $\boldsymbol{X}$ is contained in its joint PDF denoted by $f_{\boldsymbol{X}}$, thus

$$f_{\boldsymbol{X}}(\boldsymbol{x}) = \frac{\partial^n F_{\boldsymbol{X}}(\boldsymbol{x})}{\partial x_1 \cdots x_n} \tag{2-23}$$

The marginalization is a reduction for obtaining derive expression for the joint density or distribution of a subset of coordinates $\boldsymbol{X}$. For instance, the joint distribution of $\boldsymbol{X}_{|i}$ is

$$F_{\boldsymbol{X}_{|i}}(\boldsymbol{x}_{|i}) = F_{\boldsymbol{X}}\left(x_1, \ldots, x_{i-1}, \infty, x_{i+1}, \ldots, x_i\right), \tag{2-24}$$

whereas

$$f_{\boldsymbol{X}_{|i}}(\boldsymbol{x}_{|i}) = \int_{-\infty}^{+\infty} f_{\boldsymbol{X}}\left(x_1, \ldots, x_i\right) dx_i \tag{2-25}$$

The marginal distribution of a given component X_i is

$$F_{X_{i(x_i)}} = F_{\boldsymbol{X}}(\infty, \ldots, \infty, x_i, \infty, \ldots, \infty) \tag{2-26}$$

and the marginal density of X_i is obtained by integrating the joint PDF over all the remaining components

$$f_{X_i}(x_i) = \int_{\mathcal{D}_{\boldsymbol{X}_{|i}}} f_{\boldsymbol{X}}(\boldsymbol{x}) d\boldsymbol{x}_{|i} \tag{2-27}$$

where $\mathcal{D}_{\boldsymbol{X}_{|i}}$ is the subset of $\mathcal{D}_{\boldsymbol{X}}$ defined by $\{\boldsymbol{x} \in \mathcal{D}_{\boldsymbol{X}}, x_i \text{ fixed}\}$.

Similarly, the joint distribution of two component (X_i, X_j) is given by:

$$f_{X_i,X_j}(x_i, x_j) = \int_{\mathcal{D}_{\boldsymbol{X}_{|(i,j)}}} f_{\boldsymbol{X}}(\boldsymbol{x}) d\boldsymbol{x}_{|ij} \tag{2-28}$$

The expextion of random vector $\boldsymbol{X}$, is the vector containing the expectation of each component:

$$\mu_{\boldsymbol{X}} = \{\mu_{X_1}, \ldots, \mu_{X_n}\} \tag{2-29}$$

The covariance matrix of $\boldsymbol{X}$ is a $n \times n$ square symetric matrix $\mathbf{C}$

$$\mathbf{C}_{i,j} = \mathrm{Cov}\left[X_i, X_j\right] \tag{2-30}$$

ad the correlation matrix

$$\mathbf{R}_{i,j} = \rho_{X_i,X_j} \tag{2-31}$$

Let $\boldsymbol{\Lambda}$ be the diagonal matrix containing the standard deviation of each component of $\boldsymbol{X}$. Then, the following relation is satisfied

$$\mathbf{C} = \boldsymbol{\Lambda}\mathbf{R}\boldsymbol{\Lambda} \tag{2-32}$$

2.2.3 Random Fields

Consider a function $X(t, \omega) : T \times \Omega \mapsto \mathbb{R}^d$ with two arguments $t \in T \subset \mathbb{R}$ and $\omega \in \Omega$, being T a countable or uncountable index set. Generally, a $\mathbb{R}^d$-valued stochastic process is a family (or an ensemble) of functions X. Each function $X(\cdot, \omega) : t \in T \mapsto \mathbb{R}^d$ for a specified outcome $\omega \in \Omega$ is called a sample path or straightforwardly a realization of a deterministic function $X(\cdot, \omega)$; whereas, $X(t, \cdot) : \omega \in \Omega \mapsto \mathbb{R}^d$ is a $\mathbb{R}^d$-valued random variable on the probability space $(\Omega, \Im, P)$ [84].

If we consider $\mathbb{R}^d$-valued random variables indexed by a spatial coordinate, i.e., $\mathbf{x} \in \mathcal{D} \subset \mathbb{R}^n$, $n \geq 1$, then, the function $H : \mathcal{D} \times \Omega \mapsto \mathbb{R}^d$, is called $\mathbb{R}^d$-valued random field.

We define $L_2(\Omega, P)$ as the Hilbert space of the second-order random variable (finite second moment $\mathbb{E}\left[X^2\right] < \infty$) defined on probability space $(\Omega, \Im, P)$ equipped with the inner product $\langle \cdot, \cdot \rangle$ and associated norm $\|\cdot\|_{L_2(\Omega,P)}$,

where the expectation operation permits to define an inner product and the related norm as follows:

$$\begin{aligned} \langle X,Y\rangle &= \mathbb{E}\left[XY\right] \\ \|X\| &= \sqrt{\mathbb{E}\left[X^2\right]} \end{aligned} \tag{2-33}$$

We will focus on a specific class of $\mathbb{R}^d$-valued random field that can be defined as a curve belonging to the space $L_2(\Omega, P)$. It implies that for a fixed-probability random field, the output $H(\mathbf{x}_0, \omega)$ is a trajectory, i.e., a curve, whereas, for a fixed-space random field, $H(\mathbf{x}, \omega_0)$ transforms into a $\mathbb{R}^d$-valued random variable.

Certain properties of random fields are characterized by its statistical moments using similar formulas in accordance with the definitions of the moments of the random variable. Thus, the expectation function is given by the first moment

$$\mu_H(\mathbf{x}) = \mathbb{E}\left[H(\mathbf{x}, \omega)\right], \tag{2-34}$$

and the variance function by the second moment

$$\sigma_H^2(\mathbf{x}) = \mathbb{E}\left[\left(H(\mathbf{x}, \omega) - \mu_H(\mathbf{x})\right)^2\right], \tag{2-35}$$

The autocovariance is a function that yields the covariance of the field with itself at pair points and is expressed by

$$C_{HH}(\mathbf{x}_1, \mathbf{x}_2) = \mathbb{E}\left[\left(H(\mathbf{x}_1, \omega) - \mu_H(\mathbf{x}_1)\right)\left(H(\mathbf{x}_2, \omega) - \mu_H(\mathbf{x}_2)\right)\right], \tag{2-36}$$

The autocorrelation function is expressed by

$$R_{HH}(\mathbf{x}_1, \mathbf{x}_2) = \mathbb{E}\left[H(\mathbf{x}_1, \omega) H(\mathbf{x}_2, \omega)\right], \tag{2-37}$$

and the correlation coefficient function expressed as

$$\rho_{HH}(\mathbf{x}_1, \mathbf{x}_2) = C(\mathbf{x}_1, \omega)/\sigma_H(\mathbf{x}_1)\sigma_H(\mathbf{x}_2), \tag{2-38}$$

Furthermore, a random field $H : \mathcal{D} \times \Omega \mapsto \mathbb{R}^d$ is called Homogeneous in the strict sense (or, for $n = 1$ called Stationary) if all its probability distribution functions are invariant under arbitrary translations of index $\mathbf{x}$ (but not rotated) in the parameter space, i.e.,

$$F_H\left(h_1, \cdots, h_n; \mathbf{x}_1, \cdots, \mathbf{x}_n\right) = F_H\left(h_1, \cdots, h_n; \mathbf{x}_1 + \tau, \cdots, \mathbf{x}_n + \tau\right) \tag{2-39}$$

This implies that all the probabilities depend only on the relative location of the points $\mathbf{x}$ at which the samples are extracted, and not on the absolute one. Accordingly, all the moments of a homogeneous random field are independent of $\mathbf{x}$.

A random field $H : \mathcal{D} \times \Omega \mapsto \mathbb{R}^d$ is called homogeneous in the wide sense if its expectation functions are invariant, i.e., $\mu\left(\mathbf{x}\right)$ is constant and

the autocorrelation function $R_{HH}(\mathbf{x}_1, \mathbf{x}_2)$, or equivalently the autocovariance $C_{HH}(\mathbf{x}_1, \mathbf{x}_2)$, depends only on the distance $\mid \mathbf{x}_1 - \mathbf{x}_2 \mid$,i.e.,

$$R_{HH}(\mathbf{x}_1, \mathbf{x}_2) = R_{HH}(\mid \mathbf{x}_1 - \mathbf{x}_2 \mid) \tag{2-40}$$

This type of a field is a special case of homogeneous fields, which exhibits certain symmetry in the domain. Otherwise, it is called a non-homogeneous random field.

A random field is said to be ergodic if its statistical properties can be deduced by considering a sample path or a realization over all $\mathbf{x}$ or by considering the whole ensemble at a specific $\mathbf{x}$. This is not feasible for a non-ergodic field. Moreover, all ergodic random fields are homogeneous, although not all homogeneous fields are ergodic [85].

Therefore, a random field can be regarded as a generalization of a stochastic process when indexed by a spatial variable, i.e., one- or multi-dimensional according to the dimension of $\mathbf{x}$; moreover, if $H(\mathbf{x}, \cdot)$. is a random variable or random vector for a point fixed $\mathbf{x}$, the random field is called univariate or multivariate, respectively.

There is a large class of random fields that can be constructed by imposing homogeneity (strictly or in the wide sense) condition. Examples include Gaussian, Poisson, and Brownian. However, the last two is not the focus of this survey.

Gaussian fields are an important family of random fields, exhibiting the property wherein all its probability density functions are multivariate normal distributions. These fields are completely characterized only by second-order statistics, i.e., by their expectation $\mu_H(\vec{x})$, and variance $\sigma_H^2(\vec{x})$, and autocovariance functions; they are stable under linear combination, and their marginal and conditional distribution are conveniently computable [86].

Homogeneous non-Gaussian random fields are more challenging to be characterized, i.e., they are not uniquely determined by their first two moments; we generally have only a partial second-order description. The unavailability of significant experimental data about the probabilistic characteristic of the random field has increased the consideration of the Gaussian assumption [87].

2.2.4 Translation Random Field

Grigoriu proposed a technique for simulating homogeneous (non-Gaussian) fields according to an autocorrelation function called Grigoriu's

translation process theory [88]. This framework, which exhibits mathematical rigorousness, is wide applicable in engineering and applied science.

Let $H(\mathbf{x},\omega)$ be a $\mathbb{R}^d$-valued homogeneous Gaussian field with zero-expectation, unit-variance, and autocovariance function C_{HH}. The translation of fields are memoryless nonlinear transformation of the form $Z(\mathbf{x},\omega) = g\left[H(\mathbf{x},\omega)\right]$, where, $Z(\mathbf{x},\omega)$ is a homogeneous non-Gaussian field in the strict sense with finite variance, and $g(\cdot)$ is a real-valued differentiable function defined on real line that increases monotonically, i.e.,

$$g(H_m) < g(H_n) \quad \forall \quad H_m < H_n, \tag{2-41}$$

Let $g = F_Z^{-1} \circ \Phi$; then, $Z(\mathbf{x},\omega)$ is obtained through the following non-linear transformation

$$Z(\mathbf{x},\omega) = F_Z^{-1} \circ \Phi\left(H(\mathbf{x},\omega)\right), \tag{2-42}$$

where $F_Z^{-1}(\cdot)$ denotes the inverse of the prescribed marginal CDF of the non-Gaussian field $Z(\mathbf{x},\omega)$ and Φ is the CDF of the standard Gaussian.

The transformation of Eq.(2-42) exactly matches the target marginal distribution of $Z(\mathbf{x},\omega)$ as

$$\begin{aligned} P\left(Z(\mathbf{x},\omega) \leq z\right) &= P\left(F_Z^{-1} \circ \Phi\left(H(\mathbf{x},\omega)\right) \leq z\right) \\ &= P\left(H(\mathbf{x},\omega) \leq \Phi^{-1}\left(F_Z\right)\right) \\ &= F_Z. \end{aligned} \tag{2-43}$$

Therefore, $Z(\mathbf{x},\omega)$ is referred to as a translation field, and its probability law is completely defined by the covariance function of $H(\mathbf{x},\omega)$ and an arbitrary CDF F_Z .

The expectation and variance of the field are

$$\mu_Z(\mathbf{x}) = \mathbb{E}\left[g\left(H(\mathbf{x}_1,\omega)\right)\right] = \int_{-\infty}^{\infty} g(h)\phi(h)dh, \tag{2-44}$$

and

$$\sigma_Z^2(\mathbf{x}) = \mathbb{E}\left[\left(g\left(H(\mathbf{x}_1,\omega)\right) - \mu_Z\right)^2\right] = \int_{-\infty}^{\infty} \left[g(h) - \mu_Z\right]^2 \phi(h)dh, \tag{2-45}$$

respectively, where, $\phi(h) = (2\pi)^{-1/2}\exp(-1/2h^2)$ is the standard Gaussian density function. The autocorrelation function is given by

$$\begin{aligned} R_{ZZ}(\mathbf{x}_1,\mathbf{x}_2) = \int_{-\infty}^{\infty}\int_{-\infty}^{\infty} & F_Z^{-1} \circ \Phi\left(H(\mathbf{x}_1,\omega)\right) \cdot F_Z^{-1}\Phi\left(H(\mathbf{x}_2,\omega)\right) \\ & \times\phi\left(\mathbf{x}_1,\mathbf{x}_2;\rho_{HH}\left(\mathbf{x}_1,\mathbf{x}_2\right)\right) d\mathbf{x}_1 d\mathbf{x}_2 \end{aligned} \tag{2-46}$$

where,

$$\phi\left(\mathbf{x}_1,\mathbf{x}_2;\rho_{HH}\left(\mathbf{x}_1,\mathbf{x}_2\right)\right) = \left[2\pi(1-\rho_{HH})\right]^{-1/2}\exp\left(\frac{-\left(\mathbf{x}_1^2 + \mathbf{x}_2^2 - \mathbf{x}_1\mathbf{x}_2\rho_{HH}\right)}{2\pi\left(1-\rho_{HH}\right)^2}\right)$$

is the density of the bivariate standard Gaussian [89].

In general, the autocovariance function of $Z(\mathbf{x},\omega)$ is not equal to C_{HH} because the autocovariance function of $H(\mathbf{x},\omega)$ is not preserved by the transformation defined by Eq.(2-42). Numerous cases are available where marginal changes to the covariance function can be omitted; e.g., when F_Z is the CDF of a symmetric and standard beta distribution. However, another case, the covariance functions of $H(\mathbf{x},\omega)$ and $Z(\mathbf{x},\omega)$, is very different and cannot be omitted.

Let $\tilde{Z}(\mathbf{x},\omega)$ be a normalized version of $Z(\mathbf{x},\omega)$ such that

$$\tilde{Z}(\mathbf{x},\omega) = \frac{Z(\mathbf{x},\omega) - \mu_Z}{\sigma_Z} \tag{2-47}$$

Then, the autocorrelation function of $\tilde{Z}(\mathbf{x},\omega)$ is denoted as

$$R_{\tilde{Z}\tilde{Z}}(\mathbf{x}_1,\mathbf{x}_2) = \frac{R_{ZZ}(\mathbf{x}_1,\mathbf{x}_2) - \mu_Y^2}{\sigma_Z^2} \tag{2-48}$$

Note, that the autocovariance function of $H(\mathbf{x},\omega)$ satisfies $\mid R_{ZZ} \mid \leq 1$, and according to Grigoriu [89], for $R_{HH} = 0$ and $R_{HH} = 1$ imply $R_{\tilde{Z}\tilde{Z}} = 0$ and $R_{\tilde{Z}\tilde{Z}} = 1$, respectively. In addition, $R_{\tilde{Z}\tilde{Z}}$ and R_{HH} satisfy the inequality $\mid R_{\tilde{Z}\tilde{Z}} \mid \leq \mid R_{HH} \mid \forall \mid \mathbf{x}_1 - \mathbf{x}_2 \mid \in \mathcal{D}$, and $R_{\tilde{Z}\tilde{Z}}$ is bounded, i.e., $-1 \leq R^*_{\tilde{Z}\tilde{Z}} \leq R_{\tilde{Z}\tilde{Z}} \leq 1$, where

$$R^*_{\tilde{Z}\tilde{Z}} = \frac{\mathbb{E}\left[g\left(H(\mathbf{x},\omega)\right) g\left(-H(\mathbf{x},\omega)\right)\right] - \mu_Z^2}{\sigma_Z^2} \tag{2-49}$$

The value of $R^*_{\tilde{Z}\tilde{Z}}$ corresponding to $R_{HH} = -1$ can be attained if, for example, g is an odd function (odd memoryless transformation), in which case $\mu_Z = 0$ and $\mathbb{E}\left[g\left(H(\mathbf{x}_1,\omega)\right) g\left(-H(\mathbf{x}_1,\omega)\right)\right] = -\sigma_Z^2$.

For the pair $\{F_Z, R_{\tilde{Z}\tilde{Z}}\}$, with $R_{\tilde{Z}\tilde{Z}}$ assuming values outside the range $\left[R^*_{\tilde{Z}\tilde{Z}}, 1\right]$, the translation functions do not exist. The requirement of $R_{\tilde{Z}\tilde{Z}} \in \left[R^*_{\tilde{Z}\tilde{Z}}, 1\right]$ is necessary but not sufficient for the existence of translation functions [90]. The existence of translation functions also requires that the image R_{HH} of R_{ZZ} in the Gaussian space must be positive definite.

The relationship between R_{HH} and R_{ZZ}, i.e., $R_{HH} = \frac{6}{\pi}\sin^{-1}\left(\frac{R_{HH}}{2}\right)$, is determined for a marginal uniform distribution of non-Gaussian field with parameters $[-1, 1]$ [91, 92]. Figure 2.9. reveals a low distortion of the autocovariance function of $Z(\mathbf{x},\omega)$ owing to the transformation. Moreover, note that for all the points, the values of R_{ZZ} within the interval $[-1, 1]$ match one-to-one with the R_{HH} values.

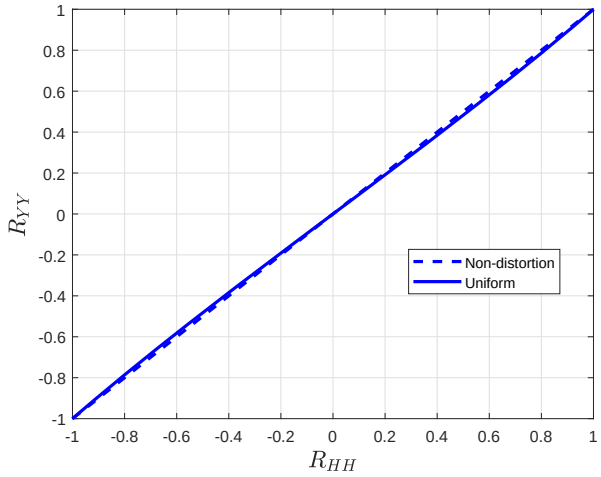

Figure 2.9: Relationship between autocreation function of non-Gaussian and Gaussian fields for a marginal uniform distribution.

2.2.5 Random Field Discretization

In the previous section, we described certain properties and types of random fields. It is necessary to represent them according to the probability distribution to model uncertain system properties. The procedure to represent a continuum-parameter random field in terms of a finite set of random variables is known as random field representation. Discretization methods can be divided into two main types: methods that seek the representation of Gaussian fields and those that seek the representation of non-Gaussian fields.

There are several methods for the discretization of Gaussian fields, which are grouped into three main categories (see e.g. [93]): point discretization, average discretization, and series expansion. In this work, we will focus on the series expansion method, which employs a finite series expansion of random variables and deterministic spatial functions to represent the field in an exact manner. For practical implementation, the approximation is obtained as a truncation of the series (finite number of terms).

The group of series expansion methods includes the orthogonal series expansion [94], expansion optimal linear estimator (EOLE) [95], perturbation methods [96], and Karhunen-Loève (K-L) expansion [97, 98], whose effectiveness in reducing dimensionality of the random field representation is highly effective. Therefore, the K-L expansion will be amply explained in the next chapter.

2.3 Uncertainties in structural analysis

Structural analysis involves the computation of the response of the structure to the design load and imposed deformations that it will be required to resist during its lifetime. In order to develop this analysis is necessary the definitions of basic input variables (loading, material properties, geometry), response variables (deformation, strain, stresser) and the relationships between these quantities. For this razon, the improving mathematical models, constitutive laws and the evolution of computational tools continues to be the attention of several researches and with the development of processor faster and powerful, the numerical constraint is no longer a problem.

However, this constitutive models and the constant enhancement of the computational tools does not solve the problem of the uncertainties associated to the parameters. As these uncertainties produce variation over space and time domains, the response of the struture are accordingly affected by theses parameters.

In order to work around this problem, it is traditionally used an average characteristics, i.e., a single design point, considering it sufficient to represent the response and at best lead to rough representations of the reality. Figure 2.10, show the response of a simulation with respect to single design point which becomes it inadequate and unrealistic when characterizing structures under varying loads or material properties. For instance, we cannot cover all types of response with a single simulation, would need more one.

Therefore, the modeling of uncertainties associated to the parameters for representing the randomness and spatial variability become extremely important and it is one of the tasks of stochastic or probabilistic model to obtain better realistic simulation.

Probabilistic models are used for representing different types of uncertainties in mechanical structures. Basic structural parameters as for example magnitude and direction of concentrated load, lengths, stiffness of joint and supports, etc. are assumed to be discrete, allowing them to be represented as radom variables. We refer to as discrete quantities when they are concentrated at discrete points in space.

However, there are others parameters that are not concentrated at a point, they are distribuited in the space. Some examples are distributed loads, material properties (Young's nodulus, strength) and geometric properties (width, thickness) they vary over the length, area or volume and cannot be represented as random variables. Figure 2.11, show uma simple beam where its Young's modulus fluctuates over the length (blue line) and also when the

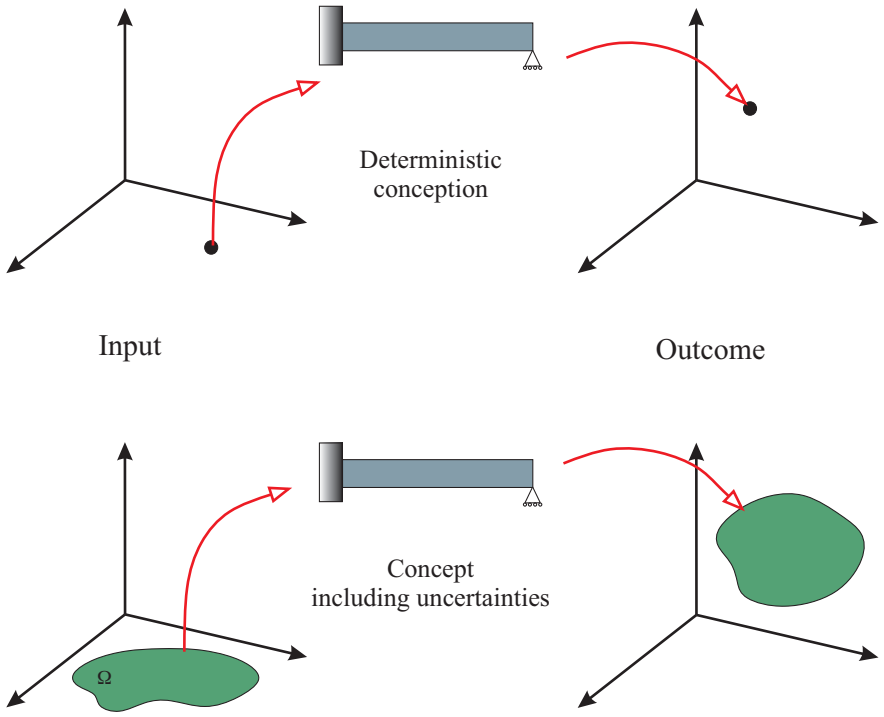

Figure 2.10: Deterministic Conception versus Concept including Uncertainties.

variation is only across the sample (green line). Then, the mathematical model of the variation over the length, parameterized by the correlation between different locations, can be characterized by means of random process. Thus, analysis of the random process is a realistic approach that can produce a whole design space instead of just a one-point result.

For the sake of simplicity, sometime the variability of Young's modulus is considered as a random variable, i.e., it would be seen as several beams but if the Young's modulus fluctuates over the length, it causes randomness in the strcutural response. Then, for representing the uncertainties in mechanical structures, we must know the nature of its random variability and classify them as well variation across samples or variation over space. If the Young's modulus consider also fluctuates over the thickness and height of beam, then it will be a multidimensional spatial and not only along one-dimensional, then in this case its characterization will be by means of a random field.

Thus, this whole procedure will allow the structural designer to select materials and member sizes that provide the structure with adequate strength and ensure that the chances of collapse are acceptably small.

2.4 General Framework for UQ

In this thesis, we follow a general framework for UQ presented and formalized in the past few years at the R&D Division of EDF ([99]; [100];[3])

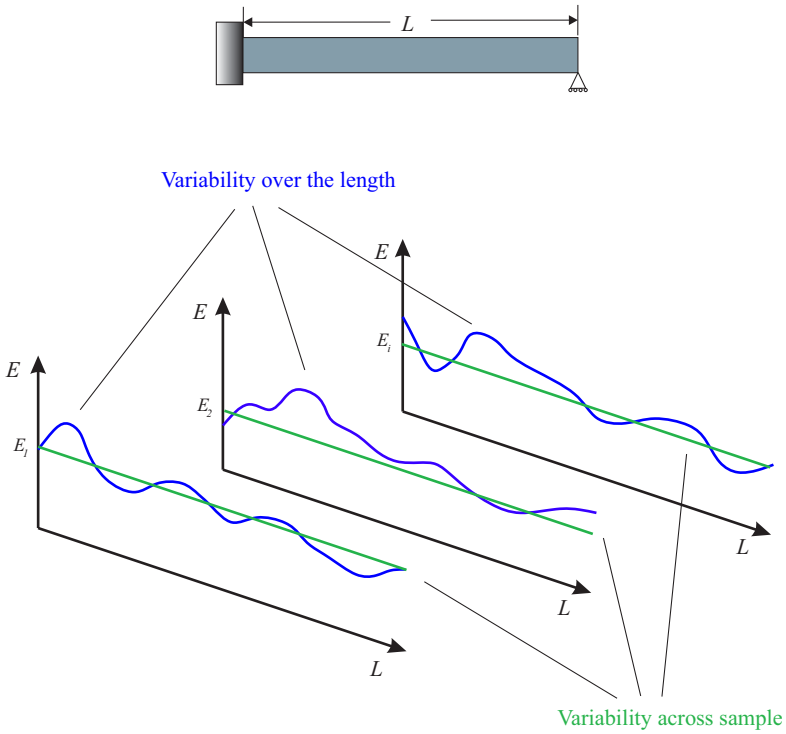

Figure 2.11: Simple beam where the Young's modulus E, fluctuates over the length.

together with various companies and academic research groups. This general framework is sketched and summarized in Figure 2.12.

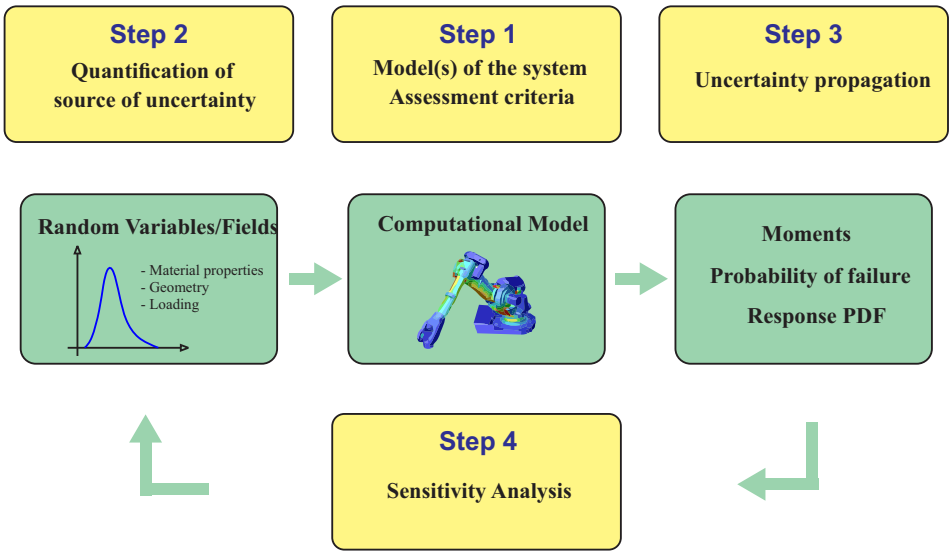

Figure 2.12: General sketch for probabilistic uncertainty analysis (Adapted from [3])

In the above figure, four steps are described as follow:

- Step 1: consists in defining the model as well as associated criteria (e.g. safety criteria) that should be used in order to assess the system under

consideration. This step gathers all the ingredients used for a classical deterministic analysis of the physical system to be analyzed.

- Step 2: This step consists in identifying and characterizing the uncertain input parameters and modelling them by random variables or random fields.
- Step 3: consists in propagating the uncertainty in the input parameters through the deterministic model, i.e. characterizing the statistical properties of the output quantities of interest.
- Step 4: consists in hierarchizing the input parameters according to their respective impact on the output variability. This study, known as sensitivity analysis, is carried out by post-processing the results obtained at the previous step.

The present thesis is focused in this four step to quantify uncertainties in mechanical structures.

2.4.1 Probabilistic Models

Let $\mathcal{M} : \mathbb{R}^n \mapsto \mathbb{R}$, $n \geq 1$ be the mathematical model of mechanical system, which can be analytical o more generally algorithmic (e.g. a finite element model), which describe a deterministic mapping, i.e.,

$$\mathcal{M} : \mathbf{x} \in \mathcal{D} \subset \mathbb{R}^n \mapsto y = \mathcal{M}(\mathbf{x}) \in \mathbb{R} \tag{2-50}$$

where, $\mathbf{x} = \{x_1, \ldots, x_n\}$ is the vector of input parameters and y is the quantity of interest (QoI) in the analysis called the model response.

The function $\mathcal{M}$ has generally no explicit expression and can be known only by pointwise evaluations: $y^{(i)} = \mathcal{M}(\mathbf{x^{(i)}})$ for each input vector $\mathbf{x^{(i)}}$ (e.g. each run of computer program). In this sense, $\mathcal{M}$ can be referred to as a black-box function that takes input values and return a result.

In the fields of mechanical structure, the vector of input parameters $\mathbf{x}$ typically may represent loading, material properties and geometrical properties. In contrast, the quantity of interest y migth for instance represent the displacements, strains or stresses at the nodes of a finite element mesh, etc.

In this thesis only models that have a single (scalar) quantity of interest are studied and used in the application of the proposed algorithm.

2.4.2 Uncertainty propagation

Consider that the model $\mathbf{x} \mapsto y = \mathcal{M}(\mathbf{x})$ of a mechanical physic include uncertainties in the input parameters and their probabilistic description is

modelled in term of a random vector $\boldsymbol{X} = [X_1, \ldots, X_n]$ with prescribed joint probability density function $f_{\boldsymbol{X}}$. Hence, the model response (quantity of interest) becomes a random variable defined by:

$$Y = \mathcal{M}(\boldsymbol{X}) \tag{2-51}$$

When the input parameters are assumed statistically independent, this joint distribution is equivalently defined by the set of marginal distribution of all input parameters, i.e., $\{f_{X_i}, i = 1, \ldots, n\}$. Otherwise, if dependence exists, the copula formalism may be used. Figure 2.13, show the uncertainty propagations through of a generic computational model.

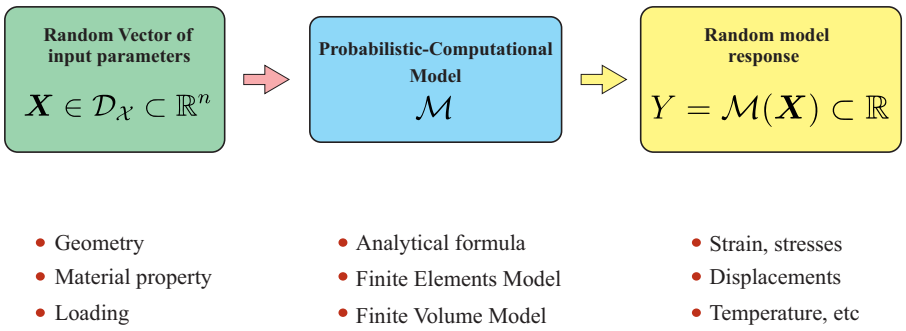

Figure 2.13: General sketch for uncertainty propagation (Adapted from [4])

The uncertainty propagation study the randomness of model response Y, through of its joint probabilistic density function $f_Y(y)$. Note, that this function is not always directly computable except in some simples cases.

The uncertainty propagation step is needed to transform the measure of uncertainty on the inputs onto a measure of uncertainty on the outputs of the pre-existing model. Depending on the information obtained in the model response, its analysis can be treated through three types according [3] (see Figure 2.14).

From Figure 2.14, the three types of model response are described as follow:

- Second moment methods: Compute and analyze the mean value μ_Y and standard deviation σ_Y of model response.
- Structural reliability methods: Investigate the tails response probability density function by computing the probability that the response exceeds a given threshold (probability of failure).
- Spectral methods: Compute and analyze the complete probability density function of the response in an intrinsic way by using suitable tools of functional analysis.

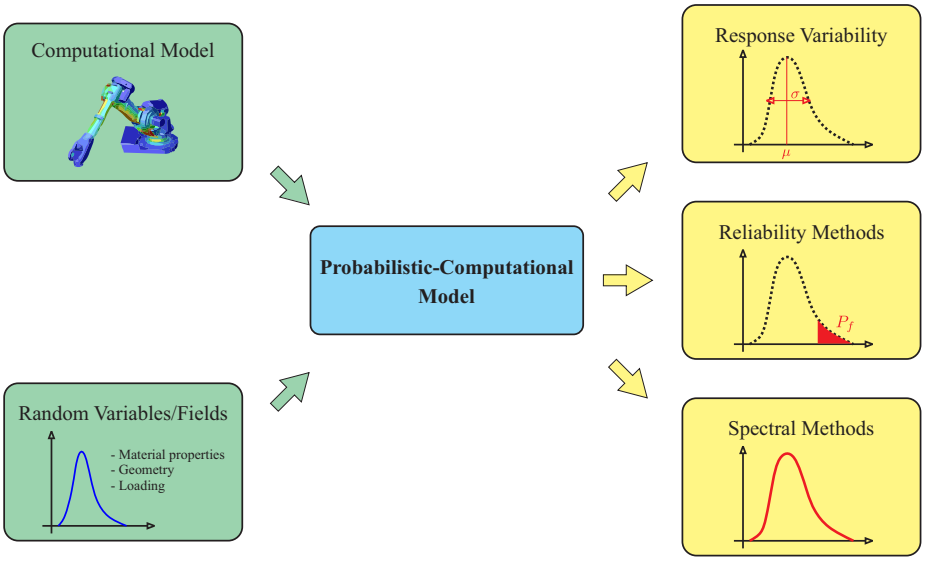

Figure 2.14: Classification of the types of model response of uncertainty propagation (Adapted from [3])

The equation of mathematical model used for representing the mechanical system can be used of two types Non-intrusive and Intrusive approach. (see Figure 2.15)

Non-Intrusive method

The non-intrusive method requires no modification in the deterministic model and only require (multiple) solutions of the original model which can be treated as a black box. The main advantages of this method is the simplicity for obtaining the response model through of repeated simulations using deterministic solver on limited number of samples and the embarrassingly parallel computing possibilities. In addition, comercial softwares can used to propagate such uncertainties due that only we need the response model.

Intrusive Models method

The intrusive method require the formulation and solution of a stochastic version of the original model, i.e., the substitution of all uncertain variables in the governing equations. The main disavantages of this method may be the dificult for formultating the equation and the high computational cost for obtaining the response of quantity of interest for many problems. Besides, the sources of most commercial codes are not accessible, and thus, it is not feasible to use.

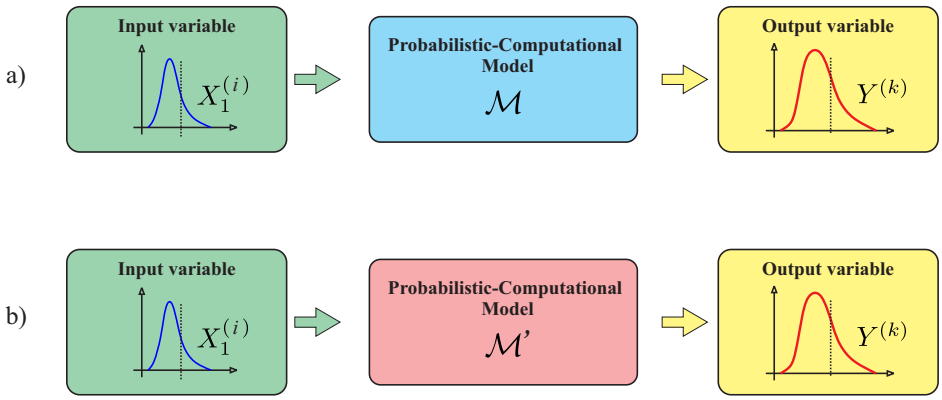

Figure 2.15: a) Non-Intrusive and b) Intrusive models

2.5 Sampling Methods

Sampling methods are advantageous because can be used directly through of experiments to obtain a probabilistic information of model response whose equations cannot be solved easily by known procedures. Sampling methods have been intensively used in uncertainty analysis due that is straightforward to apply and convergence rate is independent of number of parameters.

2.5.1 Monte Carlo Simulation (MCS)

The Monte Carlo simulation is known as a simples random sampling method to solve problems that might be deterministic in principle [101]. This method is a powerful computerized mathematical tool and consists in making realizations based on pseudo-randomly generated sampling sets for determining the approximate probability of the outcome of a specific event.

Monte Carlo simulation can be used in order to estimate the mean value μ_Y and the standard deviation σ_Y^2 of a response quantity Y. Then, a sample set of independent realizations $\{\boldsymbol{x}^{(1)}, \ldots, \boldsymbol{x}^{(N)}\}$ of the input random vector $\boldsymbol{X}$ is generated from the joint probability density function $f_{\boldsymbol{X}}$. To each of these realization corresponds a unique solution of the model $y^{(k)} = \mathcal{M}(\boldsymbol{x}^{(k)})$

Then, the estimators of the second order moments of Y are as follow:

$$\hat{\mu}_Y = \frac{1}{N}\sum_{k=1}^{n} \mathcal{M}(\boldsymbol{x}^{(k)}) \tag{2-52}$$

$$\hat{\sigma}_Y^2 = \frac{1}{N-1}\sum_{k=1}^{n} \left(\mathcal{M}(\boldsymbol{x}^{(k)}) - \hat{\mu}_Y\right)^2 \tag{2-53}$$

One of the advantages of Monte Carlo Simulation is the minimum effort

developed to propagate the uncertanties through of invidual deterministic model realization, i.e., it is only sufficient to resolve the deterministic model (applicable to nonlinear models).

However, the rate of convergence of Monte Carlo Simulation is the main limitation because depende on of number N of realizations, i.e., the convergence of variance estimates behaves as $\mathcal{O}(N^{-1/2})$ which is relatively low compared to the convergence of other methods, e.g., spectral methods. Thus many model evaluations are usually required in order to reach a good accuracy requiring a large computational effort.

High order moments can also be computed through the Monte Carlo Simulation, but their convergence is slower than the mean and standard deviation. Several sampling methods have been proposed in order to accelerate the convergence of MCS, but these are generally insufficient to provide accurate characterization of uncertainties systems.

2.5.2 Latin Hypercube Sampling (LHS)

Latin Hypercube Sampling was first proposed by McKay [102] and is one the widely used random sampling method for Monte Carlo-based uncertainty quantification and reliability analysis.

In this method, the points are randomly generated in a square grid across the design space, but no two points share the same value. (i.e., so no point shares a row or a column of the grid with any other point). A Latin hypercube is the generalisation of this concept to an arbritray number of dimension.

LHS operates by dividing the distribution function F_{X_i} of each variable X_i, $i = 1, \ldots, n$, into N non-overlapping intervals of equal probability $1/N$.

One value from each interval is selected at random according to the probability density in the interval. The N values obtained for X_1 are randomly paired with N other values of X_2. These N pairs are combined in a random manner with the N values of X_3 to form N triplets, and so on, until a set of N n-tuples is formed. This set of n-tuples is a LHS. Figure 2.16, illustrates an LHS in a two-dimensional space with sample size $N = 5$.

LHS represents a multivariate sampling method that guarantees non-overlapping designs. Several examples show that more than 50% of the computer effort is saved through this method. Figure 2.17, show the LHS are generated in such a way that each sample is randomly generated, but no two points share input parameters of the same value as its Monte Carlo sampling counterpart.

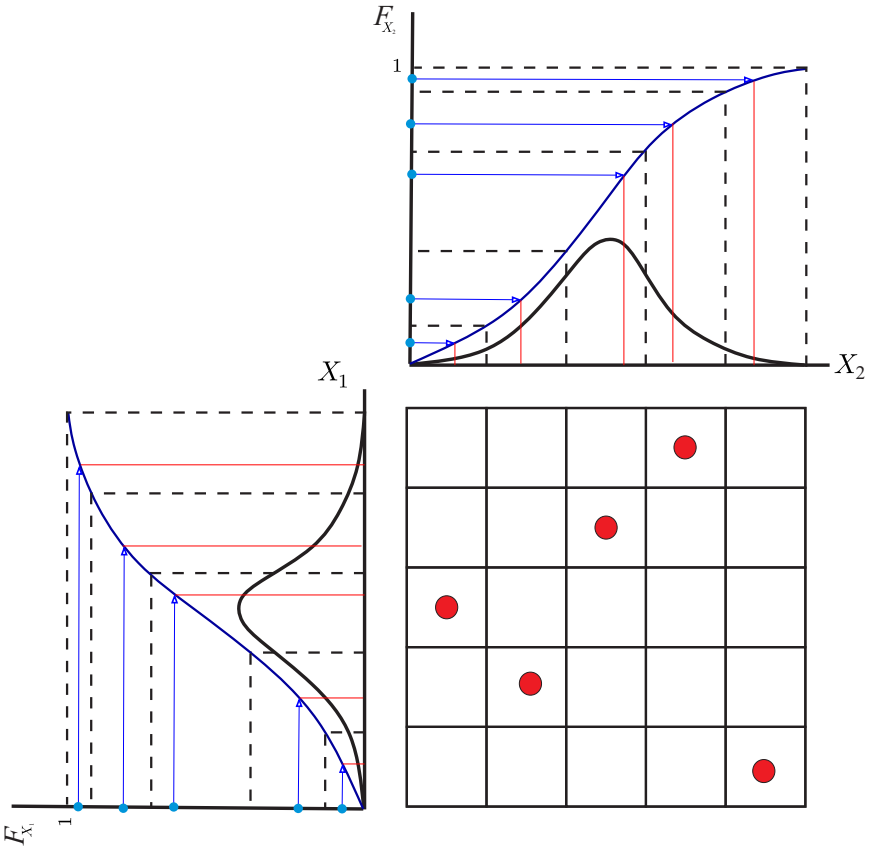

Figure 2.16: Basic Concept of LHS: Two Variables and Five Realizations

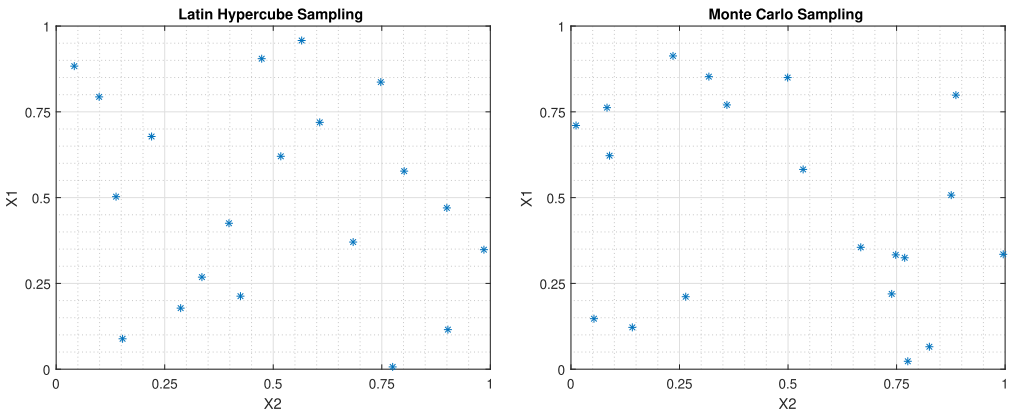

Figure 2.17: Monte Carlo Simulation with LHS and without LHS

Therefore, the LHS reduce the number of samples required for a given accuracy, but the number of analyses still remains too high for practical use, particularly in the case of computationally demanding analysis codes

3
Stochastic Spectral Methods

This chapter explores two approaches to forming stochastic expansions: the Polynomial Chaos expansion to propagate uncertainties, which employs bases of multivariate orthogonal polynomials, and the Karhunen-Loeve expansion, which provides an representation of random field in term of countable uncorrelated random variables. Also, it present several non-intrusives methodos for computing the coefficients of polnomial chaos. Both approaches capture the functional relationship between a set of output response metrics and a set of input random variables.

3.1
Spectral Methods

Let $\boldsymbol{\xi} = \{\xi_i(\omega)\}_{i=1}^{N}$ be a set of N independent and identically distributed random variables for ω. We denote $L_2(\Omega, P)$ the space of second-order random variable defined on $(\Omega, \mathfrak{F}, P)$ with the inner product $\langle \cdot, \cdot \rangle$ and associated norm $\| \cdot \|_{L_2(\Omega,P)}$.

Let $X(w)$ be a second-order random variable (finite second moment) belonging to the space:

$$L_2(\Omega, P) = \left\{ X : \Omega \to \mathbb{R} \;\middle|\; \mathbb{E}[X^2] \equiv \int_{\Omega} X^2 dP(w) < +\infty \right\}, \tag{3-1}$$

where $\mathbb{E}[\cdot]$ is the expected operator. This space is an Hilbert Space with respect to the inner product between two random variables $X(w)$ and $Y(w)$ belonging to $L_2(\Omega, P)$:

$$\langle X(\omega), Y(\omega) \rangle \equiv \mathbb{E}[X\omega)Y(\omega)] \equiv \int_{\Omega} X(\omega)Y(\omega)dP(\omega) \tag{3-2}$$

This inner product induces the norm:

$$\|X\|^2_{L_2(\Omega,P)} = \langle X^2 \rangle \tag{3-3}$$

Generally, spectral representation of random functionals aim at finding a series expansion of the form:

$$X(\omega) = \sum_{j=0}^{\infty} u_j \Psi_j(\boldsymbol{\xi}(w)) \tag{3-4}$$

where $\{\Psi_j(\boldsymbol{\xi})\}_{j=0}^{\infty}$ is the set of basis functions and $\{u_j\}_{j=0}^{\infty}$ is the set of coefficients to be determined. Therefore, stochastic spectral expansion may be seen as a particular case of the response surface methods where the approximation of the functional is given in terms of orthogonal polynomials basis.

3.2 Polynomial Chaos Expansion

Polynomial Chaos Expansion (PCE) theory was first introduced in the form of Wiener's Hermite-chaos by N. Wiener, in 1938 [103]. It is also called Homogeneous Chaos and was also developed as a framework by Ghanem and Spanos [104].

For a sequence of centered, normalized and mutually orthogonal Gaussian random variables $\{\xi_i\}_{i=1}^{\infty}$, define $\hat{\Gamma}_p$ to be the space of polynomials in $\{\xi_i\}_{i=1}^{\infty}$ having a polynomial degree of less than or equal to $p \in \mathbb{N}$. Furthermore, define $\Gamma_p \subset \hat{\Gamma}_p$ to be the set of polynomials, which belong to $\hat{\Gamma}_p$ and which are orthogonal to $\hat{\Gamma}_{p-1}$. The space spanned by Γ_p shall be denoted by $\tilde{\Gamma}_p$. Then, the Cameron and Martin theorem [105] yields:

$$\hat{\Gamma}_n = \hat{\Gamma}_{n-1} \oplus \tilde{\Gamma}_n, \qquad L_2(\Omega, P) = \bigoplus_{i=0}^{\infty} \tilde{\Gamma}_i \tag{3-5}$$

Here, the subspace $\tilde{\Gamma}_p$ of $L_2(\Omega, P)$ is called the p-th Homogeneous Chaos, whereas Γ_p is called the Polynomial Chaos of order p. Therefore, The Polynomial Chaos of order p consists of all polynomials of order p, involving all possible combinations of the random variables $\{\xi_i\}_{i=1}^{\infty}$. Note that since random variables are functions, the polynomials chaoses are functions of functions, and are thus regarded as functionals.

This expansion technique employs Hermite polynomials based on independent Gaussian random variables ξ which are associated with an individual random event $w \in \Omega$.

Thus, a general second-order Gaussian random response $X(\omega) \in L_2(\Omega, P)$, viewed as a function of w as the random event, admitted a poly-

nomial chaos expansion represented in the form:

$$\begin{aligned} X(\omega) &= u_0\Gamma_0 + \sum_{i_1=1}^{+\infty} u_{i_1}\Gamma_1(\xi_{i_1}(\omega)) \\ &+ \sum_{i_1=1}^{+\infty}\sum_{i_2=1}^{i_1} u_{i_1 i_2}\Gamma_2(\xi_{i_1}(\omega),\xi_{i_2}(\omega)) \\ &+ \sum_{i_1=1}^{+\infty}\sum_{i_2=1}^{i_1}\sum_{i_3=1}^{i_2} u_{i_1 i_2 i_3}\Gamma_3(\xi_{i_1}(\omega),\xi_{i_2}(\omega),\xi_{i_3}(\omega)) \\ &+ \sum_{i_1=1}^{+\infty}\sum_{i_2=1}^{i_1}\sum_{i_3=1}^{i_2}\sum_{i_4=1}^{i_3} u_{i_1 i_2 i_3 i_4}\Gamma_4(\xi_{i_1}(\omega),\xi_{i_2}(\omega),\xi_{i_3}(\omega),\xi_{i_4}(\omega)) + \ldots, \end{aligned} \tag{3-6}$$

The second-order random process from (3-6) represents the infinite space of a complete multidimensional orthogonal polynomial space. $\Gamma_p(\xi_{i_1},\ldots,\xi_{i_p})$ denotes the Hermite-Chaos of order p in the variables $(\xi_{i_1},\ldots,\xi_{i_p})$, where the Γ_p are set orthogonal Hermite polynomials in term of the standard Gaussian random variable ξ with zero expected and unit variance, which constitutes a complete basis in the Hilbert space $L_2(\Omega,P)$. $u_{i_1},\ldots,u_{i_p}$ are deterministic constants.

According to the theorem by Cameron and Martin [105], it can approximate any functionals in $L_2(\Omega,P)$ and as consequence it converges in the mean-square $L_2(\Omega,P)$ sense, i.e.:

$$\lim_{p\to\infty}\mathbb{E}[(u_0\Gamma_0 + \cdots + \sum_{i_1=1}^{+\infty}\cdots\sum_{i_p=1}^{i_p-1} u_{i_1\cdots i_p}\Gamma_p(\xi_{i_1},\ldots,\xi_{i_p}) - X)^2] = 0 \tag{3-7}$$

Therefore, PCE provides a means for expanding second-order random processes in terms of Hermite polynomials. Second-order random processes are the ones with finite variances, and this applies to most physical processes. Then, the p^{th} order polynomial chaos expansion consists of all orthogonal polynomials of order p, including any combination of $\{\xi_i\}_{i=1}^{\infty}$; furthermore, $\Gamma_p \perp \Gamma_q$ for $p \neq q$. This orthogonality greatly simplifies the procedure of statistical calculations, such as moments. Thus, PCE could be used to approximate non-Gaussian distributions using a least-square scheme: for example in order to compare the skewness and kurtosis distributions. By construction, the chaos polynomials whose orders are greater than one have vanishing expectation:

$$\mathbb{E}[\Gamma_{p>0}] = 0 \tag{3-8}$$

The original Wiener polynomial chaos expansion is composed of continuous integrals and were replaced by summations to get a discrete version in

(3-6). The general expression to obtain the multi-dimensional Hermite polynomials of order n is given by:

$$\Gamma_n(\xi_{i_1}, \ldots, \xi_{i_n}) = e^{\frac{1}{2}\boldsymbol{\xi}^T\boldsymbol{\xi}}(-1)^n \frac{\partial^n}{\partial\xi_{i_1}\cdots\partial\xi_{i_n}} e^{-\frac{1}{2}\boldsymbol{\xi}^T\boldsymbol{\xi}} \tag{3-9}$$

Therefore, Hermite-Chaos provides a means for expanding not only second-order random variables but also random fields in terms of orthogonal polynomials. Second-order random field is a generalization of random processes whose variance is also finite.

For notational convenience and in order to facilitate the manipulation of the PC expansion, we rely on an univocal relation between the $\Gamma()$ and a new functionals $\Psi()$. Then, the expression (3-6), can be rewritten as:

$$X(\omega) = \sum_{j=0}^{+\infty} \hat{u}_j \Psi_j(\boldsymbol{\xi}) \qquad \boldsymbol{\xi} = \{\xi_1, \xi_2, \ldots\} \tag{3-10}$$

Thus, this results is a more compact expression where there is a one-to-one correspondence between the functionals $\Gamma_p(\xi_{i_1}, \ldots, \xi_{i_p})$ and $\Psi_j(\boldsymbol{\xi})$, and also between the coefficients $u_{i_1 \cdots i_p}$ and $\hat{u}_j$. The deterministic expansion coefficients $\hat{u}_j$ are simply called PC coefficients.

The expansion above involves an infinite collection of ξ_i. In practice, it is necessary to restrict the representation to a finite number of random variables. Specifically, the PC of dimension N and order p is the subspace of $\tilde{\Gamma}_p$ generated by the elements of Γ_p that only involve N independent random variables $\xi_1, \ldots, \xi_N$. Therefore, each of the $\Psi_j(\boldsymbol{\xi})$ are multi-dimensional polynomials which involve products of the one-dimensional Hermite polynomials.

Let $\{\psi_{i_k}(\xi_k)\}_{k=1}^N$ be the one-dimensional Hermite polynomials of order i_k less than equal to p whit $\{\psi_0(\xi_k)\}_{k=1}^N \equiv 1$, and let $\lambda = i_1 + \cdots + i_N$ be a multi-index such that $0 \leq \lambda \leq p$. Then Γ_p can be represented as:

$$\Gamma_p(\xi_{i_1}, \ldots, \xi_{i_p}) = \Psi_j(\boldsymbol{\xi}) = \prod_{k=1}^{N} \psi_{i_k}(\xi_k) \qquad \lambda = p \tag{3-11}$$

Furthermore, the polynomial basis $\{\Psi_j\}$ of Hermite-Chaos forms a complete orthogonal basis of $L_2(\Omega, P)$, i.e.:

$$\langle \Psi_i, \Psi_j \rangle = \mathbb{E}[\Psi_i \Psi_j] = \langle \Psi_i^2 \rangle \delta_{ij} \tag{3-12}$$

where δ_{ij} is the Kronecker delta and the inner product in the Hilbert space is determined by the support of the Gaussian variables.

In the one-dimensional case, we can expand the random response U using orthogonal polynomials in ξ, which has a known probability distribution such as unit normal, $\mathcal{N}(0, 1)$. If X is a function of a normally distributed random

variable Y, which has the known mean μ_Y and variance σ_Y^2, ξ is a normalized variable:

$$\xi = \frac{X - \mu_Y}{\sigma_Y} \tag{3-13}$$

Generally, the one-dimensional Hermite polynomial are defined by:

$$\psi_p(\xi) = (-1)^p \frac{\varphi^{(p)}(\xi)}{\varphi(\xi)} \tag{3-14}$$

where $\varphi^{(p)}(\xi)$ is the $p^{(th)}$ derivative of the normal density function, $\varphi(\xi) = \frac{1}{\sqrt{2\pi}} e^{-\xi^2/2}$. This is simply the single-variable version of equation 3-9 For example, the one-dimensional Hermite polynomials are:

$$\begin{aligned}
\Psi_0(\boldsymbol{\xi}) &= \psi_0(\xi_1) = 1 \\
\Psi_1(\boldsymbol{\xi}) &= \psi_1(\xi_1) = \xi \\
\Psi_2(\boldsymbol{\xi}) &= \psi_2(\xi_1) = \xi^2 - 1 \\
\Psi_3(\boldsymbol{\xi}) &= \psi_3(\xi_1) = \xi^3 - 3\xi, \quad \dots
\end{aligned}$$

In the case of a two-dimensional expansion, we can write

$$\begin{aligned}
X(\omega) &= u_0\Gamma_0 + \sum_{i_1=1}^{2} u_{i_1}\Gamma_1(\xi_{i_1}) + \sum_{i_1=1}^{2}\sum_{i_2=1}^{i_1} u_{i_1 i_2}\Gamma_2(\xi_{i_1}, \xi_{i_2}) \\
&\quad + \sum_{i_1=1}^{2}\sum_{i_2=1}^{i_1}\sum_{i_3=1}^{i_2} u_{i_1 i_2 i_3}\Gamma_3(\xi_{i_1}, \xi_{i_2}, \xi_{i_3}) \\
&\quad + \sum_{i_1=1}^{2}\sum_{i_2=1}^{i_1}\sum_{i_3=1}^{i_2}\sum_{i_4=1}^{i_3} u_{i_1 i_2 i_3 i_4}\Gamma_4(\xi_{i_1}, \xi_{i_2}, \xi_{i_3}, \xi_{i_4}) + \dots,
\end{aligned}$$

or alternatively:

$$\begin{aligned}
X &= u_0\Gamma_0 + u_1\Gamma_1(\xi_1) + u_2\Gamma_2(\xi_2) \\
&\quad + u_{11}\Gamma_2(\xi_1, \xi_1) + u_{21}\Gamma_2(\xi_2, \xi_1) + u_{22}\Gamma_2(\xi_2, \xi_2) \\
&\quad + u_{111}\Gamma_3(\xi_1, \xi_1, \xi_1) + u_{211}\Gamma_3(\xi_2, \xi_1, \xi_1) + u_{221}\Gamma_3(\xi_2, \xi_2, \xi_1) \\
&\quad + u_{222}\Gamma_3(\xi_2, \xi_2, \xi_2) + u_{1111}\Gamma_4(\xi_1, \xi_1, \xi_1, \xi_1) + \dots,
\end{aligned}$$

and using the simplified form (3-10):

$$\begin{aligned}
X &= \hat{u}_0\Psi_0(\boldsymbol{\xi}) + \hat{u}_1\Psi_1(\boldsymbol{\xi}) + \hat{u}_2\Psi_1(\boldsymbol{\xi}) \\
&\quad + \hat{u}_3\Psi_3(\boldsymbol{\xi}) + \hat{u}_4\Psi_4(\boldsymbol{\xi}) + \hat{u}_5\Psi_5(\boldsymbol{\xi}) \\
&\quad + \hat{u}_6\Psi_6(\boldsymbol{\xi}) + \hat{u}_7\Psi_7(\boldsymbol{\xi}) + \hat{u}_8\Psi_8(\boldsymbol{\xi}) + \hat{u}_9\Psi_9(\boldsymbol{\xi}) + \cdots
\end{aligned}$$

Then calculating the multi-dimensional basis polynomials over two random

dimensions, we get:

$$\begin{aligned}
\Psi_0(\boldsymbol{\xi}) &= \psi_0(\xi_1)\psi_0(\xi_2) = 1 \\
\Psi_1(\boldsymbol{\xi}) &= \psi_1(\xi_1)\psi_0(\xi_2) = \xi_1 \\
\Psi_2(\boldsymbol{\xi}) &= \psi_0(\xi_1)\psi_1(\xi_2) = \xi_2 \\
\Psi_3(\boldsymbol{\xi}) &= \psi_2(\xi_1)\psi_0(\xi_2) = \xi_1^2 - 1 \\
\Psi_4(\boldsymbol{\xi}) &= \psi_1(\xi_1)\psi_1(\xi_2) = \xi_1\xi_2 \\
\Psi_5(\boldsymbol{\xi}) &= \psi_0(\xi_1)\psi_2(\xi_2) = \xi_2^2 - 1 \\
\Psi_6(\boldsymbol{\xi}) &= \psi_3(\xi_1)\psi_0(\xi_2) = \xi_1^3 - 3\xi_1 \\
\Psi_7(\boldsymbol{\xi}) &= \psi_2(\xi_1)\psi_1(\xi_2) = \xi_1^2\xi_2 - \xi_2 \\
\Psi_8(\boldsymbol{\xi}) &= \psi_1(\xi_1)\psi_2(\xi_2) = \xi_2^2\xi_1 - \xi_1 \\
\Psi_9(\boldsymbol{\xi}) &= \psi_0(\xi_1)\psi_3(\xi_2) = \xi_2^3 - 3\xi_2, \quad \ldots
\end{aligned}$$

and, finally, the expansion of X is given by:

$$\begin{aligned}
X &= \hat{u}_0 + \hat{u}_1\xi_1 + \hat{u}_2\xi_2 + \hat{u}_3(\xi_1^2 - 1) + \hat{u}_4(\xi_1\xi_2) + \hat{u}_5(\xi_2^2 - 1) + \hat{u}_6(\xi_1^3 - 3\xi_1) \\
&\quad + \hat{u}_7(\xi_1^2\xi_2 - \xi_2) + \hat{u}_8(\xi_2^2\xi_1 - \xi_1) + \hat{u}_9(\xi_2^3 - 3\xi_2) + \ldots,
\end{aligned}$$

$$\begin{aligned}
X &= \hat{u}_0 + \hat{u}_1\xi_1 + \hat{u}_2\xi_2 \\
&\quad + \hat{u}_3(\xi_1^2 - 1) + \hat{u}_4(\xi_1\xi_2) + \hat{u}_5(\xi_2^2 - 1) \\
&\quad + \hat{u}_6(\xi_1^3 - 3\xi_1) + \hat{u}_7(\xi_1^2\xi_2 - \xi_2) \\
&\quad + \hat{u}_8(\xi_2^2\xi_1 - \xi_1) + \hat{u}_9(\xi_2^3 - 3\xi_2) + \ldots,
\end{aligned}$$

3.2.1 Truncated PC Expansion

When the examined system contains multiple uncertain parameters, a single variable polynomial basis is no longer sufficient to perform the polynomial expansion. Multi-dimensional polynomials must be constructed to have the correct number of variables and polynomial order.

In practical computations, a finite number of basic variables shall be chosen, and the polynomial expansion (3-10), must be limited to a finite number of dimensions.

The number of basis functions $(M + 1)$ is dependent on the number of stochastic dimensions and the order of truncation of the chaos expansion.

The selection of the number of independent sources of uncertainty (i.e.

the number of independent random variables used to describe the process $\boldsymbol{\xi} = (\xi_1, \ldots, \xi_N)^T)$ in the system is denoted by N. The maximum order p of the multi-dimensional polynomial basis also has to be defined. Then, given the two values N and p, the total number of polynomials terms is truncated to a $(M+1)$ finite number defined by the following equation:

$$(M+1) = \binom{N+p}{p} = \frac{(N+p)!}{N!\,p!} \tag{3-15}$$

while for the tensor polynomial basis we have:

$$(M+1) = (p+1)^N \tag{3-16}$$

Therefore, the truncated expression of the random variable U can be expressed as:

$$X(\xi) = \sum_{j=0}^{M} \hat{u}_j \Psi_j(\boldsymbol{\xi}) + \epsilon(N,p) \tag{3-17}$$

The truncated expansion also converges in the mean square sense as N and p go to infinite, i.e.:

$$\lim_{N,\,p\to\infty} \langle \epsilon(N,p); \epsilon(N,p) \rangle = 0 \tag{3-18}$$

The PC representation will be computationally efficient when small values de N and p are sufficient for an accurate representation of U, or in other words, when $\langle \epsilon^2(N,p) \rangle \to 0$ rapidly with N and p.

Note that the Table 3.1 provides values de $(M+1)$ for p and N in the interval $[1-8]$. The dependence of $(M+1)$ on N and p is illustrated in the Figure 3.1.

Table 3.1: Number of terms $(M+1)$ in the N-dimensional PC expansion truncated at order p

p/N	1	2	3	4	5	6	p/N	1	2	3	4	5	6
1	2	3	4	5	6	7	5	6	21	56	126	252	462
2	3	6	10	15	21	28	6	7	28	84	210	462	924
3	4	10	20	35	56	84	7	8	36	120	330	792	1716
4	5	15	35	70	126	210	8	9	45	165	495	1287	3003

For example, consider the case where $N = 2$ and $p = 6$. That means 49 tensor polynomial basis and 21 basis function for the complete polynomial basis. If we increase the stochastic dimension to $N = 5$ by keep $p = 6$,

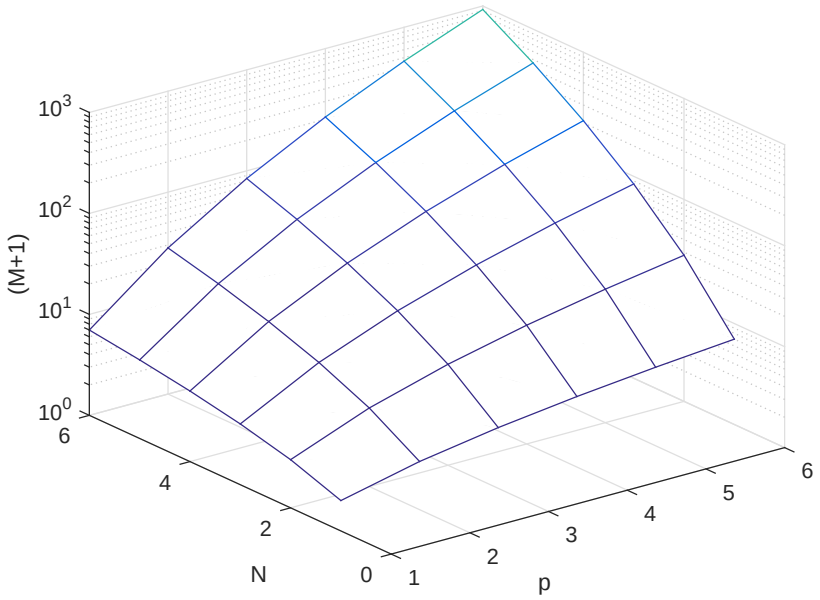

Figure 3.1: Number of terms in the PC expansion plotted against the order p and the number of dimensions N (Adapted from [5]).

the complete polynomial basis contain 462 basis functions. In contrast, the corresponding tensor polynomial basis contain as many as 16807 basis.

An increase in the number of random parameters corresponds to an exponential increase in the terms of the series. This quickly leads to infeasible numerical problems and has spurred broad interest in alternative formulations not based on the tensorization introduced earlier.

3.3 Generalized Polynomial Chaos

The Wiener's Hermite-chaos expansion has been quite effective in solving stochastic differential equation with Gaussian inputs but many stochastic problems involve certain types of non-Gaussian inputs, e.g., Lognormal distributions; this can be justified by the Cameron-Martin theorem [105]. Moreover, for general non-Gaussian random inputs when these are approximated with Wiener's Hermite-chaos chaos expansions, the convergence may be slow and in some cases, the convergence rate is, in fact, severely deteriorated [106]. The main reason for this is that, when expressed as functions of a collection of Gaussian basic random variables, these function are often highly non-linear and can only be well approximated by truncated Wiener's Hermite-chaos expansions of very high order. A possible remedy is to base the expansion on non-Gaussian basic random variables whose distribution is closer to the random variables under expansion, thus permitting good approximations of lower order. As a

consequence, such expansions involve polynomials orthogonal with respect to non-Gaussian measures replacing the Hermite polynomials. In principle a sequence of orthogonal polynomials exists for any probability distribution on $\mathbb{R}$ with finite moments of all orders [107].

Xiu and Karniadakis [108, 109] introduce the term generalized polynomial chaos (gPC) expansions and have in fact shown that for a large number of common probabilities laws, any random functions can be represented by the corresponding families of the set of hypergeometric polynomial from the Askey-scheme (Wiener-Askey polynomial chaos) as generalization of the original Wiener's Hermite-chaos expansion.

The expansion basis of the Wiener-Askey polynomial chaos by the complete set of orthogonal polynomials from the Askey-scheme can be used to represented both Gaussian and non-Gaussian random functions instead of the Hermite polynomial. For instance we represent the general second-order random response $U(\xi)$ as:

$$\begin{aligned} X(\xi) &= u_0 I_0 + \sum_{i_1=1}^{+\infty} u_{i_1} I_1(\zeta_{i_1}(\xi)) \\ &\quad + \sum_{i_1=1}^{\infty}\sum_{i_2=1}^{i_1} u_{i_1 i_2} I_2(\zeta_{i_1}(\xi), \zeta_{i_2}(\xi)) \\ &\quad + \sum_{i_1=1}^{\infty}\sum_{i_2=1}^{i_1}\sum_{i_3=1}^{i_2} u_{i_1 i_2 i_3} I_3(\zeta_{i_1}(\xi), \zeta_{i_2}(\xi), \zeta_{i_3}(\xi)) + \ldots, \end{aligned} \tag{3-19}$$

where $I_p(\zeta_{i_1}, \ldots, \zeta_{i_p})$ denote the Wiener-Askey polynomial chaos expansion of order p in terms of the multi-dimensional random variable $\boldsymbol{\zeta} = (\zeta_{i_1}, \ldots, \zeta_{i_p})$. In the Wiener-Askey chaos expansion the polynomial I_p are not restricted to Hermite polynomial but instead they could be any member of the Askey-scheme [110]. As it was described above, for notational convenience we rewrite (3-19) as:

$$X(w) = \sum_{j=0}^{\infty} \hat{c}_j \Phi_j(\boldsymbol{\zeta}) \tag{3-20}$$

where also there is a one-to-one correspondence between the functional $I_p()$ and $\Phi_j(\boldsymbol{\zeta})$, and between the coefficients $u_{i_1 \cdots i_2}$ and $\hat{c}_j$.

Each type of polynomial $\{\Phi_j\}$ from the Askey-scheme forms a complete basis in the Hilbert space determined by its corresponding support and converge in the $L_2(\Omega, P)$ sense. The orthogonality relation of the Wiener-Askey polynomial chaos takes the form:

$$\langle \Phi_i, \Phi_j \rangle = \langle \Phi_i^2 \rangle \delta_{ij} \tag{3-21}$$

where δ_{ij} is the Kronecker delta and the inner product in the Hilbert space of the variable $\boldsymbol{\zeta}$ denoted by:

$$\langle f(\zeta), g(\zeta) \rangle = \mathbb{E}[f(\zeta)g(\zeta)] = \int_{\Omega} f(\zeta)g(\zeta)\varrho(\boldsymbol{\zeta})d(\boldsymbol{\zeta}) \tag{3-22}$$

whereas probability measure may be represented by the joint probability density function (weighting function $\varrho(\boldsymbol{\zeta})$ corresponding to the Wiener-Askey polynomial chaos) of the multi-dimensional independent random variable ζ:

$$\varrho(\boldsymbol{\zeta}) = \prod_{i=1}^{N} \varrho_i(\zeta_i) \tag{3-23}$$

For instance, in the case of multi-dimensional independent Gaussian random variables:

$$\varrho(\boldsymbol{\zeta}) = \frac{1}{\sqrt{(2\pi)^n}} e^{-\frac{1}{2}\boldsymbol{\zeta}^t\boldsymbol{\zeta}} = \frac{dP}{d(\boldsymbol{\zeta})} \tag{3-24}$$

and similarly for the discrete case:

$$\langle f(\zeta), g(\zeta) \rangle = \mathbb{E}[f(\zeta)g(\zeta)] = \sum_{\Omega} f(\zeta)g(\zeta)\varrho(\boldsymbol{\zeta}) \tag{3-25}$$

Then, we observe that some types of orthogonal polynomials from the Askey-scheme have weighting functions of the same form as the probability density function of certain types of random distributions. Then, this establishes a corresponding relation between the distributions of the independent random variable $\boldsymbol{\zeta}$ and the type of orthogonal polynomial $\{\Phi_j(\boldsymbol{\zeta})\}$ of the Askey-scheme (gPC basis), according to Table 3.2.

For instance, for Uniform and Binomial distribution, the Legendre and Krawtchouk polynomials are more appropriate choices to be optimally represented with respect to their weighting functions, respectively. It is clear that the original Wiener polynomial chaos corresponds to the Hermite-chaos and is a subset of the Wiener-Askey polynomial chaos.

Furthermore, in the case of the probability functions for which one does not readily dispose of an orthogonal family of polynomials, it is generally possible to rely on a numerical construction of the PC basis, following a Gram-Schmidt orthogonalization process [111].

The optimality of the choice of stochastic expansion pertains to the representation of the input; the representation of the output of a nonlinear problem will likely be highly nonlinear as expressed in the basis of the input [112]. The Cameron-Martin theorem [105] applies also to gPC with non-Gaussian random variable, but only when the probability distribution (measure) of the stochastic expansion variable ζ is uniquely determined by the sequence of moments.

Table 3.2: Correspondence between the type of gPC and their underlying random variables

	Distribution of ζ	gPC basis polynomials	Weight function	Support
Continuous	Uniform	Legendre	$\frac{1}{2}$	$[-1,1]$
	Gaussian	Hermite	$\frac{1}{\sqrt{2\pi}}e^{-\frac{\zeta^2}{2}}$	$(-\infty,+\infty)$
	Gamma	Laguerre	$\frac{\zeta^\alpha e^\zeta}{\Gamma(\alpha+1)}$	$[0,+\infty)$
	Beta	Jacobi	$\frac{(1+\zeta)^\alpha(1-\zeta)^\beta}{2^{\alpha+\beta+1}B(\alpha+1,\beta+1)}$	$[-1,1]$
Discrete	Poisson	Charlier	$e^{-\lambda}\frac{\lambda^\zeta}{\zeta!}$	$\{1,2,\ldots\}$
	Binomial	Krawtchouk	$\binom{N}{\zeta}p^\zeta(1-p)^{N-\zeta}$	$\{1,2,\ldots,N\}$
	Negative Binomial	Meixner	$\frac{(\beta)_\zeta}{\zeta!}(1-c)^\beta c^\zeta$	$\{1,2,\ldots\}$
	Hipergeometric	Hahn	$\frac{\binom{\alpha}{\zeta}\binom{\beta}{N-\zeta}}{\binom{\alpha+\beta}{N}}$	$\{1,2,\ldots,N\}$

This is not always the case in situations commonly encountered. For instance, probability distributions, for which the moment problem is uniquely solvable are the uniform, beta, gamma and the normal distributions. By contrast, the moment problem is not uniquely solvable for the lognormal distribution, so that the sequence of orthogonal polynomial with respect to the lognormal random variable does not constitute a basis of the Hilbert space, and there will be some elements (random variables) in this space which are not the limit of their gPC expansion. Thus, there are cases where the gPC expansion does not converge to the true limit of the random variable under expansion. Further examples of random variables with indeterminate distribution are certain power of random variables with normal or gamma distribution (see e.g. [113, 114]). However, lognormal random variables may be successfully represented by gPC satisfying the determinacy of moments, e.g. Hermite polynomial [107].

Another possible choice for PCE of non-Gaussian cases is the transformation technique introduced by Isukapalli [11] in the stochastic response surface method. In this procedure, the random input variables, which include non-normal distributions, are transformed into standard normal random variables [115]. According to Table 3.3, the input random variable z can be represented

by a function of standard normal random variable ζ. The μ and σ are the mean and standard deviation of the input random variable, respectively, while a, b and λ are scale parameters of each distributions. Then, the original PCE can be employed as the response surface model for uncertain systems.

Table 3.3: Representation of Various Distributions as Functionals of Normal Random Variables (According to [11])

Distribution Type	Transformation
Normal (μ, σ)	$\mu + \sigma\zeta$
Lognormal (μ, σ)	$\exp(\mu + \sigma\zeta)$
Uniform (a, b)	$a + (b-a)\left(\frac{1}{2}\frac{1}{2}\,\mathrm{erf}\left(\frac{\zeta}{\sqrt{2}}\right)\right)$
Gamma (a, b)	$ab\left(\zeta\sqrt{\frac{1}{9a}} + 1 - \frac{1}{9a}\right)^3$
Exponential (λ)	$-\frac{1}{\lambda}\log\left(\frac{1}{2}\frac{1}{2}\,\mathrm{erf}\left(\frac{\zeta}{\sqrt{2}}\right)\right)$

3.3.1 Stochastic Quantities

The stochastic spectral expansion of a random quantity gives us a convenient representation of their information available implicitly (measures do the probability, statistic moments, analysis of correlations, local and global sensitivity analysis, etc) at low computational cost provided that the coefficients of the representation of relevant quantities are known.

Let X be a second-order random variable defined on a probability space $(\Omega, \mathfrak{F}, P)$ with a distribution function $F_X(x) = P(X \leq x)$ and finite moments $\mathbb{E}[X^2] < +\infty$. Its expansion on the orthogonal gPC basis $\{\Phi_j\}_{j=0}^{\infty}$ is given by:

$$X = \sum_{j=0}^{\infty} \hat{c}_j \Phi_j(\boldsymbol{\zeta}) \tag{3-26}$$

where we assume an indexation such that $\Phi_0(\boldsymbol{\zeta}) = 1$ and satisfying the property of orthogonal polynomials

$$\langle \Phi_0(\boldsymbol{\zeta}), \Phi_j(\boldsymbol{\zeta}) \rangle = \mathbb{E}[\Phi_i(\boldsymbol{\zeta})\Phi_j(\boldsymbol{\zeta})] = \gamma_i \delta_{ij} \tag{3-27}$$

where $\gamma_i = \mathbb{E}[\Phi_i^2(\boldsymbol{\zeta})]$ are the normalization factors. Then, as a consequence, important properties from (3-27) can be obtained:

$$\begin{aligned} &\mathbb{E}[\Phi_0(\boldsymbol{\zeta})\Phi_j(\boldsymbol{\zeta})] = 0 \qquad \forall j > 0 \\ &\mathbb{E}[\Phi_0(\boldsymbol{\zeta})\Phi_0(\boldsymbol{\zeta})] = 1 \end{aligned} \tag{3-28}$$

The expression that calculates the expectation of X is given by:

$$\mathbb{E}[X] = \mathbb{E}[\Phi_0(\boldsymbol{\zeta})X] = \langle \Phi_0(\boldsymbol{\zeta}), X\rangle = \sum_{j=0}^{N} \hat{c}_j \langle \Phi_0(\boldsymbol{\zeta}), \Phi_j(\boldsymbol{\zeta})\rangle \tag{3-29}$$

then:

$$\mathbb{E}[X] = \hat{c}_0 \tag{3-30}$$

Therefore, we obtain the expected value of the random variable X, from the indexation convention, whose value is the coefficient $\hat{c}_0$.

From (3-29), we can also calculate the variance of X as:

$$\begin{aligned} \sigma_X^2 &= \mathbb{E}[(X - \mathbb{E}[X])^2] = \mathbb{E}[(\sum_{j=1}^{N} \hat{c}_j \Phi_j(\boldsymbol{\zeta}))] \\ &= \sum_{i,j=1}^{N} \hat{c}_i \hat{c}_j \langle \Phi_i(\boldsymbol{\zeta}), \Phi_j(\boldsymbol{\zeta})\rangle = \sum_{j=1}^{N} \hat{c}_j^2 \langle \Phi_j^2 \rangle \end{aligned} \tag{3-31}$$

Note the variance of X is given as a weighted sum of its squared gPC coefficients. If the bases are orthonormal polynomials so, $\langle \Phi_j^2 \rangle = 1$ and the variance depends only of the sum of its squared gPC coefficients. Similar expressions can be derived for higher order moments of X in terms of its gPC coefficients, e.g. skewness, kurtosis and others. However higher order moments do not have an expression as simple as that for the first and second-order ones.

Another alternative can be used to estimate the expectation and variance values and another moments using sampling strategies. Realization of X can be obtained by sampling of $\boldsymbol{\zeta}$ following its density function followed by the evaluation of the gPC expansion at sample point $\boldsymbol{\zeta}(\omega)$.

Note that in the context of the analysis of any model, the sampling scheme for a output known from its gPC expansion is simpler and more efficient than the full evaluation of the model realization such as in Monte Carlo methods.

3.4 Non-Intrusive Spectral Method (NISP)

Let $\mathcal{M}$ be a real scalar model in function of N independent real-valued random variables $\boldsymbol{X}(\omega) = \{X_1(\omega), \ldots, X_N(\omega)\}$, such that, $\boldsymbol{X}(\omega) : \omega \in \Omega \mapsto \mathcal{D}_{\boldsymbol{X}} \subset \mathbb{R}$ with prescribed joint probability density function $f_{\mathbf{X}}(\mathbf{x})$ with respect to the support $\mathcal{D}_{\boldsymbol{X}}$:

$$f_{\mathbf{X}}(\mathbf{x}) = \prod_{i=1}^{N} f_{Xi}(x_i) \tag{3-32}$$

If we denote Y as the model response, then:

$$\mathcal{M} \ : \boldsymbol{X} \in \mathcal{D}_{\boldsymbol{X}} \mapsto Y = \mathcal{M}(\boldsymbol{X}) \in \mathbb{R} \tag{3-33}$$

Note that the model response is also a random variable $Y(w) = \mathcal{M}(\boldsymbol{X}(w))$. The NISP aims at computing the projection coefficients of random model response Y on a finite dimensional stochastic subspace $\mathbb{P}_M^N$ of $L_2(\mathcal{D}_{\boldsymbol{X}}, f_{\boldsymbol{X}})$ which is a Hilbert space.

Let us suppose that its random response $Y \in L_2(\mathcal{D}_{\boldsymbol{X}}, f_{\boldsymbol{X}})$ is a second-order random variable:

$$\mathbb{E}[Y^2] =< +\infty \tag{3-34}$$

and $\{\Psi_j\}_{j=0}^M$ are the orthogonal basis of $\mathbb{P}_M^N$ which consists of the set of gPC truncated to order p.

Let $P_M Y$ be the projection of Y onto $\mathbb{P}_M^N$ via the inner product $\langle \cdot, \cdot \rangle_{L_2}$, then we define its gPC orthogonal projection as:

$$P_M Y = \sum_{j=0}^{M} \hat{y}_j \Psi_j(\boldsymbol{X}) \tag{3-35}$$

where $\{\hat{y}_j\}$ are the generalized Fourier coefficients. Due to the orthogonality of the selection of basis of $\mathbb{P}_M^N$, the projection coefficients $\hat{y}_j$ are given by:

$$\hat{y}_j = \frac{\langle Y, \Psi_j \rangle}{\langle \Psi_j^2 \rangle} = \frac{1}{\langle \Psi_j^2 \rangle} \int_{\mathcal{D}_{\boldsymbol{X}}} Y \Psi_j(\boldsymbol{X}) f_{\boldsymbol{X}}(\boldsymbol{x}) d\boldsymbol{x} \tag{3-36}$$

furthermore, for all $\{\Psi_j\} \in \mathbb{P}_M^N$:

$$Y - P_M Y \perp \mathbb{P}_M^N \Leftrightarrow \langle Y - P_M Y, \Psi_j \rangle = 0 \qquad 0 \leq j \leq M \tag{3-37}$$

The existence and convergence of the projection follow directly from the classical approximation theory; i.e.:

$$\| Y - P_M Y \|_{L_2} \to 0, \qquad M \to \infty \tag{3-38}$$

which is also referred to as mean-square convergence or strong norm sense. Furthermore, it implies that $P_M Y$ converges to Y in probability, i.e. $P_M Y \xrightarrow{P} f$, which further implies the convergence in distribution, i.e., that $P_M Y \xrightarrow{d} f$, as $M \to \infty$.

From the expression (3-35) the factor $\langle \Psi_j^2 \rangle$ depends only on the basis used which are known analytically for gPC bases and classical probability density functions, but the determination of the numerator is to be discussed. Note that $\hat{y}_j$ does not depend on the dimension of the projection subspace, but only on the basis function Ψ_j. This implies that since the basis has been selected, the determination of $\hat{y}_j$ are independent from each other.

Two different techniques have been proposed to numerically estimate the right-hand side of (3-36): Simulation method, where one relies on pseudo-random sampling strategies, and cubature methods which involve deterministic schemes to numerically estimate the integrals.

3.4.1 Sampling Method

In this approach, the correlation between Y and $\Psi_j(\boldsymbol{X})$ is estimated by means of a pseudo-random sampling of the parameter space $\mathcal{D}_{\boldsymbol{X}}$.

The Monte Carlo method (MCM) is one of the simplest crude simulation techniques to compute $\hat{y}_j$. Then, a sample of set of independent realizations of $\boldsymbol{X}$ is generated from $f_{\boldsymbol{X}}$ using a pseudo-random number generator. Denoting $\boldsymbol{X}^{(i)}$ the i-th element of the sample set, and $Y^{(i)} = \mathcal{M}(\boldsymbol{X}^{(i)})$ the corresponding model response and as $\langle Y, \Psi_j \rangle = \mathbb{E}[Y\Psi_j]$. Then the empirical mean is evaluated by:

$$\langle Y, \Psi_j \rangle \approx \frac{1}{m} \sum_{i=1}^{m} Y^{(i)} \Psi_j(\boldsymbol{X}^{(i)}) \tag{3-39}$$

where m is the sample set dimension. The convergence rate of Monte Carlo simulation is well known and a variance of ϵ_m asymptotically goes to zero as $\mathcal{O}(1/\sqrt{m})$ for sufficiently large m according to the law of large numbers. There exists another sampling techniques that can achieve lower sampling errors. This strategies are known as Latin Hypercube Sampling and Quasi Monte Carlo sampling. The main idea is to force the sampler to draw points that cover the parameter domain in a more uniform way than the MCM. Hence, in general, the accuracy of another sampling methods increases faster than the Monte Carlo method.

3.4.2 Cubature Method

The integrals over the stochastic domains of the gPC projections defined by (3-36) can be approximated employing numerical quadratures schemes.

We denote $g(\boldsymbol{X}) = Y\Psi_j(\boldsymbol{X})$ over $\mathcal{D}_{\boldsymbol{X}}$ with non-negative weight $f_{\boldsymbol{X}}$ having a product form. Then, the numerator of right-hand expression (3-36) can be represented as:

$$I(g) = \langle Y, \Psi_j \rangle = \int_{\mathcal{D}_{\boldsymbol{X}}} g(\boldsymbol{X}) f_{\boldsymbol{X}} d\boldsymbol{x} \tag{3-40}$$

This integral can be determined employing effectively deterministic cubatures. A cubature is an approximation of the multidimensional integral as a discrete sum:

$$I(g) = \int_{\mathcal{D}_{\boldsymbol{X}}} g(\boldsymbol{X}) f_{\boldsymbol{X}} d\boldsymbol{x} \;\approx\; I_m(g) = \sum_{i=1}^{m_Q} g(\boldsymbol{X}^{(i)}) W^{(i)} \tag{3-41}$$

where $\boldsymbol{X}^{(i)} \in \mathcal{D}_{\boldsymbol{X}}$ and $W^{(i)} \in \mathbb{R}$, $i = 1, \ldots, m_Q$, are the nodes and weights of the m_Q-node cubature.

In the context of NISP, the integration weights $W^{(i)}$ are the product probability density functions $f_{X_i} > 0$ of the random parameter over their

respective domains. Consequently $I(g)$ can be approximated using Gauss quadrature formulas.

The Gauss quadrature chooses the points $\{X^{(i)}\}_{i=0}^{m_Q}$ over $\mathcal{D}_{\boldsymbol{X}}$ for evaluations in an optimal distribution rather than equally spaced way. The Gauss formula is closely related to the orthogonal polynomial family for the weight functions f_{X_i}, which is also the basis for gPC expansions. For instance, we choose $\{X^{(i)}\}$ to be the set of Gauss-Legendre quadrature points for the case of uniformly distribution, and the set of Gauss-Hermite quadrature point for the case of gaussian distribution.

For multiples stochastic dimensions another techniques more efficient can be used as tensor product and Smolyak quadrature (sparse grid) scheme.

3.4.3 Sparse Grid

Non-intrusive spectral method by using the tensor product as strategies of integration achieves an exponential convergence. However, as the number of random variables increases ($N >> 1$) , the collocation points (nodes) that employ a selected subset of Gaussian quadrature points grows very rapidly for large N, i.e., $m_c = (p+1)^N$, and the rate of convergence deteriorates drastically owing to a very slow convergence. Moreover, if each collocation point requires a large computing time, it becomes highly expensive computationally. This is the well-known "curse of dimensionality". Therefore, tensor product is mostly used for low dimensional problems, i.e., with less than five [116].

An efficient alternative approach to the tensor product is using the Smolyak sparse grid [117]. The algorithm is based on the sparse tensor product construction by using quadrature nested formulas [118]. Nested rules generally involve nested sets of nodes whose dimensions double each time the level is incremented. The level is used to distinguish quadrature formulas with different orders of accuracy. In the literature, several nested rules are available, e.g., Trapezoidal, Clenshaw-Curtis, Ferjèr, and Gauss-Patterson rules.

Let $Q_l^{(1)} f$ be a family of quadrature rules and define the difference relations:

$$\Delta_l^{(1)} f = \left(Q_l^{(1)} - Q_{l-1}^{(1)} \right) f \tag{3-42}$$

with $Q_0^{(1)} = 0$. Note that $\Delta_l^{(1)} f$ is also a quadrature rule and contains the set of nodes in $Q_l^{(1)} f$ with weights equal to the difference of weights between levels l and $l-1$.

Then, we introduce the multi-index $\mathbf{I} = (I_1, \ldots, I_N) \in \mathbb{N}^N$to construct the sparse grid such that

$$| \mathbf{I} |= \sum_{i=1}^{N} l_i \tag{3-43}$$

Therefore, using the multi-index, the sparse quadrature formula at level l is expressed by

$$Q_l^{(N)} f = \sum_{|\mathbf{I}| \leq l+N-1} \left(\Delta_{l_1}^{(1)} \otimes \Delta_{l_2}^{(1)} \otimes \cdots \otimes \Delta_{l_N}^{(1)} \right) \tag{3-44}$$

It is observed that the sparse grid method involves a significantly reduced number of nodes from the construction of grids and weights that yields similar accuracy as the tensor product, albeit with a low computational cost.

In this work, we use the 1D Gaussian nested quadrature rules with Gaussian weight. These rules are shown in Figure 3.2 for four points of integration.

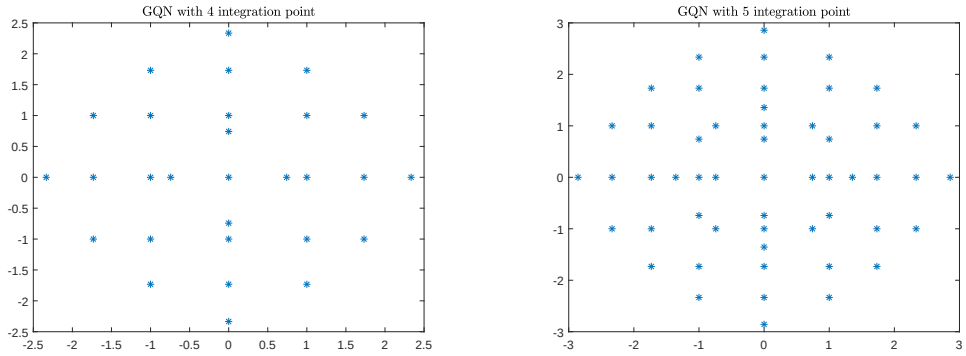

3.2(a): Univariate Gaussian quadrature rules as basis

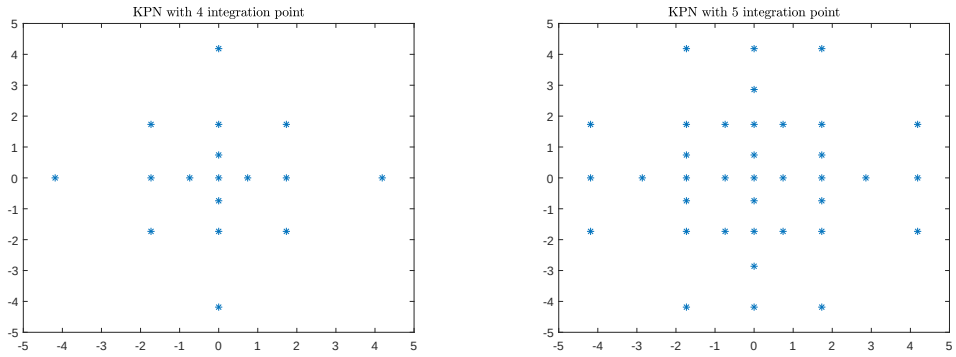

3.2(b): Univariate Kronrod-Patterson nested quadrature rules as basis

Figure 3.2: Sparse grids with four integration points by sparsification of tensor products of 1D.

3.5 Regression Method

In this work, a different non-intrusive approach based on linear regression is employed. Let $\mathbf{u} = \left[\hat{u}_0, \ldots, \hat{u}_{\nu_{pc}})\right]^T$ be a vector of unknown coefficients,

$\mathbf{\Psi} = \psi_j$ a matrix with the gPC and Y is the random field (variable) of interest that is evaluated in a finite set of ν_{gq} possible realizations of the germ ξ, and thus the coefficients of the expansion are obtained through $\mathbf{u} = (\mathbf{\Psi}^T \mathbf{\Psi})^{-1} \mathbf{\Psi}^T \mathbf{Y}$, the solution of the mean-square problem

$$\mathbf{\Psi}\,\mathbf{u} \;\approx\; \mathbf{Y}, \tag{3-45}$$

where

$$\underbrace{\begin{bmatrix} \psi_0(\xi_1) & \cdots & \psi_{\nu_{pc}}(\xi_1) \\ \vdots & \ddots & \vdots \\ \psi_0(\xi_{\nu_{gq}}) & \cdots & \psi_{\nu_{pc}}(\xi_{\nu_{gq}}) \end{bmatrix}}_{\mathbf{\Psi}} \underbrace{\begin{bmatrix} \hat{u}_0 \\ \hat{u}_1 \\ \vdots \\ \hat{u}_{\nu_{pc}} \end{bmatrix}}_{\mathbf{u}} \approx \underbrace{\begin{bmatrix} Y(\mathbf{x}, \xi_1) \\ \vdots \\ Y(\mathbf{x}, \xi_{\nu_{gq}}) \end{bmatrix}}_{\mathbf{Y}}. \tag{3-46}$$

For further information about the basic aspects of gPC expansion the reader is encouraged to see the references [119–124], and for more advanced topics [125–129].

3.6 Karhunen-Loève Expansion

The KL expansion [119, 120] is one of the most widely used and powerful techniques for analysis and synthesis of random fields, providing a denumerable representation, in terms of the spectral decomposition of the correlation function, for a random field parametrized by a nondenumerable index [125, 130].

Let $\tilde{H}(\mathbf{x}, \omega) : \mathcal{D} \times \Omega \mapsto \mathbb{R}$ be second-ordered Homogeneus Gaussian field (finite second order $\mathbb{E}[\tilde{H}(\mathbf{x}, \omega)]^2$), where $\tilde{H}(\mathbf{x}, \omega)$ is called centered, if $\mathbb{E}[\tilde{H}(\mathbf{x}, \omega)] = 0 \;\forall\; \mathbf{x} \in \mathcal{D}$. Let $H(\mathbf{x}, \omega) : \mathcal{D} \times \Omega \mapsto \mathbb{R}$ be an arbitrary random field and we note that

$$\tilde{H}(\mathbf{x}, \omega) = H(\mathbf{x}, \omega) - \mathbb{E}[H(\mathbf{x}, \omega)] \tag{3-47}$$

Suppose that random field $\tilde{H}(\mathbf{x})$ is mean-square continuous, if

$$\lim_{\epsilon \to 0} \mathbb{E}[H(\mathbf{x}_{1+\epsilon}, \omega) - H(\mathbf{x}_1, \omega)]^2 = 0. \tag{3-48}$$

The autocorrelation function of $\tilde{H}(\mathbf{x})$ is $R_{\tilde{H}\tilde{H}}(\cdot, \cdot) : \mathcal{D} \times \mathcal{D} \to \mathbb{R}$ defined for any pair of vectors $\mathbf{x}_1, \mathbf{x}_2 \in \mathcal{D}$ by means of

$$R_{\tilde{H}\tilde{H}}(\mathbf{x}_1, \mathbf{x}_2) = \mathbb{E}[\tilde{H}(\mathbf{x}_1, \omega)\tilde{H}(\mathbf{x}_2, \omega)] = C_{\tilde{H}\tilde{H}}(\mathbf{x}_1, \mathbf{x}_2) \tag{3-49}$$

The following well-known result states that for a random field the continuity of its autocorrelation function is a necessary and sufficient condition

for the mean-square continuity of the field.

We call a function $k : \mathcal{D} \times \mathcal{D} \mapsto \mathbb{R}$ a Hilbert-Schmidt kernel if

$$\int_{\mathcal{D}} \int_{\mathcal{D}} |k(\mathbf{x}_1, \mathbf{x}_2)|^2 d\mathbf{x}_1 d\mathbf{x}_2 < +\infty \tag{3-50}$$

that is, $k \in L_2(\mathcal{D} \times \mathcal{D})$. Then, we define the integral operator $\mathcal{K}$ on $L_2(\mathcal{D})$, $\mathcal{K} : u \mapsto \mathcal{K}u$ for $u \in L_2(\mathcal{D})$, by

$$[\mathcal{K}u](\mathbf{x}_1) = \int_{\mathcal{D}} k(\mathbf{x}_1, \mathbf{x}_2) u(\mathbf{x}_2) d\mathbf{x}_2 \tag{3-51}$$

It is simple to show that $\mathcal{K}$ is a bounded operator on $L_2(\mathcal{D})$, where convergence is absolute and uniform on $\mathcal{D} \times \mathcal{D}$.

The following Mercer's theorem [131], provides a series representantion for the kernel function k based on spectral representation through Hilbert-Schmidt operator $\mathcal{K}$. Suppose further that the corresponding Hilbert-Schmidt operator $\mathcal{K} : L_2(\mathcal{D}) \mapsto L_2(\mathcal{D})$ given by Eq.(3-51) is possitive. If $\lambda_i \in [0, +\infty\rangle$ and $\phi_i : \mathcal{D} \mapsto \mathbb{R}$ are the eigenvalues and eigenvectors of $\mathcal{K}$ then $\forall\ \mathbf{x}_1,\ \mathbf{x}_2 \in \mathcal{D}$

$$\mathcal{K}(\mathbf{x}_1, \mathbf{x}_2) = \sum_{i=1}^{+\infty} \lambda_i \phi_i(\mathbf{x}_1) \phi_i(\mathbf{x}_2) \tag{3-52}$$

Under these assumptions, the linear integral operator, i.e., $k(\mathbf{x}_1, \mathbf{x}_2) = R_{\tilde{H}\tilde{H}}(\mathbf{x}_1, \mathbf{x}_2)$

$$R_{\tilde{H}\tilde{H}}\, \phi\,(\mathbf{x}_1) = \int_{\mathcal{D}} R_{\tilde{H}\tilde{H}}(\mathbf{x}_1, \mathbf{x}_2)\, \phi(\mathbf{x}_2)\, d\mathbf{x}_2 \tag{3-53}$$

defines a Hilbert-Schmidt operator [125, 130]. In this context, based on Eq.(3-52), the eigenvalues and associated eigen functions can be obtained by solving the Fredholm integral equation of the second kind

$$\int_{\mathcal{D}} R_{\tilde{H}\tilde{H}}(\mathbf{x}_1, \mathbf{x}_2) \phi_i(\mathbf{x}_2) d\mathbf{x}_2 = \lambda_i \phi_i(\mathbf{x}_1), \qquad \mathbf{x} \in \mathcal{D}, \tag{3-54}$$

which has denumerable family of eigenpairs $\{(\lambda_i, \phi_i)\}_{i=1}^{+\infty}$, where λ_i are the eigenvalues and ϕ_i the corresponding eigenfunctions of the operator defined by Eq.(3-53). Besides that, the sequence of eigenvalues is such that $\sum_{i=1}^{+\infty} \lambda_i < +\infty$ and $\lambda_1 \geq \lambda_2 \geq \cdots \geq \lambda_i \geq \cdots \to 0$; and the family of functions $\{\phi_n\}_{i=1}^{+\infty}$ defines an orthonormal Hilbertian basis in $L_2(\mathcal{D})$, i.e.,

$$\phi_i \phi_j = \delta_{ij}\,, \tag{3-55}$$

where Kronecker delta is such that $\delta_{ij} = 1$ if $i = j$ and $\delta_{ij} = 0$ for $i \neq j$.

By definition, $R_{\tilde{H}\tilde{H}}(\mathbf{x}_1, \mathbf{x}_2)$ is bounded, symmetric, and positive definite. Therefore, the eigen functions $\phi_i(\mathbf{x})$ of $R_{\tilde{H}\tilde{H}}(\mathbf{x}_1, \mathbf{x}_2)$ form a complete orthogonal set that satisfy

$$\int_{\mathcal{D}} \phi_i(\mathbf{x}) \phi_j(\mathbf{x}) d\mathbf{x} = \delta_{ij} \tag{3-56}$$

Therefore, applying two standard results of functional analysis [132], the

theorems of Hilbertian basis and orthogonal projection, it is possible to show that the random field $\tilde{H}(\mathbf{x})$ admits a decomposition

$$\tilde{H}(\mathbf{x},\omega) = \sum_{i=1}^{+\infty} \sqrt{\lambda_i}\, \phi_i(\mathbf{x})\, \xi_i(\omega)\,, \tag{3-57}$$

Susbtituting Eq.(3-47) in Eq.(3-57) the Karhunen-Loève expansion of $H(\mathbf{x},\omega)$ is given by

$$H(\mathbf{x},\omega) = \mu_H(\mathbf{x}) + \sum_{i=1}^{+\infty} \sqrt{\lambda_i}\, \phi_i(\mathbf{x})\, \xi_i(\omega)\,, \tag{3-58}$$

where $\{\xi_i(\omega) : \Omega \mapsto \mathbb{R}\}_{i=1}^{+\infty}$ is a family of random variables which are centered (zero mean) and mutually uncorrelated, i.e.,

$$\mathbb{E}[\xi_i] = 0, \qquad \text{and} \qquad \mathbb{E}[\xi_i\, \xi_j] = \delta_{ij}\,. \tag{3-59}$$

In addition, if we calculate the orthogonality relation of ξ_i from Eq.(3-59), this implies that ξ_i forms a set of orthonormal random variable with respect to the inner product. Therefore, from Eqs.(3-59), the set of uncorrelated random variables straightforwardly attains a closed form expressed by

$$\xi_i = \frac{1}{\sqrt{\lambda_i}} \int_{\mathcal{D}} \left(H(\mathbf{x},\omega) - \mu_{\,H}(\mathbf{x})\right) \phi_i(\mathbf{x}) d\mathbf{x}, \tag{3-60}$$

As the homogeneous field is Gaussian, the mutually independent, uncorrelated random variables can be obtained from a standard Gaussian distribution [98].

To computationally implement the K-L expansion, it is convenient to use a series expansion involving a finite number of random variables. Thus, a finite dimensional approximation for $H(\mathbf{x},\omega)$, denoted by $\hat{H}(\mathbf{x},\omega)$, is constructed by truncation of the series in Eq.(3-58) i.e.

$$H(\mathbf{x},\omega) \approx \hat{H}(\mathbf{x},\omega) = \mu_{\,H}(\mathbf{x}) + \sum_{i=1}^{\nu_{kl}} \sqrt{\lambda_n}\, \phi_i(\mathbf{x})\, \xi_i, \tag{3-61}$$

where the integer ν_{kl} is chosen such that

$$\texttt{Energy}(\nu_{kl}) = \frac{\sum_{i=1}^{\nu_{kl}} \lambda_i}{\sum_{i=1}^{+\infty} \lambda_i} \geq \tau, \tag{3-62}$$

for a heuristically chosen threshold τ (e.g. $\tau = 90\%$). In practice, as a closed formula for λ_i is not available in general, $\texttt{energy}(\nu_{kl})$ is estimated using a finite (but large) number of eigenvalues, instead of an infinite quantity. This procedure is justified in light of the eigenvalues decreasing property.

The error variance when truncating the expansion after terms, may be

obtained as follows

$$\begin{aligned} \mathrm{Var}\left[H(\mathbf{x},\omega)-\hat{H}(\mathbf{x},\omega)\right] &= \sigma_H^2-\mathbb{E}\left[\left(\sum_{i=1}^{\nu_{kl}}\sqrt{\lambda_i}\phi_i(\mathbf{x})\xi_i\right)^2\right] \\ &= \mathrm{Var}\left[H(\mathbf{x},\omega)\right]-\sum_{i=1}^{\nu_{kl}}\lambda_i\phi_i^2(\mathbf{x}) \end{aligned} \tag{3-63}$$

It is known that the variance of a quantity is always positive. This means that the K-L expansion always under-represents the true variance of the field [133].

One of the main difficulties to apply KL expansion to discrete random fields is the determination of the eigenvalues and corresponding eigenfunctions of the correlation function. Analytical solutions for the Fredholm integral equation in (3-54) are almost never available. However, for some special cases, such as exponential and Gaussian autocovariance functions, an analytical solution can be obtained by converting the integral equation into a differential equation through successive derivatives [119, 120].

Several numerical methods can be used to solve the eigenvalue problem of Eq.(3-54), such as the direct method, projection methods, among others [134, 135]. In this study, the direct method is employed to transform the Fredholm integral equation into a finite dimensional eigenvalue problem, whose the solution provides an approximation for the desired eigenvalues/eigenvectors of the infinite dimensional problem.

In this numerical procedure, a set of M realizations of the random field $H(\mathbf{x})$ and its mean function $\mu_H(\mathbf{x})$ are numerically generated (These numerical realizations are defined in a computational mesh $\mathbf{x}_1,\mathbf{x}_2,\cdots,\mathbf{x}_n$.) and grouped into the matrices

$$\begin{aligned} \mathbf{H} &= \begin{bmatrix} H^1(\mathbf{x}_1) & H^2(\mathbf{x}_1) & \dots & H^M(\mathbf{x}_1) \\ H^1(\mathbf{x}_2) & H^2(\mathbf{x}_2) & \dots & H^M(\mathbf{x}_2) \\ \vdots & \vdots & \ddots & \vdots \\ H^1(\mathbf{x}_n) & H^2(\mathbf{x}_n) & \dots & H^M(\mathbf{x}_n) \end{bmatrix} \\ \boldsymbol{\mu}_H &= \begin{bmatrix} \mu_H(\mathbf{x}_1) & \mu_H(\mathbf{x}_1) & \dots & \mu_H(\mathbf{x}_1) \\ \mu_H(\mathbf{x}_2) & \mu_H(\mathbf{x}_2) & \dots & \mu_H(\mathbf{x}_2) \\ \vdots & \vdots & \ddots & \vdots \\ \mu_H(\mathbf{x}_n) & \mu_H(\mathbf{x}_n) & \dots & \mu_H(\mathbf{x}_n) \end{bmatrix} \end{aligned} \tag{3-64}$$

which are used to define the zero mean matrix $\hat{\mathbf{H}} = \mathbf{H} - \boldsymbol{\mu}_H$. Then, the correlation matrix is estimated with the aid of

$$R_{\hat{\mathbf{H}}} = \frac{1}{M}\hat{\mathbf{H}}\hat{\mathbf{H}}^T, \tag{3-65}$$

and the discrete eigenvalue problem

$$R_{\hat{\mathbf{H}}}\mathbf{\Phi} = \mathbf{\Lambda}\mathbf{\Phi}, \tag{3-66}$$

is solved to obtain the matrices $\mathbf{\Phi}$ and $\mathbf{\Lambda}$, which present approximations for the first M eigenfunctions/eigenvalues on the columns/main diagonal.

For further details on theoretical and practical aspects of K-L expansion the reader is encouraged to see [121, 122, 136, 137].

From Eq.(3-58), the mean square truncation error decreases monotonically with the increase in the number of terms in the expansion. The selection of ν_{kl} depends on the correlation function of the random field. This implies that the more correlated the random field, the smaller the number ν_{kl} required to achieve a desired marginal error. Conversely, if the random field is less correlated, a high number ν_{kl} will be required. Figure 3.3. shows the first twenty eigenvalues of exponential autocovariance function 1D for different sizes of length correlation and their variance error.

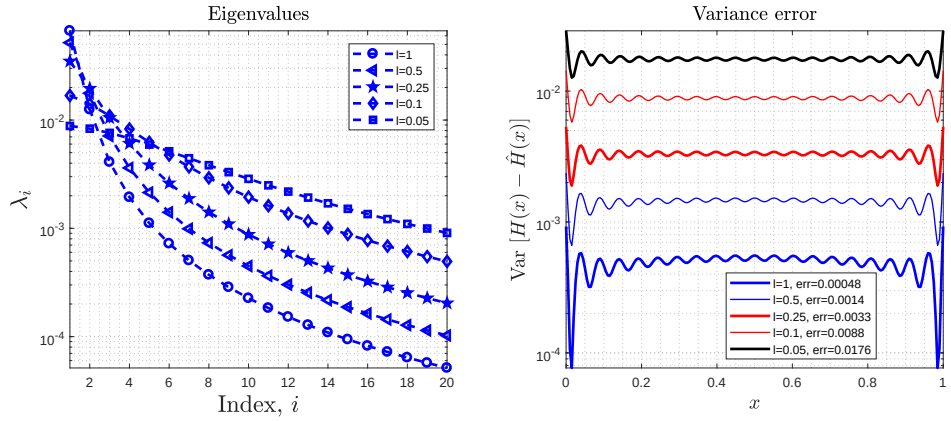

Figure 3.3: Eigenvalues of exponential autocovariance function 1D and variance error

Figure 3.4 illustrates the autocorrelation surface of an exponential kernel and their approximation using an 8-term K-L expansion. Then, it can be observed that both the surfaces are in good agreement.

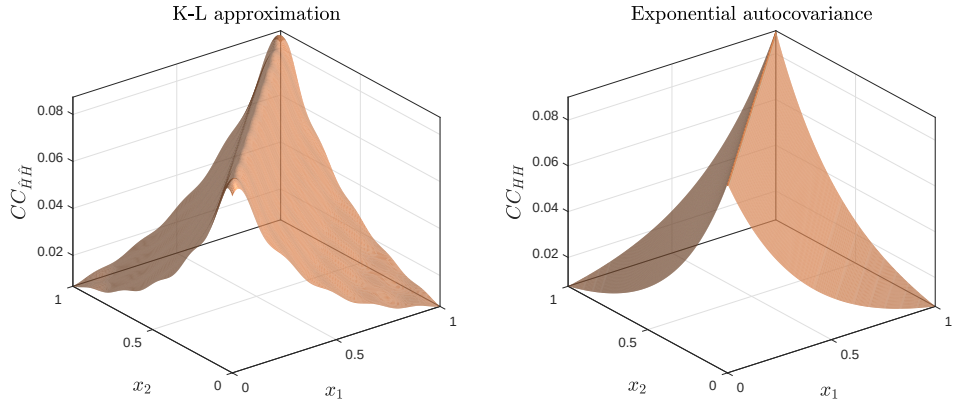

Figure 3.4: Approximated exponential autocovariance function using 8-term K-L expansion.

4
Structural Optimization

This chapter we provides brief background information on structural optimization where the principal aim is to find a structure which can carry with the loads applied doing this in an efficient way. For this, three main optimization techniques can be grouped into Sizing optimization, Shape optimization and Topology optimization whose objective of the optimization can be to minimize the stress weight or compliance for a given amount of material and boundary conditions. In addition, the presence of uncertainties in the optimization problems is treated and studied in this chapter presenting an overvierw the main approaches.

4.1
Mathematical Formulation

According to J.E. Gordon [138], a structure is defined as any assemblage of materials that is intended to support different loads (statics or dynamics).

Optimization means how to make things in the best possible way (optimum) to achieve the desired goal among the several available alternatives. Therefore, structural optimization is a sub-area of structural analysis that allows one to obtain an assemblage of materials to sustain loads in the best way.

Consider the cantilever beam, whose initial geometry and boundary conditions are illustrated in figure 4.1. To find the structure that presents the best performance we first need to specify the term "best". As a first idea, we can try to design a structure as light as possible, i.e., to minimize its weight. Another idea might be to make the structure as stiff as possible, and yet another one could be to make it as insensitive to buckling or instability as possible.

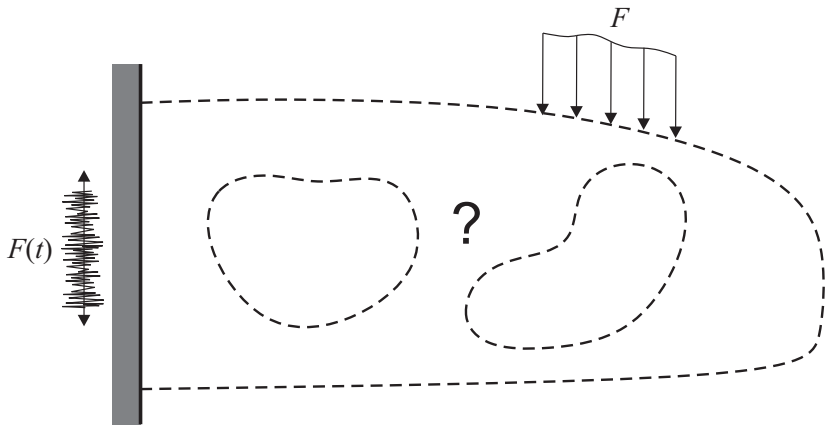

Figure 4.1: Structural Optimization Problem (Adapted from [6])

In structural optimization problems the following functions and variables can be defined as:

- Objective Function (f): This function is used to classify possible designs, i.e., f evaluates possible solutions and returns a number which indicates the characteristics of the design. Usually, we choose f such that a smaller value is better than a larger one (minimization problem). Frequently, in structural optimization f represents: weights, displacements, effective stress, compliance or cost of production;
- Design variables ($\mathbf{x}$): Describes the design of the problem, and can be changed during the process of optimization. Also, it may represent geometry or choice of material. When it describes geometry, it can be related to a sophisticated interpolation of shape or it can be associated to the areas of the bars, or the thickness of a sheet;
- State variable ($\mathbf{y}$): For a given design $\mathbf{x}$ of a mechanical structure, $\mathbf{y}$ is a function or vector that represents the response related to displacements, stresses, strains or forces.

A general Structural Optimization problem can be expressed as:

$$(\text{SO}) = \begin{cases} \text{minimize} & f(\mathbf{x},\mathbf{y}) \text{ with respect to } \mathbf{x} \text{ and } \mathbf{y} \\ \text{subject to} & \begin{cases} \text{behavioral constraints on } \mathbf{y} \\ \text{design constraints on } \mathbf{x} \\ \text{equilibrium constraints} \end{cases} \end{cases} \tag{4-1}$$

We might find a problem with several objective functions, a so-called multiple criteria, or multi-objective optimization problems, i.e.:

$$\text{minimize } (f_1(\mathbf{x},\mathbf{y}), f_2(\mathbf{x},\mathbf{y}), \ldots, f_n(\mathbf{x},\mathbf{y}))$$

where n, is the number of objective functions, and the constraints are the

same as for (SO). To solve these kind of problems, we often use the so-called Pareto optimality. A given design is a Pareto optimal if there is not any design that satisfies all the goals better. In this work we will consider only structural optimization problems of form (SO), i.e. problems with only one objective function.

In 4-1, three types of constraints are indicated:

(1) Behavioral constraints are the ones applied to the variables $\mathbf{y}$. Usually they are written $g(\mathbf{y}) \leq 0$, where g is a function which represents, for example, a displacement in a certain direction;
(2) Design constraints are applied to the design variables $\mathbf{x}$. Obviously, these two types of constraints can be combined;
(3) Equilibrium constraints are usually represented by a partial differential equation. Moreover, in a dynamic structural optimization problem, equilibrium should be seen as the dynamic equilibrium equation.

Moreover, in a naturally discrete problem or in a discretized problem the equilibrium constraints can be expressed as:

$$\mathbf{K}(\mathbf{x})\mathbf{u} = \mathbf{F}(\mathbf{x}) \tag{4-2}$$

where $\mathbf{K}(\mathbf{x})$ is the stiffness matrix of the structure, which generally is a function of the design, $\mathbf{u}$ is the displacement vector and $\mathbf{F}(\mathbf{x})$ is the force vector which may also depend on the design. Note that, in the equation (4-2), the displacement vector $\mathbf{u}$ represents the general state variables $\mathbf{y}$.

4.2 Techniques for Structural Optimization

In this work $\mathbf{x}$ represents some kind of geometrical feature of the structure. Therefore, we divide the problem of structural optimization in three types:

Sizing optimization is a type of optimization where the design variables are associated whit the dimensions of the structures, such as, cross-section areas of bars, thickness of plates, etc.

It is a powerful tool for efficient structural designs, and has been employed by several industries to systematically achieve structural configurations with better performance and reduced cost. Figure 4.2 shows two examples of sizing optimization problems for a truss structure and a bike. Note that, sizing optimization in both designs is used to find an optimal cross-section.

Shape optimization consists of finding the best contour shape of a given structure in order to minimize some cost function, such as, weight, compliance, etc.

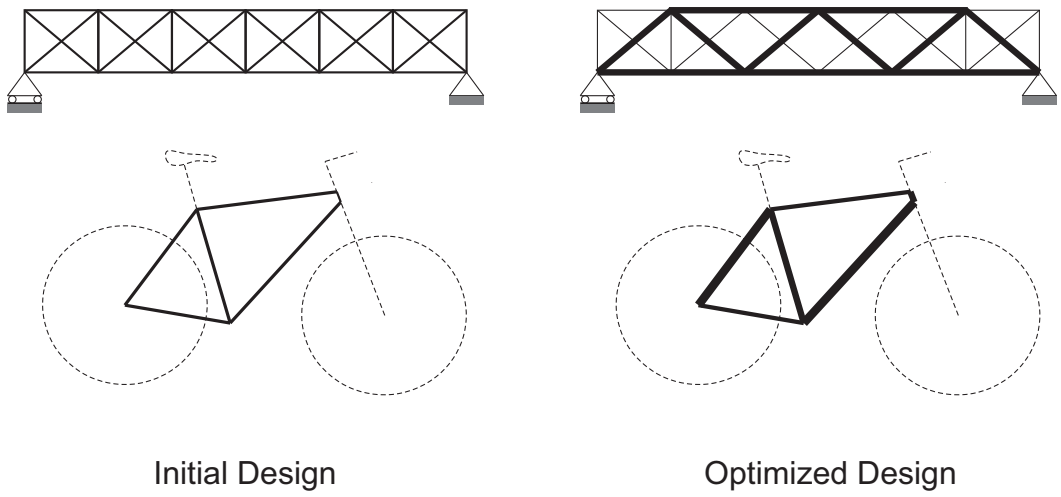

Figure 4.2: Sizing structural optimization problem (Adapted from [7, 8])

Figure 4.3, presents two examples of shape optimization problems for a truss structure and a bike. Note that, the connectivity (or topology) of the structure is not changed by the shape optimization process, i.e. new boundaries are not created.

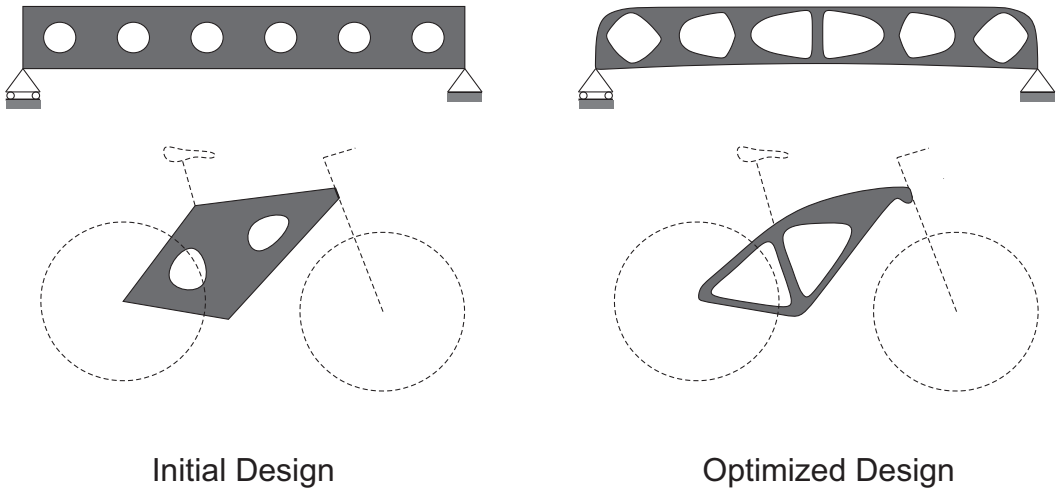

Figure 4.3: Shape structural optimization Problem (Adapted from [7, 8])

Topology optimization is the most general form of structural optimization. This process involves the determination of new layouts of the structures, i.e., the number and location of holes and the connectivity (or topology) of the domain.

Figure 4.4 illustrates two examples of topology optimization problems for a truss structure and a bike. Note that, the original continuum structures are changed during the optimization process by removing material where is not necessary.

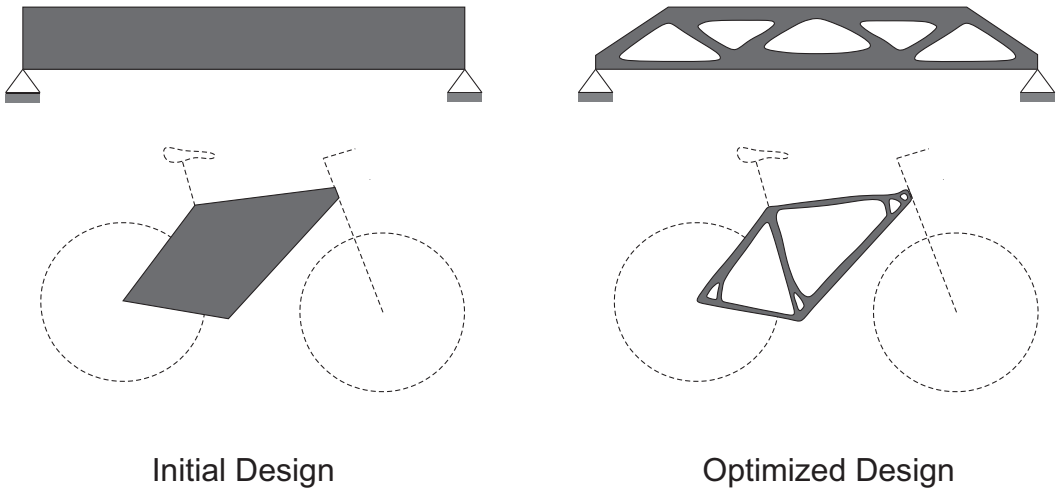

Figure 4.4: Topology structural optimization problem (Adapted from [7, 8])

Topology Optimization differs from shape optimization method in that it seeks the best layout for a structure by optimizing the material distribution in a predefined design domain. The popularity of topology optimization is demonstrated by its widely application in many different fields of engineering. However, most of the applications of topology optimization are limited to deterministic conditions, i.e., the sources of uncertainties are not taken into account.

4.3 Topology Optimization (TO)

The main objective of TO is to find the optimal distribution of materials, for every point $\mathbf{x}$ in a given design domain $\bar{\Omega} \subset \mathbb{R}^d$, $d = 2$ or 3, which maximize a certain performance measure subjected to a set of design constraints, i.e., to determine which regions in $\bar{\Omega}$ should not present material (void regions), and obtain the final topology of the structure.

By convention, points where material exists are represented by a density value of 1, otherwise, the density value is 0. Note that, in this way, one has an integer-programming problem, where the distribution of material is defined by the density map $\boldsymbol{x} \in \bar{\Omega} \mapsto \rho(\mathbf{x}) \in \{0, 1\}$, for

$$\rho(\mathbf{x}) = \begin{cases} 1 & \text{if } \mathbf{x} \text{ is structural member,} \\ 0 & \text{if } \mathbf{x} \text{ is void.} \end{cases} \tag{4-3}$$

4.3.1 Minimum Compliance design

Commonly, the topology optimization problem seeks to minimize an objective function defined by the continuum structure compliance, denoted here by c, subject to a constraint on the final volume of the structure and satisfying the equilibrium equations for a linear Hookean solid material. This formulation, which is equivalent to maximize the structural stiffness subject to the same constraints (see reference [9] for further details), can be stated as

$$\begin{aligned} \min_{\rho} \quad & c\left(\mathbf{u}(\rho),\rho\right) = \int_{\bar{\Omega}} \frac{1}{2}\,\boldsymbol{\sigma} : \boldsymbol{\epsilon}\; d\bar{\Omega}, \\ \text{subject to} \quad & v(\rho) = \int_{\bar{\Omega}} \rho(\mathbf{x})\, d\bar{\Omega} \leq v_S, \end{aligned} \tag{4-4}$$

where $\boldsymbol{\sigma}$ and $\boldsymbol{\epsilon}$ represent the tensors of stress and strain, respectively, v_S is a specified upper bound on the optimized structure volume, and the map $\mathbf{x} \in \bar{\Omega} \mapsto \mathbf{u}(\rho(\mathbf{x})) \in \mathbb{R}^d$ is the continum structure displacement, parametrized by ρ and implicitly defined by the elasticity equations

$$\begin{aligned} \nabla \cdot \boldsymbol{\sigma}(\mathbf{u}) &= \mathbf{0}, \\ \boldsymbol{\sigma}(\mathbf{u}) &= \boldsymbol{\sigma}(\mathbf{u})^T, \\ \boldsymbol{\epsilon}(\mathbf{u}) &= \tfrac{1}{2}\left(\nabla \mathbf{u} + \nabla \mathbf{u}^T\right), \\ \boldsymbol{\sigma}(\mathbf{u}) &= \boldsymbol{\mathcal{C}}(\rho) : \boldsymbol{\epsilon}(\mathbf{u}), \end{aligned} \tag{4-5}$$

and the boundary conditions

$$\begin{aligned} \boldsymbol{\sigma}(\mathbf{u}) \cdot \mathbf{n} &= \boldsymbol{t} \;\text{ in}\, \Gamma_N, \\ \mathbf{u} &= \mathbf{0} \;\text{ in}\, \Gamma_D, \end{aligned} \tag{4-6}$$

where Γ_D is the partition of $\partial\bar{\Omega}$ on which the displacements are prescribed, Γ_N is the complimentary partition of $\partial\Omega$ on which tractions $\boldsymbol{t}$ are prescribed such that $\overline{\Gamma_D} \cup \overline{\Gamma_N} = \partial\Omega$ and $\Gamma_D \cap \Gamma_N = \emptyset$ and $\boldsymbol{\mathcal{C}}(\rho)$ is the $4th$ order stiffness tensor that depends on the density function ρ. As posed, finding ρ and $\boldsymbol{\mathcal{C}}(\rho)$ becomes a large integer programming problem, which can be impractical to solve. Thus, we recast ρ as a continuous scalar field, $\rho(\mathbf{x}) \in [0,1]$. In order to recover the binary nature of the problem, the SIMP [9] model is employed and the stiffness tensor can be expressed as

$$\boldsymbol{\mathcal{C}}(\rho) = \left[\varepsilon + (1-\varepsilon)\rho^p\right]\boldsymbol{\mathcal{C}}^0, \tag{4-7}$$

where $p > 1$ is the penalty parameter, $0 < \varepsilon \ll 1$ is a positive parameter ensuring well-posedness of the governing equations and $\boldsymbol{\mathcal{C}}^0$ is the elasticity tensor of the constituent material, i.e., is Young's modulus of the material in the solid phase corresponding to the density $\rho = 1$.

In terms of computational implementation, the domain is splited into N_e elementary regions, i.e., $\bar{\Omega} = \cup_{e=1}^{N_e} \bar{\Omega}^e$, and the finite element method is employed for the solution of the elasticity equations. Thus, the following finite dimensional version of the optimization problem is considered

$$\begin{aligned} \min_{\boldsymbol{\rho}} \quad & C(\boldsymbol{\rho}) = \mathbf{F}^T \mathbf{U}(\boldsymbol{\rho}) \\ \text{subject to} \quad & V(\boldsymbol{\rho}) = \sum_{e=1}^{N_e} \rho_e \, |\bar{\Omega}^e| - v_S \leq 0, \\ \text{with} \quad & \mathbf{K}(\boldsymbol{\rho}) \, \mathbf{U}(\boldsymbol{\rho}) = \mathbf{F}, \\ & 0 < \rho_{\min} \leq \boldsymbol{\rho}(\bar{\Omega}) \leq 1. \end{aligned} \tag{4-8}$$

where $\boldsymbol{\rho} = (\rho_1, \rho_2, \cdots, \rho_{N_e})$ is a discretized version of the density map, $|\bar{\Omega}^e|$ denotes the volume of the element e, $\mathbf{U}$ is the discrete displacement vector, parametrized by $\boldsymbol{\rho}$ and implicitly defined by the equilibrium equation, $\mathbf{F}$ is the global loading vector and $\mathbf{K}$ represents the global stiffness matrix, which is also dependent on $\boldsymbol{\rho}$. To prevent singularity of the stiffness matrix, a small positive lower bound, e.g. $\rho_{\min} = 10^{-3}$ is placed on the density.

4.3.2 Algorithm

During the solution of a TO problem it is very common to deal with numerical anomalies, such as checkerboards, which are traditionally treated through the use of higher-order elements or filters [139, 140]. However, Talischi et al. [14] have shown that the use of the `PolyTop` framework, which employs polygonal finite elements, can naturally address the checkerboard problem. Besides that, this approach also allows flexibility in the optimization strategy to be used, being compatible with the classical approaches based on the optimality criteria (OC) [141] and the method of moving asymptotes (MMA) [142].

An overview of the classical TO procedure, used in `PolyTop` framework to obtain an optimal design, is illustrated in Figure 4.5. The sensitivity analysis step described in this schematic is explained in details in section 4.3.3.

4.3.3 Sensitivity analysis

Most optimization algorithms use gradients during the optimization steps to reach a solution. Due to the high computational cost associated, sensitivity analysis plays an important role in the field of structural optimization.

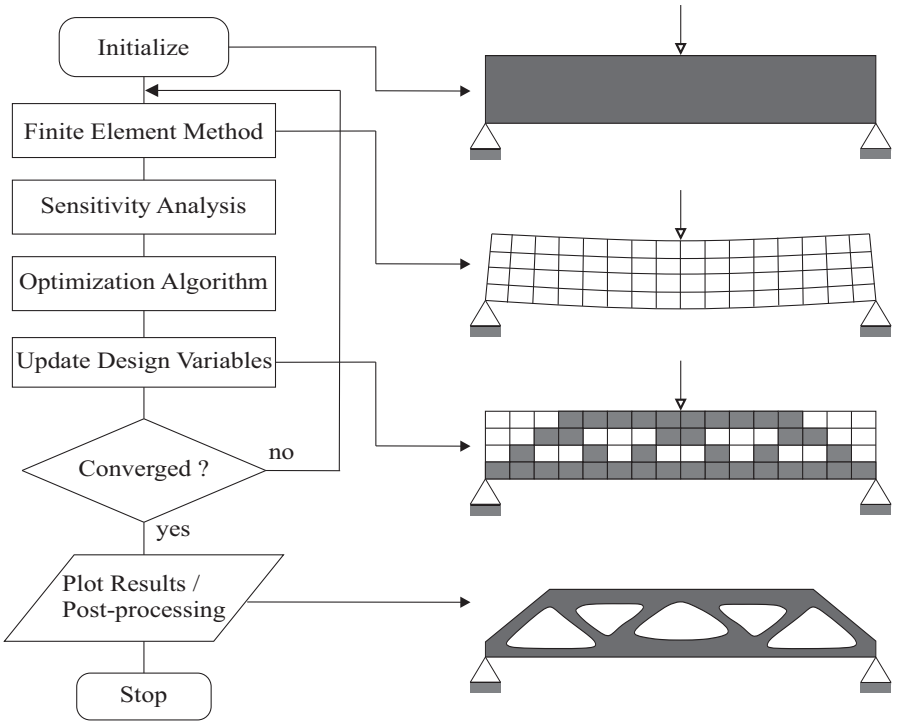

Figure 4.5: Overview of the classical topology optimization procedure (adapted from [9]).

An efficient method to calculate the sensitivity of the objective function with respect to the element design variable is the well-known adjoint method. Its basic idea consists of adding to the objective function the equilibrium equation (4-2), i.e.,

$$C(\boldsymbol{\rho}) = \mathbf{F}^T \mathbf{U} - \boldsymbol{\lambda}^T (\mathbf{K}\,\mathbf{U} - \mathbf{F}), \tag{4-9}$$

where the Lagrange multiplier $\boldsymbol{\lambda}$ is an arbitrary real vector. Then, taking the derivatives of C with respect to the design variable ρ_e, one obtains

$$\frac{\partial C}{\partial \rho_e} = \left(\mathbf{F}^T - \boldsymbol{\lambda}^T \mathbf{K}\right) \frac{\partial \mathbf{U}}{\partial \rho_e} - \boldsymbol{\lambda}^T \frac{\partial \mathbf{K}}{\partial \rho_e} \mathbf{U}. \tag{4-10}$$

By choosing $\boldsymbol{\lambda} = \mathbf{U}$ in Eq.(4-10), the following equation is obtained

$$\frac{\partial C}{\partial \rho_e} \;=\; -\mathbf{U}^T \frac{\partial \mathbf{K}}{\partial \rho_e} \mathbf{U} \tag{4-11}$$

The global stiffness matrix from equation (4-8) can be expressed as

$$\mathbf{K} = \sum_{e=1}^{N_e} \mathbf{K}_e(\rho_e) \tag{4-12}$$

Let $(\mathbf{K}_e)_{ij}$ be the e-th element stiffness matrix,

$$[\mathbf{K}_e]_{ij} = \int_{\bar{\Omega}_e} [\varepsilon + (1-\varepsilon)\rho^p]\, \boldsymbol{\mathcal{C}}^0 \nabla \mathbf{N}_i : \nabla \mathbf{N}_j d\mathbf{x} \tag{4-13}$$

where $\mathbf{N}_i$ is the base of the discrete displacement field and subindex i represent the number of displacement degrees of freedom. The integral inside the summation is the (i,j)-th entry of the stiffness matrix for element $\bar{\Omega}_e$ in the global node numbering.

Then the Eq. (4-13) can be represented as:

$$\mathbf{K}_e = [\varepsilon + (1-\varepsilon)\rho^p]\, \mathbf{K}_e^0 \tag{4-14}$$

where $\mathbf{K}_e^0$ is the element stiffness matrix of the solid material

Then, substituting the equation (4-12) in (4-11) $\frac{\partial C}{\partial \rho_e}$ is expressed as

$$\frac{\partial C}{\partial \rho_e} \;=\; -\mathbf{U}_e^T \frac{\partial \mathbf{K}_e}{\partial \rho_e} \mathbf{U}_e, \tag{4-15}$$

where $\mathbf{U}_e$ denote the displacement vector of the element e and once the partial derivative of the stiffness matrix with respect to the element design variable is computed straightforwardly. , then

$$\frac{\partial C}{\partial \rho_e} = -p\ (1-\varepsilon)\ \rho_e^{p-1}\, \mathbf{U}_e^T\, \mathbf{K}_e^0\, \mathbf{U}_e, \tag{4-16}$$

The gradient of the volume constraint function $V(\boldsymbol{\rho})$ with respect to the design variable ρ_e is given as

$$\frac{\partial V}{\partial \rho_e} = |\bar{\Omega}^e|. \tag{4-17}$$

4.4 Optimization under Uncertainties

We should understand that optimization under uncertainty differs from the field of stochastic programming since there exists a lack of specific mathematical structure that is often found in stochastic programming (e.g. linear objective and constraint functions).

Sometimes optimization under uncertainty can be thought of as a highly nonlinear programming under uncertainty because it involves nonlinear implicit objective and constraint functions and non-deterministic parameters, where the evaluation of these functions might require the execution of expensive computation models (e.g. finite element method, finite volume method, etc).

Optimization under uncertainty is an important line of research due to

the increasing need for robust and reliable designs, where the key objective is to quantify and propagate uncertainties into the optimization process [143].

4.4.1 Robust Design Optimization

Robust optimization, also known as robust design optimization (RDO), is a mathematical procedure that simultaneously addresses optimization and robustness analysis, obtaining an optimal design that is less susceptible to variabilities (uncertainties) in the system parameters. In contrast to conventional optimization, that is deterministic, RDO considers uncertain parameters and statistical measures in the objective function and/or constraint specifications. Figure 4.6, show as comparative between RDO and conventional optimization problem.

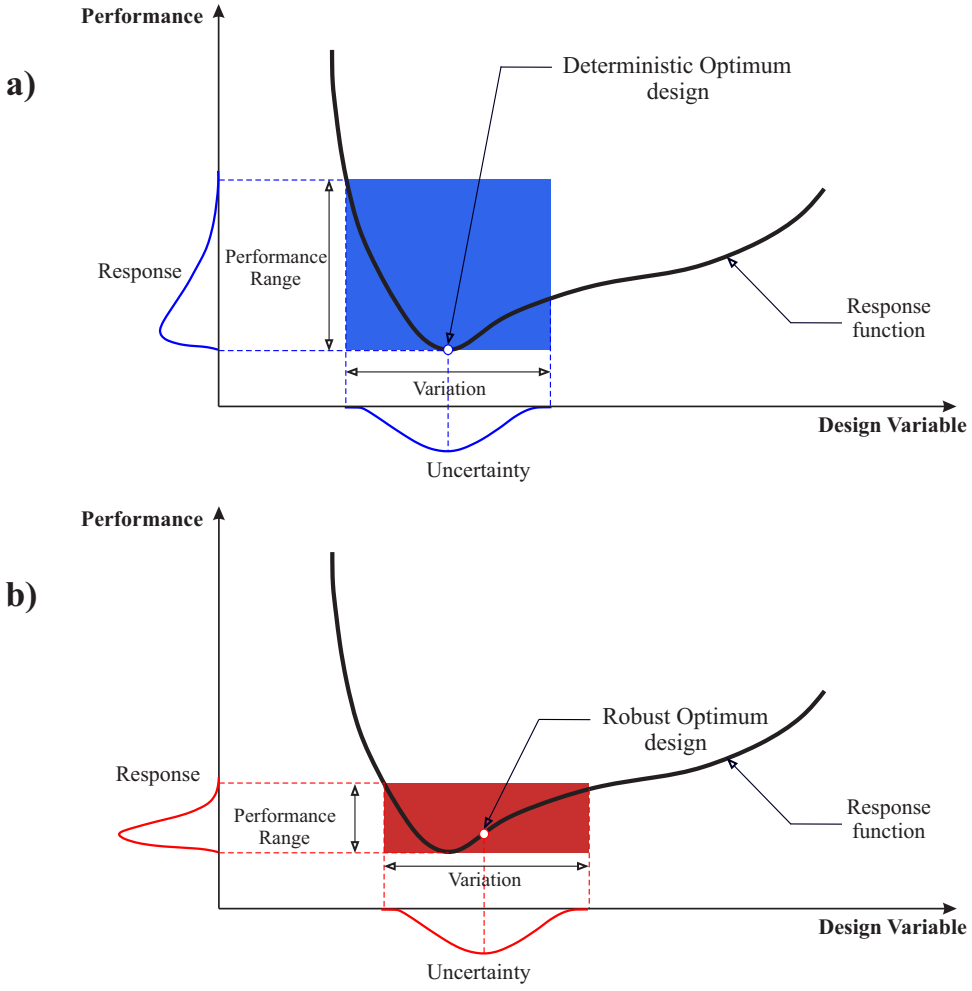

Figure 4.6: Comparison between: a) Conventional deterministic optimization and b) Robust optimization.

From figure 4.6(a), we can see that the performance range increase to small variations of the parameters at the optimal point. Through the

same magnitude of variation for a point near the optimal, we can see that performance range is smaller figure 4.6(b). Therefore, it is important to find a suitable balance between effort and accuracy of the robustness measures with a particular insight on their sensitivity due to random perturbation of design variables or parameters (see references [144, 145]). The general overview of RDO is explained in Figure 4.7,

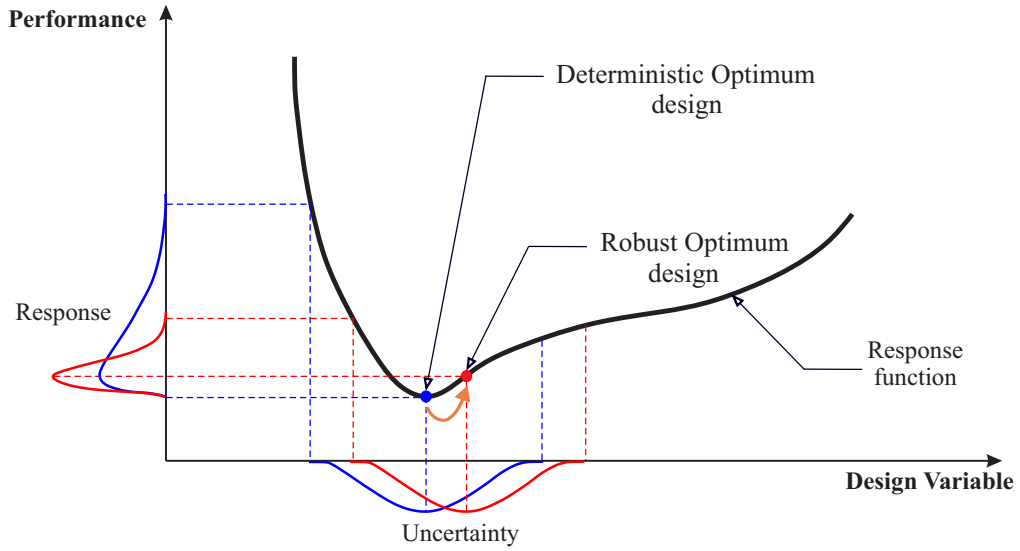

Figure 4.7: Robust Design Optimization (RDO).

RDO is advantageous because seeks to locate a robust optimum with low performance variation directly evaluating robustness measures. Another approaches widely used are the Taguchi method and its variants. According to Taguchi [146, 147], through a systematic method of application of experimental designs, one can achieve a robust design [148].

According to Chen [149], it is important for designers to identify where the uncertainty sources reside in a system model in order to employ an appropriate uncertainty management method. For this reason, the Robust design was categorized in type I and II. The type I is refered to uncertainty in uncontrollable independent system parameters which are known as noise factors. The type II is refered to uncertainty in uncontrollable system variables which are known as control factors. From this same approach a type III is defined in [10] which identify adjustable ranges for control factors (design variable), that satisfy a set of performance requirement targets and/or performance requirements ranges and are insensitive to the variability within the model. Figure 4.8 show the three type of Robust Design.

The general procedure of RDO in this thesis is explained in Figure 4.9, which shows a computational model where the input is subjected to uncertainties — that can be in material or geometrical properties, loadings, boundary

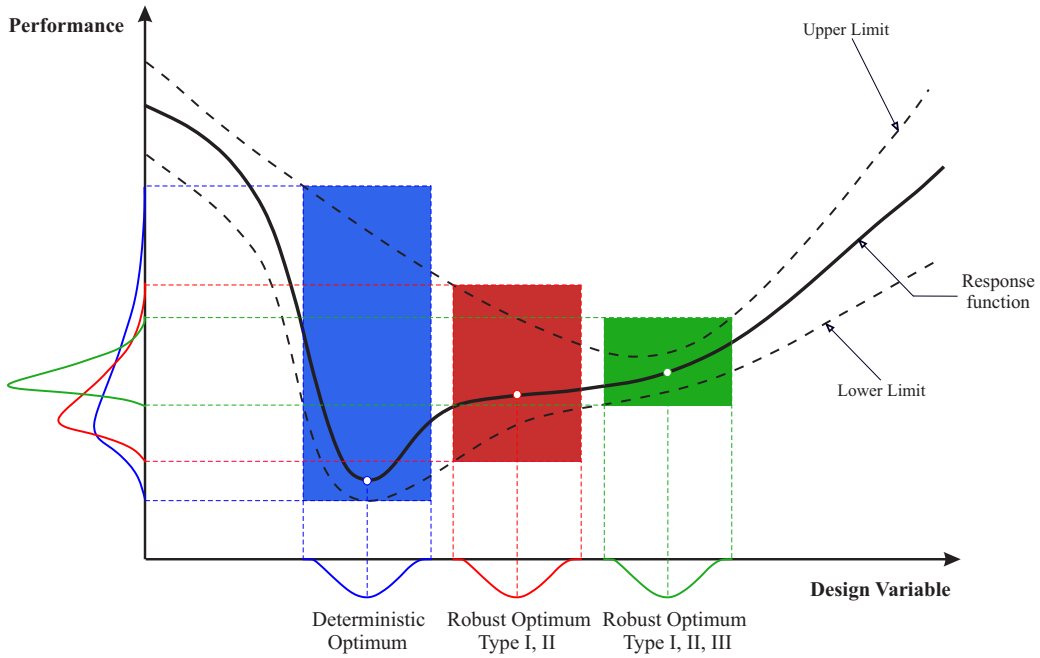

Figure 4.8: An illustration of Type I, II, and III robust design (see reference [10]).

conditions etc. — and, therefore, the model response has a certain probability distribution. This distribution is used to compute some kind of statistical response of the system, which is conveniently used to update the model input, in order to reduce the output uncertainty.

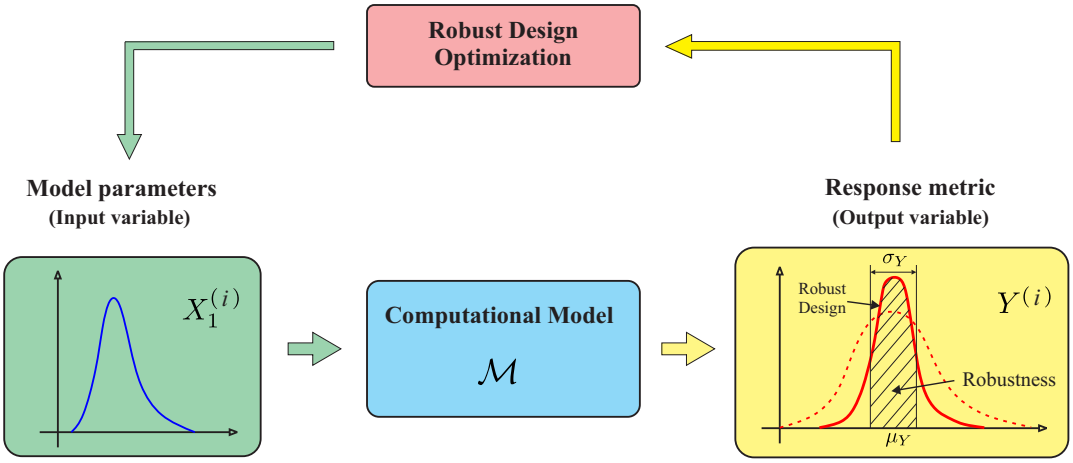

Figure 4.9: Overview of the classical Robust Design Optimization procedure (RDO).

In this context, it is essential to understand the mathematical definition of robustness, i.e., the choice of the robustness measure that is generally expressed by the combination of statistical properties of the objective function. Several definitions of measures of robustness have been proposed in literature

[150–153] and the weighted sum of both the mean and the standard deviation of the objective function is often considered. The tradeoff between these two statistical measures gives rise to a final design that is less sensitive to parameters variations, i.e., a kind of robust design.

Example 4.4.1

This example shows the procedure that RDO performs for finding robust solutions. Consider the objective function that must be minimized:

$$y(x,\xi) = x^4\xi^2 + \xi^3(3x^3 + 2x) + 5\xi$$

where ξ is an arbitrary parameter. If we replace the value of $\xi = 1$ the function y becames as follows

$$y(x) = x^4 + 3x^3 + 2x + 5$$

The unconstrained optimization problem is formulated as

$$x_d^* = \underset{x}{\operatorname{argmin}} \left\{ x^4 + 3x^3 + 2x + 5 \right\}$$

where the optimal solution was found for $x_d^* = -2.3412$.

Now, consider ξ to be a random parameter represented by a normal distribution, i.e., $\xi \in \mathcal{N}(1,1)$ and we want to find the optimal solution of $y(x,\xi)$ that is robust to the variability of parameter ξ. The latter is practically an optimization problem in presence of uncertainties.

To find a robust solution we use weighted sum of the mean and standard deviation value of $y(x,\xi)$. This robustness measure gives an optimal solution that is less sensitive to the variability of ξ.

The mean and standard deviation value of $y(x,\xi)$ can be computed analytically from Eqs. (2-53) and (2-53)

$$\begin{aligned} \mathbb{E}\left[y(x,\xi)\right] &= 2x^4 + 12x^3 + 8x + 5 \\ \sigma\left[y(x,\xi)\right] &= \sqrt{6x^8 + 108x^7 + 540x^6 + 72x^5 + 740x^4 + 180x^3 + 240x^2 + 120x + 25} \end{aligned}$$

In most cases, these analytical expressions are not easily calculable. Therefore, the Monte Carlo Simulation can be used for estimating the mean and standard deviation value through of a set of independent realizations of ξ. Figure 4.10 shows the mean and standard deviation value of $y(x,\xi)$ in function of x.

To get better estimates through MCS, a big number of realization of ξ is necessary. Figure 4.11, shows the error between the analytical value and the

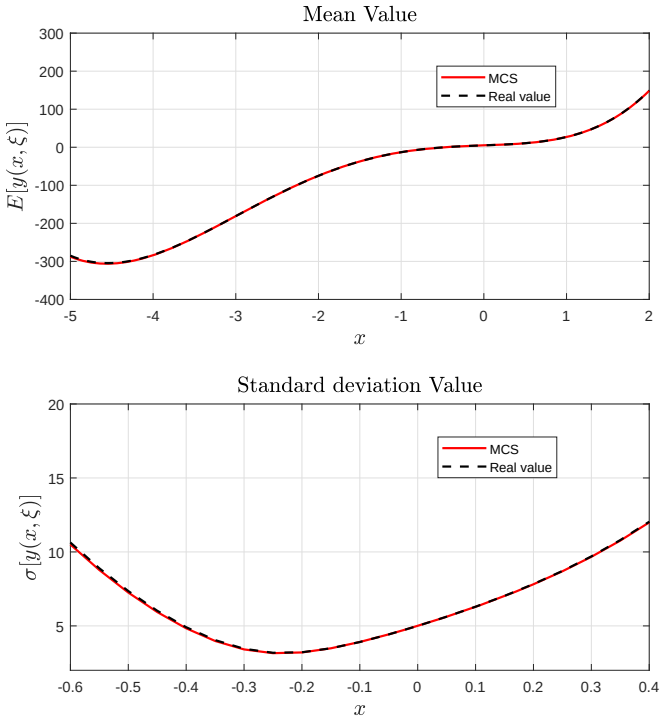

Figure 4.10: Estimation of the mean and standard deviation value of $y(x, \xi)$ through Monte Carlo Simulation usign 1000 realizations.

estimation obtained through different quantities of realizations for ξ. Note that as the number of realizations increases the error tends to be close to zero

Then, the unconstrained optimization problem is formulated as:

$$x_r^* = \underset{x}{\text{argmin}} \left\{ \mathbb{E}\left[y(x,\xi)\right] + \mathsf{k}\,\text{std}\left[y(x,\xi)\right] \right\}$$

where the optimal value was found for $x_r^* = -0.4$. This value is different from that was found when the parameter has its deterministic value. Figure 4.12 show the two objective functions with their respective optimal solutions.

Until now, we found the optimal solution of y when $\xi(\omega)$ is considered a random parameter (uncertainties) and in the case when the ξ takes a fixed value. The difference between two solution is in the robustness of y.

For $x = -0.3225$, the mean and standard deviation value of y was 2.0361 and 3.6864 respectively and for $x = -2.3412$, the mean and standard deviation value of y was -107.6322 and 262.6252 respectively.

From this results, we can conclude that the variation of y is smaller in $x = -0.3225$ that $x = -2.3412$, which means that the function y is more robust to the variability of ξ.

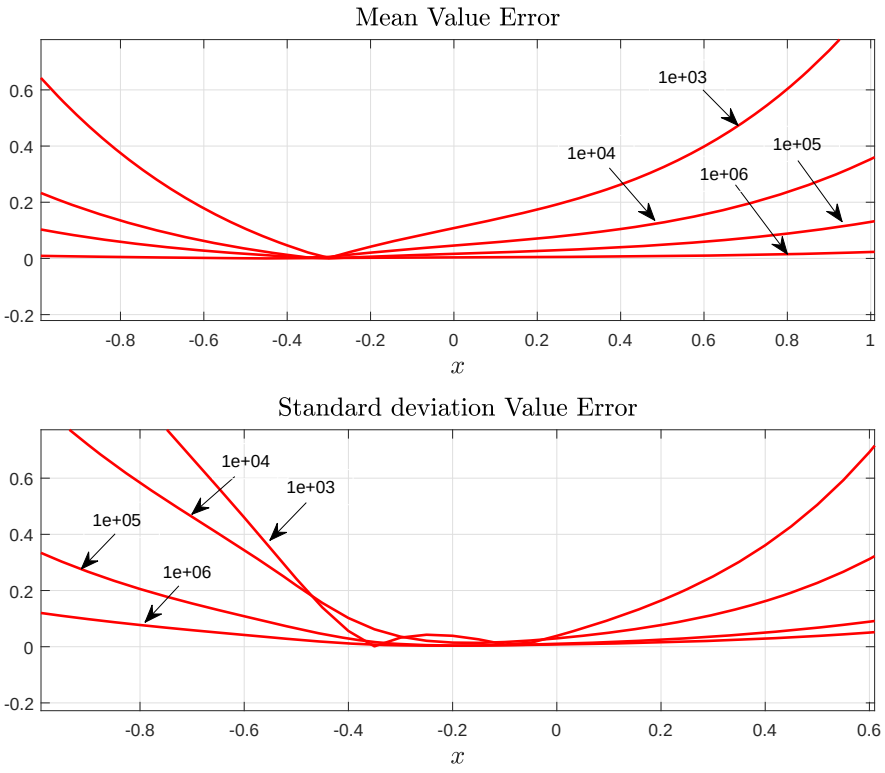

Figure 4.11: The error of estimation of mean and standard value of $y(x, \xi)$ using different quantities of realizations.

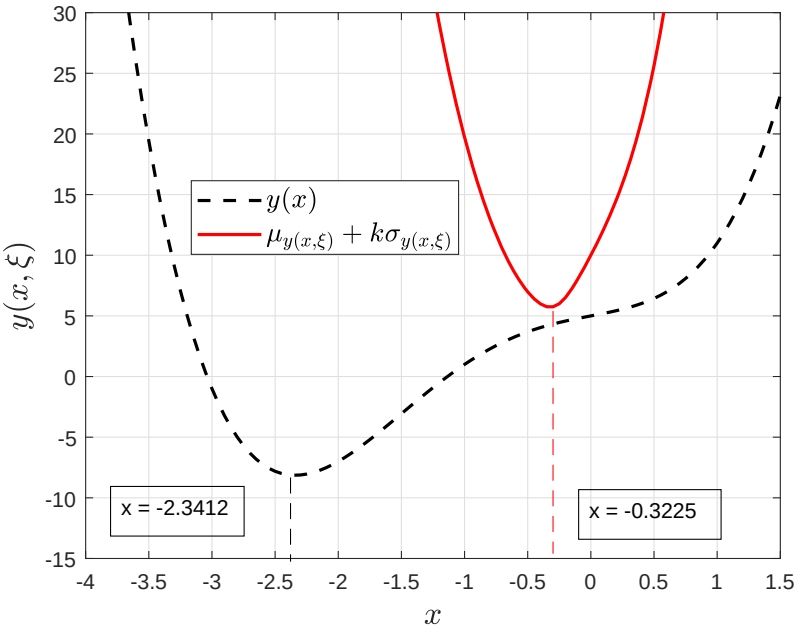

Figure 4.12: Robust and non-Robust solution of the function y.

5
Robust Topology Optimization

In this chapter it is presented the computational strategy to formulate the Robust Topology Optimization. The strategy combines deterministic topology optimization techniques with the generalized polynomial chaos (gPC) for the quantification of uncertainties associated with loading and material properties. The mathematical formulation for computing the statistical measures of complainces are developed. Finally, the calculation of sensitivity of Compliance function is showed using two non-intrusives methods to evaluate the performance of gPC.

5.1
Topology Optimization considering Load uncertainty

In order to increase the optimal design robustness, the concept of robust optimization described in section 4.4.1 can be applied to TO. This possibility is addressed in this thesis where variabilities in the external loading acting on the structure of interest are taken into account. Thus, the force vector and the compliance function become random objects, more precisely, a random vector $\boldsymbol{F}(\omega)$ and a random variable $C(\boldsymbol{\rho}, \omega)$, both defined on the probability space $(\Omega, \Im, P)$.

For the sake of computational implementation, these objects are parametrized by a set of ν_{rv} suitable random variables that are lumped into the random variable $\boldsymbol{\xi}(\omega) = \{\xi_i(\omega)\}_{i=1}^{\nu_{rv}}$ so that force vector and compliance can be expressed as $\boldsymbol{F}(\boldsymbol{\xi})$ and $C(\boldsymbol{\rho}, \boldsymbol{\xi})$.

5.1.1
Mathematical Formulation

This procedure, called robust topology optimization (RTO), can be mathematically formulated as

$$\begin{aligned} \min_{\boldsymbol{\rho}} \quad & \tilde{C} = \mathbb{E}\left[C(\boldsymbol{\rho},\boldsymbol{\xi})\right] + \mathsf{k}\,\sigma\left[C(\boldsymbol{\rho},\boldsymbol{\xi})\right], \\ \text{subject to} \quad & V(\boldsymbol{\rho}) = \sum_{e=1}^{N_e} \rho_e\,|\bar{\Omega}^e| \leq v_S;\ e = 1, 2, \ldots, N_e. \\ \text{with} \quad & \mathbf{K}(\boldsymbol{\rho})\,\boldsymbol{U}(\boldsymbol{\rho},\boldsymbol{\xi}) = \boldsymbol{F}(\boldsymbol{\xi}), \\ & 0 < \boldsymbol{\rho}_{\min} \leq \boldsymbol{\rho}(\bar{\Omega}) \leq 1 \end{aligned} \tag{5-1}$$

$\tilde{C}$ is the objective function of the RTO problem to be minimized and at the same time is the structural performance measure (robustness), so that it is a linear combination between the mean $\mu_{C(\boldsymbol{\rho},\boldsymbol{\xi})} = \mathbb{E}[C(\boldsymbol{\rho},\boldsymbol{\xi})]$ and standard deviation $\sigma_{C(\boldsymbol{\rho},\boldsymbol{\xi})} = \sigma[C(\boldsymbol{\rho},\boldsymbol{\xi})]$ of the random compliance $C(\boldsymbol{\rho},\boldsymbol{\xi})$, which depends on the weight $\mathsf{k} \geq 0$ and on the random displacement map $\boldsymbol{U}(\boldsymbol{\rho},\boldsymbol{\xi})$, implicitly defined by the random equilibrium equation.

The RTO problem defined in (5-1) can be solved by considering non-intrusive methods for stochastic computation. The basic idea of non-intrusive methods is to use a set of deterministic model evaluations to construct an approximation of the desired (random) output response. The deterministic evaluations are obtained for a finite set of realizations of parameter $\boldsymbol{\xi}$ with the aid of a deterministic solver (e.g. finite element code), that is used as a black box. Thus, non-intrusive methods offer a very simple way to propagate uncertainties in complex models, such as structural optimization, where only deterministic solvers are available. In this study the focus is on two non-intrusive techniques, namely, MC simulation [154, 155] and gPC expansion [120, 123].

5.1.2 Low-order statistics for compliance

Monte Carlo Simulation (MCS) method is one of the simplest crude techniques for stochastic simulation and may be used to construct mean-square consistent and unbiased estimations (approximations) — see [154] for details — for $\hat{\mu}_C \approx \mu_{C(\boldsymbol{\rho},\boldsymbol{\xi})}$ and $\hat{\sigma}_C \approx \sigma_{C(\boldsymbol{\rho},\boldsymbol{\xi})}$, respectively defined by

$$\hat{\mu}_C = \frac{1}{\nu_{mc}} \sum_{k=1}^{\nu_{mc}} C^{(k)}, \tag{5-2}$$

and

$$\hat{\sigma}_C = \left(\frac{1}{\nu_{mc} - 1} \sum_{k=1}^{\nu_{mc}} \left(C^{(k)} - \hat{\mu}_C\right)^2 \right)^{1/2}, \tag{5-3}$$

where $C^{(k)} = C(\boldsymbol{\rho}, \boldsymbol{\xi}^{(k)})$, $\boldsymbol{\xi}^{(k)}$ is the k-th realization of the random variable $\boldsymbol{\xi}$

and ν_{mc} denotes the number of MC realizations.

Despite its simplicity, the slow convergence rate of MC method ($\sim 1/\sqrt{\nu_{mc}}$) usually makes it a very expensive stochastic solver in terms of computational cost, particularly for TO problems, where a large number of deterministic model resolutions needs to be obtained to achieve an adequate response characterization. For this reason, a gPC procedure for low-order statistics estimation is also considered in this work.

Using the gPC approach, an spectral representation of the compliance function can be written as

$$C(\boldsymbol{\rho}, \boldsymbol{\xi}) = \sum_{j=0}^{+\infty} \hat{c}_j(\boldsymbol{\rho}) \Phi_j(\boldsymbol{\xi}) \tag{5-4}$$

in a way that, because of properties $\mathbb{E}[\Phi_0] = 1$ and $\mathbb{E}[\Phi_j] = 0,\ j \geq 1$, the mean value of $C(\boldsymbol{\rho}, \boldsymbol{\xi})$ writes as

$$\mu_C = \mathbb{E}[C(\boldsymbol{\rho}, \boldsymbol{\xi})] \approx \hat{\mu}_C^{'} = \hat{c}_0(\boldsymbol{\rho}), \tag{5-5}$$

where an approximation for the gPC coefficient $\hat{c}_0$ is obtained from the linear regression (3-45). This procedure induces a Gaussian quadrature estimation of μ_C, defined by the estimator

$$\hat{\mu}_C^{'} = \sum_{j=1}^{\nu_{gq}} W_j \, C_j, \tag{5-6}$$

where $C_j = C(\boldsymbol{\rho}, \boldsymbol{\xi}_j)$ corresponds to the evaluation of the compliance at the Gauss points and the quadrature weights $W_j = \Psi^{\dagger}_{1j}$ are given by the first line entries of $\boldsymbol{\Psi}^{\dagger} = (\boldsymbol{\Psi}^T \boldsymbol{\Psi})^{-1} \boldsymbol{\Psi}^T$, the pseudoinverse of the $\nu_{gq} \times \nu_{pc}$ regression matrix $\boldsymbol{\Psi}$ defined in Eq. (3-46).

By definition, the standard deviation of compliance is written as

$$\sigma_C = \left(\mathbb{E}\left[C(\boldsymbol{\rho}, \boldsymbol{\xi})^2\right] - \mathbb{E}[C(\boldsymbol{\rho}, \boldsymbol{\xi})]^2\right)^{1/2}, \tag{5-7}$$

so that a procedure similar to that used to construct the estimator of Eq.(5-6) can be adopted now to propose

$$\hat{\sigma}_C^{'} = \left(\sum_{j=1}^{\nu_{gq}} W_j \, C_j^2 - \left(\hat{\mu}_C^{'}\right)^2\right)^{1/2}, \tag{5-8}$$

as an estimator for σ_C.

The gPC-based estimators defined by Eqs.(5-6) and (5-8) provide a very accurate and efficient framework for estimation of the compliance low-order statistics, that demands a small number of deterministic model evaluations, once in practice $\nu_{gq} \ll \nu_{mc}$.

5.1.3 Sensitivity analysis

The partial derivative of the objective function $\tilde{C}$, defined in the optimization problem (5-1), with respect to the element density function ρ_e is given by

$$\frac{\partial \tilde{C}}{\partial \rho_e} = \frac{\partial \mu_C}{\partial \rho_e} + \mathsf{k}\,\frac{\partial \sigma_C}{\partial \rho_e}, \tag{5-9}$$

where the partial derivatives on the right hand side can be approximated, via crude MC, with the aid of the estimators

$$\frac{\partial \mu_C}{\partial \rho_e} \approx \frac{\partial \hat{\mu}_C}{\partial \rho_e} = \frac{1}{\nu_{mc}} \sum_{k=1}^{\nu_{mc}} \frac{\partial C^{(k)}}{\partial \rho_e} \tag{5-10}$$

and

$$\frac{\partial \sigma_C}{\partial \rho_e} \approx \frac{\partial \hat{\sigma}_C}{\partial \rho_e} = \frac{1}{(\nu_{mc}-1)\,\hat{\sigma}_C} \left(\left(\sum_{k=1}^{\nu_{mc}} C^{(k)}\,\frac{\partial C^{(k)}}{\partial \rho_e} \right) - \nu_{mc}\,\hat{\mu}_C\,\frac{\partial \hat{\mu}_C}{\partial \rho_e} \right). \tag{5-11}$$

However, from the point of view of computational cost, it is more efficient to obtain these sensitivity coefficients using the gPC estimators, i.e.

$$\frac{\partial \mu_C}{\partial \rho_e} \approx \frac{\partial \hat{\mu}_C^{'}}{\partial \rho_e} = \sum_{j=1}^{\nu_{gq}} W_j\,\frac{\partial C_j}{\partial \rho_e} \tag{5-12}$$

and

$$\frac{\partial \sigma_C}{\partial \rho_e} \approx \frac{\partial \hat{\sigma}_C^{'}}{\partial \rho_e} = \frac{1}{\hat{\sigma}_C^{'}} \left(\left(\sum_{j=1}^{\nu_{gq}} W_j\,C_j\,\frac{\partial C_j}{\partial \rho_e} \right) - \hat{\mu}_C^{'}\,\frac{\partial \hat{\mu}_C^{'}}{\partial \rho_e} \right), \tag{5-13}$$

obtained from Eqs.(5-6) and (5-8) by differentiation with respect to ρ_e.

5.1.4 Algorithm for robust topology optimization

The results obtained from the TO algorithm, i.e., the compliance and sensitivities, are used to compute statistical measures in a non-intrusive way. Therefore, the RTO algorithm, for problems with uncertain loading, can be described as follows:

1. Topology Optimization Data: define finite element model, set optimizer and underlying numerical and control parameters;
2. Stochastic Model: parametrize aleatory objects with a set of independent random variables defined by the germ $\boldsymbol{\xi}$. Choose an appropriate family of orthogonal polynomials, define weight factor k and gPC order p_{pc};
3. Objective Function
   - for each germ realization $\boldsymbol{\xi}^{(k)}$ perform finite element analysis using Eq.(4-2) and compute compliance sensitivities with Eq.(4-15);

- Compute gPC coefficients from Eq.(3-45);
- Compute statistical estimates for mean and standard deviation with aid of Eqs.(5-6) and (5-8);
- Compute the sensitivity of the objective function from Eq.(5-9).

4. Constraint Function: compute volume constraint using Eq.(5-1) and its sensitivity with Eq.(4-17);
5. Update the design variables $\boldsymbol{\rho}$ according to the optimizer. Repeat from step 3 until convergence is achieved;

A flowchart of the proposed RTO algorithm is depicted in Figure 5.1.

5.2 Topology Optimization considering uncertainties in material properties

The RTO problem in this case consider uncertainty material and it is formulated for minimizing the volume of the structure subjected to the compliance constraint whose limit is chosen for the designer. We must have in mind that for each value of the limit we can obtain a different topology.

5.2.1 Mathematical Formulation

The RTO problem is mathematically formulated as

$$\begin{aligned} \min_{\boldsymbol{\rho}} \quad & V(\boldsymbol{\rho}) = \sum_{e=1}^{N_e} \rho_e \, |\bar{\Omega}^e|; \; e = 1, 2, \ldots, N_e \\ \text{subject to} \quad & \tilde{C} = \mathbb{E}\left[C(\boldsymbol{\rho}, \mathbf{x})\right] + \mathsf{k}\, \sigma\left[C(\boldsymbol{\rho}, \mathbf{x})\right] \leq C_s, \\ \text{with} \quad & \boldsymbol{K}(\boldsymbol{\rho}, \mathbf{x})\, \boldsymbol{U}(\boldsymbol{\rho}, \mathbf{x}) = \mathbf{F}, \\ & 0 < \boldsymbol{\rho}_{\min} \leq \boldsymbol{\rho}(\Omega) \leq 1. \end{aligned} \tag{5-14}$$

The objective function Eq.(5-14) that in this case represents the volume of structure does not depend on the properties of the material related to stiffness, therefore is considered deterministic so that the uncertainties are presented only in the compliance constraint limted for C_s.

5.2.2 Modeling the uncertainty of material properties

Numerous physical phenomena can be modeled using random fields when the variability is over space, i.e., stochastic variation along each dimension. Moreover, in various practical situations, only upper and lower limits are available.

For all these reasons, the Young's modulus is considered as spatially varying uncertain and is described by a 2D non-Gaussian random field.

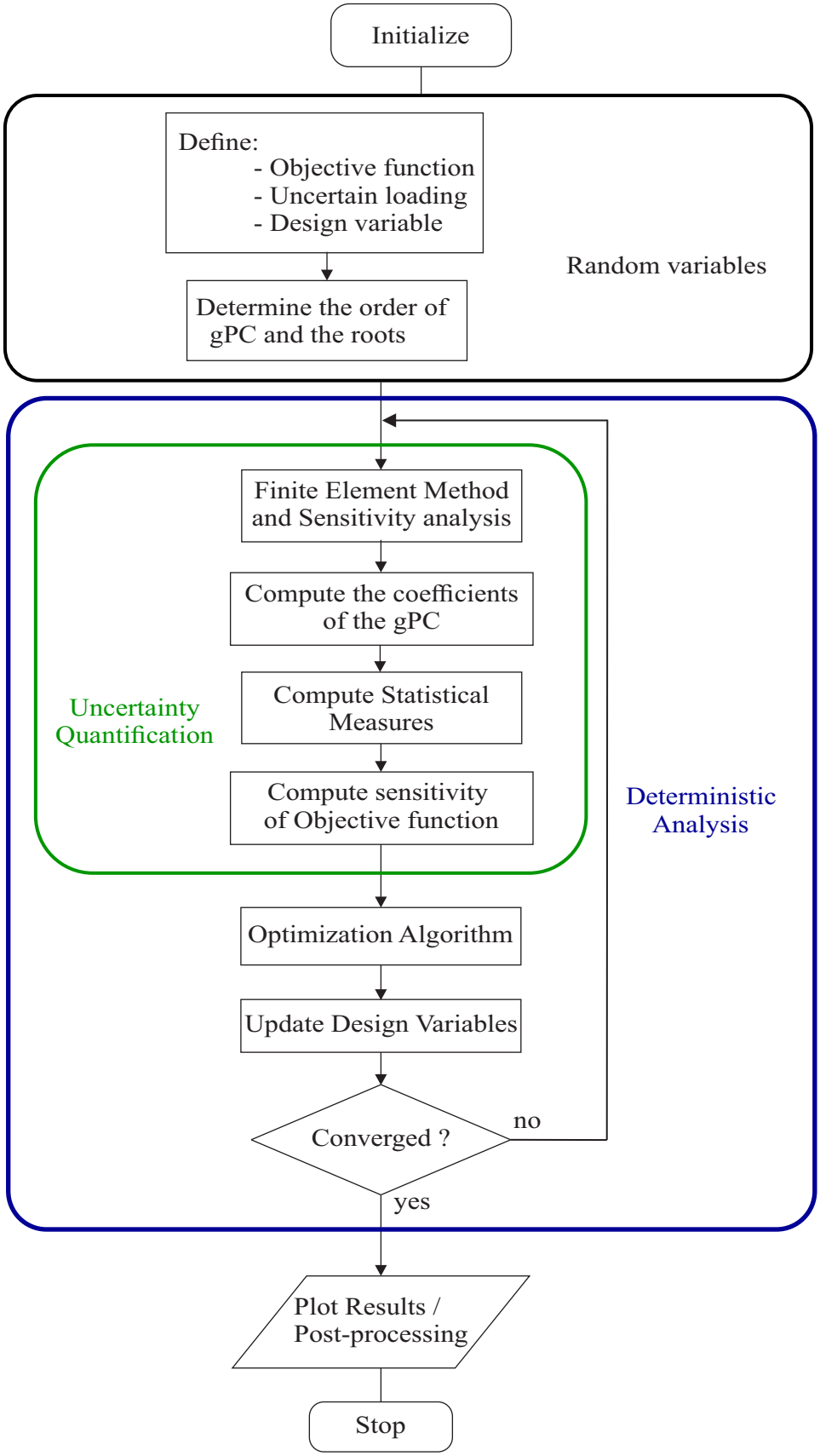

Figure 5.1: General flow chart of the gPC RTO integrated procedure.

Let $H(\mathbf{x})$ be the Gaussian field that represent the Young's modulus and its discretization consist in approximating it by $\hat{H}(\mathbf{x})$, which is defined by means of a finite set of random variables $\boldsymbol{\xi}(\omega) = \{\xi_i(\omega)\}_{i=1}^{\nu_{rv}}$ gathered into a random vector denoted by

$$H(\mathbf{x}, \omega) \approx \hat{H}(\mathbf{x}, \omega) \tag{5-15}$$

From Eq.(2-42)., the Young's modulus can be modeled as

$$E^0(\mathbf{x}, \omega) = g\left[H(\mathbf{x}, \omega)\right], \tag{5-16}$$

where $g(\cdot)$ is a real-valued differentiable function by prescribing the marginal distribution of a non-Gaussian field $E(\mathbf{x}, \omega)$. Then, the memoryless non-linear transformation becomes

$$E^0(\mathbf{x}, \omega) = F_E^{-1} \circ \Phi\left(H(\mathbf{x}, \omega)\right) \tag{5-17}$$

Typically, F_E^{-1} can involve a log-normal, beta, or uniform distribution for modeling the uncertainties in material properties. In this work, the latter is used as the admissible marginal distribution to model the elastic properties. Then, the support of uniform distribution is defined by two parameters, a and b , which are its minimum and maximum values, respectively. Then, Eq.(5-17) becomes

$$E^0(\mathbf{x}, \omega) = a + (b - a)\Phi\left(H(\mathbf{x}, \omega)\right) \tag{5-18}$$

To discretize a non-Gaussian field, the method of translation of field is used and can be interpreted as a memoryless nonlinear transformation of Gaussian field $H(\mathbf{x}, \omega)$. Then, we adopt an empirical and hypothetical model for the Kernel that defines the correlation characteristic of the Gaussian field. Therefore, the random field $H(\mathbf{x}, \omega)$ is described by a 2D Gaussian autocovariance kernel

$$C_{HH}(\mathbf{x}_1, \mathbf{x}_2) = \exp\left(-\frac{\left(x_1 - x_1^{'}\right)^2}{l_1^2} - \frac{\left(x_2 - x_2^{'}\right)^2}{l_2^2}\right) \tag{5-19}$$

where l_1 and l_2 are the correlation lengths parameters in different directions.

Figure 5.2 illustrates the first 12 2D eigenfunctions of the Gaussian Kernel usign correlation lengths $l_1 = 20$ and $l_2 = 15$.

In practice, it is common to distribute the random material properties uniformly over the FE mesh for simplification; however, the inherent material heterogeneity that is related to the manufacturing process implies that it is not necessarily identical. For obtaining reasonable accuracy, we use two types of meshes for the random field and FE, albeit with an identical boundary shape.

Each value of the random field is placed in each nodal point of the mesh.

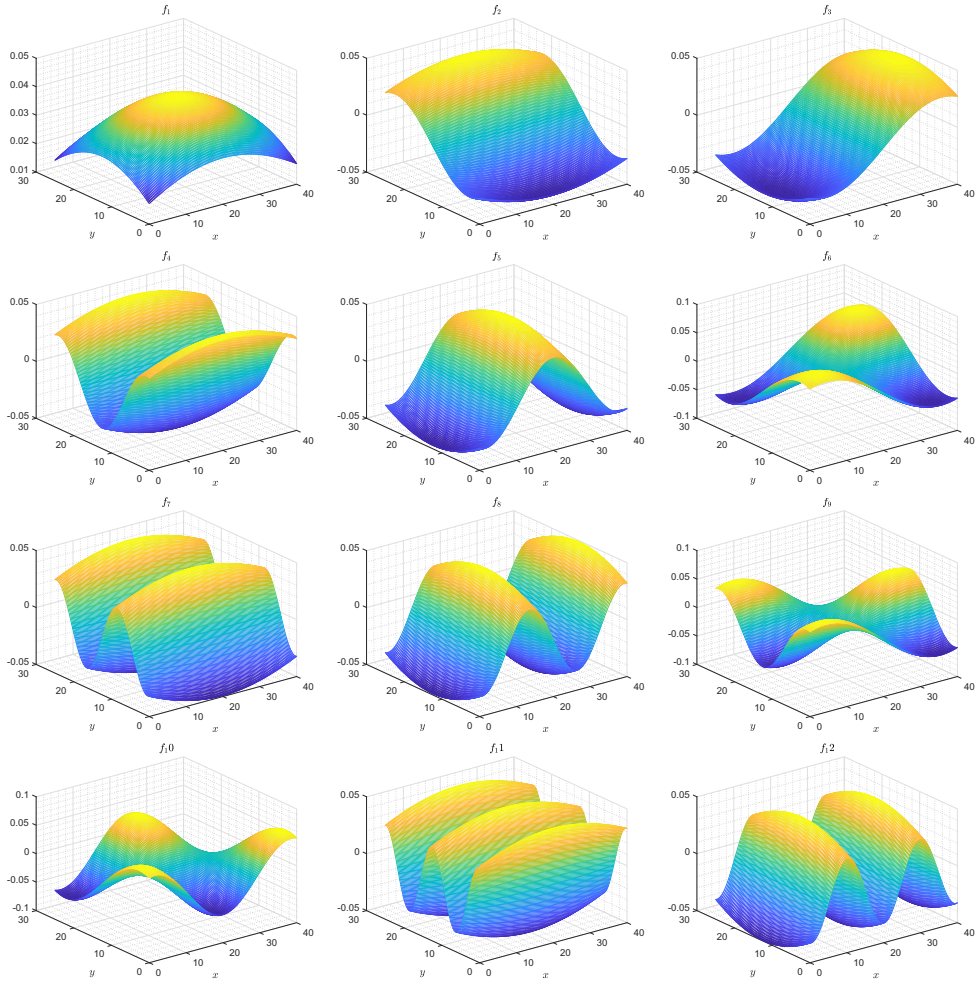

Figure 5.2: 2D Eigenfunction of Gaussian Kernel (Eq.(5-19)).

A regular rectangular mesh was used for the random field to facilitate the discretization. As the RF mesh is different from the FE mesh (because it uses a polygonal mesh) a mapping-interpolation method is required to transfer the spatially-distributed material properties to the centroid of the FE mesh.

Figure 5.3 shows the fundamental concept underlying the mapping-interpolation method.

5.2.3
Low-order statistics for compliance

As was seen in the previous formulation, the mean and standard deviation of the compliance $C(\boldsymbol{\rho}, \mathbf{x})$ is in function of the coefficients of the gPC and they were computed through linear regression.

From Eqs. 3-30 and 3-31, the mean and standard deviation of Compliance given by:

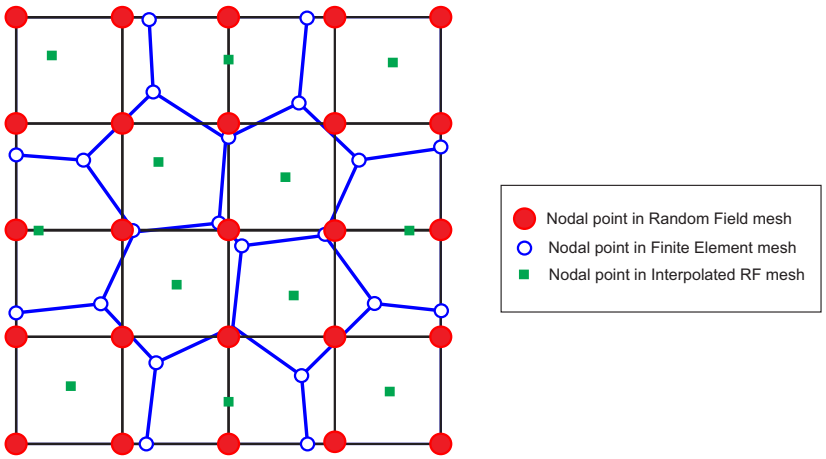

Figure 5.3: Illustration of RF and FE nodal points used for the mapping interpolation .

$$\begin{aligned} \mu_C &= \mathbb{E}\left[C(\boldsymbol{\rho},\mathbf{x})\right], \\ \sigma_C &= \left(\mathbb{E}\left[C(\boldsymbol{\rho},\mathbf{x})^2\right] - \mathbb{E}\left[C(\boldsymbol{\rho},\mathbf{x})\right]^2\right)^{1/2} \end{aligned} \tag{5-20}$$

are represented as

$$\begin{aligned} \hat{\mu}_C^{'} &= \hat{c}_0, \\ \hat{\sigma}_C^{'} &= \sum_{j=0}^{\nu_{gq}} \hat{c}_j^2 \langle \Psi_j^2(\xi) \rangle - \hat{c}_0^2 \end{aligned} \tag{5-21}$$

In this case the coefiicients of gPC is computated through of spectral projection approach.

5.2.4 Sensitivity analysis

The sensitivity of the objective function is straightforwardly determined and is expressed by

$$\frac{dV}{d\rho_e} = \sum_{e=1}^{N_e} |\bar{\Omega}^e| \tag{5-22}$$

From the equilibrium equation $\boldsymbol{K}(\boldsymbol{\rho},\mathbf{x})\,\boldsymbol{U}(\boldsymbol{\rho},\mathbf{x}) = \mathbf{F}$, and Eqs. (4-16;4-14) the partial derivative of the Compliance with respect to the element design variable is straightforwardly computed:

$$\frac{\partial C}{\partial \rho_e} = -p\,\left[1-\varepsilon\right]\,\rho_e^{p-1}\,\mathbf{U}_e^T\,\mathbf{K}_e^0(\boldsymbol{x})\,\mathbf{U}_e, \tag{5-23}$$

The sensitivity of the constraint $\hat{C}$ with respect to the design variable ρ_e is expressed as

$$\frac{\partial \tilde{C}}{\partial \rho_e} = \frac{\partial \hat{\mu}_C^{'}}{\partial \rho_e} + \mathsf{k}\,\frac{\partial \hat{\sigma}_C^{'}}{\partial \rho_e} \tag{5-24}$$

Similarly, with a direct derivative of the equations that compute the statistical measures through the gPC, we can obtain the sensitivity of $\hat{C}$

$$\begin{aligned} \frac{\partial \hat{\mu}_C^{'}}{\partial \rho_e} &= \Big\langle \frac{\partial C(\boldsymbol{\rho}, \mathbf{x})}{\partial \rho_e} \Big\rangle \\ \frac{\partial \hat{\sigma}_C^{'2}}{\partial \rho_e} &= \sum_{j=1}^{\nu_{gq}} \frac{\partial \hat{c}_j^2}{\partial \rho_e} \langle \Psi_j^2(\boldsymbol{\xi}) \rangle \end{aligned} \tag{5-25}$$

if since

$$\frac{\partial \hat{c}_j^2}{\partial \rho_e} = \frac{\Big\langle \dfrac{\partial C(\boldsymbol{\rho}, \mathbf{x})}{\partial \rho_e}, \Psi_j(\boldsymbol{\xi}) \Big\rangle}{\langle \Psi_j^2(\boldsymbol{\xi}) \rangle} \tag{5-26}$$

we substitute it in Eq.(5-25). to determine the sensitivity of the variance

$$\frac{\partial \hat{\sigma}_C^{'}}{\partial \rho_e} = \frac{1}{\hat{\sigma}_C^{'}} \left[\sum_{j=1}^{\nu_{gq}} \hat{u}_j \Big\langle \frac{\partial C(\boldsymbol{\rho}, \mathbf{x})}{\partial \rho_e}, \Psi_j(\boldsymbol{\xi}) \Big\rangle \right] \tag{5-27}$$

5.2.5 Algorithm

The values computed through the TO algorithm, i.e., the compliance and sensitivity information, are used to compute the statistical measures in a non-intrusive manner. Therefore, the topology optimization algorithm for problems with uncertain material properties can be formulated as follows:

1. Initialize the problem to represent the uncertain material properties by using a probabilistic modeling, i.e. through a non-Gaussian random field;
2. A Gaussian field is used for obtaining a non-Gaussian field through the memoryless transformation Eq.(2-42) and a desired marginal CDF;
3. Use the K-L expansion for discretizing the Gaussian field and obtaining the eigenfunction and eigenvalue from the autocovariance function Eq.(3-54);
4. Set the order of the gPC and select the roots of each random variable according to the orthogonal polynomial;
5. Set the boundary condition for the problem and generate the polygonal element mesh with PolyMesh;
6. Solve the finite element equation $\mathbf{K}\mathbf{U}^{(i)} = \mathbf{F}^{(i)} \quad \text{for} \quad i = 1, \ldots, \nu_{gq}$

7. Calculate the sensitivity of the compliance C and with respect to ρ_e according to Eq.(5-22) and (5-23);
8. Calculate the coefficients $\hat{u}_j$ of the gPC using the sparse grid from Eq.(3-44);
9. Calculate the statistical measures ($\mathbb{E}[\cdot]$ and $\sigma[\cdot]$) according to Eqs.(5-21);
10. Calculate the sensitivity of the objective function $\hat{C}$ according to Eqs.(5-25) and (5-27);
11. Update the design variables ρ by the optimizer. Repeat from step 6 until convergence;

Figure 5.4. depicts the flowchart of the proposed TO algorithm.

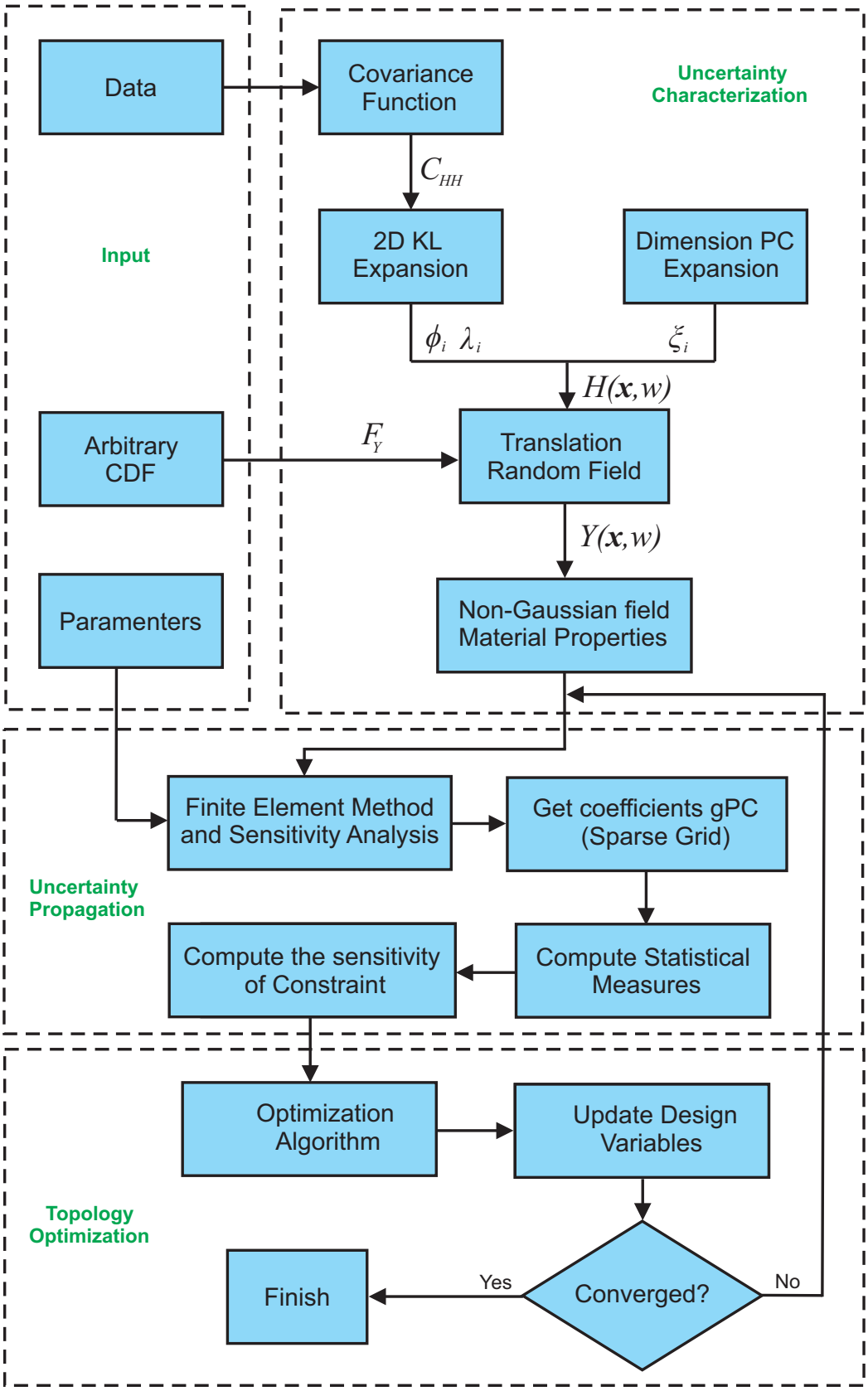

Figure 5.4: General flow-chart of TO algorithm under uncertain material properties.

6
Numerical Results

The effectiveness of the proposed gPC RTO algorithm is addressed in this section by means of a study that considers bidimensional mechanical systems subjected to uncertain loads. The goal is to show that different statistical responses can be obtained when using the proposed gPC RTO design algorithm and a non-robust design strategy, where TO is done first (deterministically) and the propagation of uncertainties is computed later, considering the deterministic optimized topology.

For the sake of accuracy verification, a reference crude Monte Carlo RTO solution is employed. This comparison allows one verify the accuracy of the statistical measures obtained with the proposed gPC approach. The influence of the weight factor in the robust design is also addressed, as well as the different effects that are observed when a random load is treated as a random variable or a random field.

For the examples presented in the following section, consistent units are used.

6.1
Cantilever beam design

As first example, we consider the same example from [156], which a simple cantilever beam subjected to a pair of vertical loads, with uncertain magnitudes, applied at the two right edge corners, such as illustrated in Figure 6.1(a).

The vertical and horizontal dimensions of the structure are 30 and 60 units of length, respectively. The structure is composed of an isotropic material with Young modulus $E_0 = 1$ and Poisson ratio $\nu = 0.3$. For the void material an elastic modulus value equal to $E_{min} = 10^{-9}$ is employed. The prescribed volume fraction of material is set as 0.3, the filter radius as 1.5, the penalization

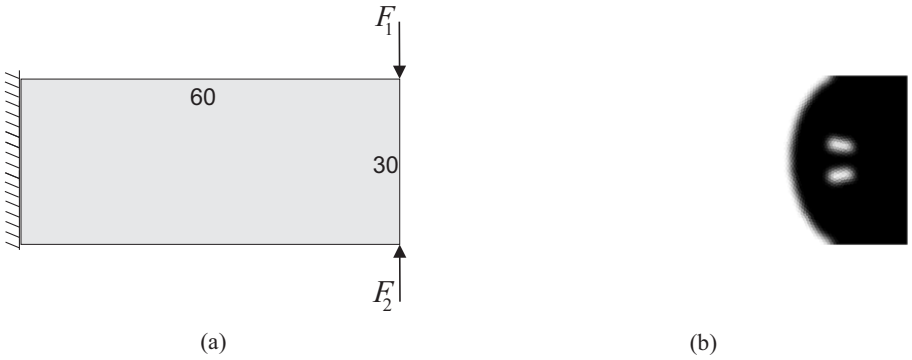

Figure 6.1: Cantilever beam structure: (a) original configuration, (b) non-robust TO design.

factor 3, and the design domain is discretized by means of a polygonal mesh with $N = 7,200$ finite elements. The nominal (deterministic) configuration for this problem adopts the magnitude of the two vertical forces as $F_1 = F_2 = 1$, respectively.

On the other hand, in the stochastic case, magnitudes of the forces are assumed to be uncertain and modeled by independent random variables $w \in \Omega \mapsto F_1(\omega) \in \mathbb{R}$ and $w \in \Omega \mapsto F_2(\omega) \in \mathbb{R}$, both defined on a suitable probability space $(\Omega, \mathfrak{F}, P)$. For the sake of simplicity, but being consistent with the physics of the mechanical problem, it is assumed that these two random variables are uniformly distributed on the same positive support $\texttt{Supp}\, F = [F_{min}, F_{max}] \subset (0, +\infty)$. Three numerical studies are conducted in this example, where $\texttt{Supp}\, F$ is chosen as $[F_{min}, F_{max}] = [0.95, 1.05]$, $[F_{min}, F_{max}] = [0.9, 1.1]$ and $[F_{min}, F_{max}] = [0.8, 1.2]$. Note that these intervals correspond to symmetrical variabilities of up to 5%, 10% and 20% around the mean values $\mu_{F_1} = \mu_{F_2} = 1$, respectively.

The non-robust TO, obtained using the `PolyTop` with MMA optimizer, is shown in Figure 6.1(b). The lack of material on the left side of the cantilever is due to the two forces of equal magnitudes applied in opposite directions. Therefore, the stress in the cantilever is distributed only on the right side of the domain. However, to avoid instability (displacements going to infinity), a minimum value of elastic modulus E_{min} is used.

In order to perform the gPC RTO one needs to define the random variable $\boldsymbol{\xi} = (F_1, F_2)$, which is over the region $[F_{min}, F_{max}] \times [F_{min}, F_{max}] \subset (0, +\infty) \times (0, +\infty)$, so that $\nu_{rv} = 2$. In this case the optimal base for gPC expansion is given by the Legendre polynomials [120]. For the three different types of uniform distribution considered, a weight factor $\mathsf{k} = 1$ is employed, together with an expansion of order $p_{pc} = 5$ (so that $1 + \nu_{pc} = 21$)(this value was heuristically chosen to ensure the stochastic convergence.). A total number

of $\nu_{gq} = 36$ collocation points is used to generate realizations of $\boldsymbol{\xi} = (F_1, F_2)$. To check the accuracy of the gPC RTO strategy, the same problem is addressed using the MC simulation with $\nu_{mc} = 10^4$ scenarios of loading magnitudes, a reference result dubbed MC RTO.

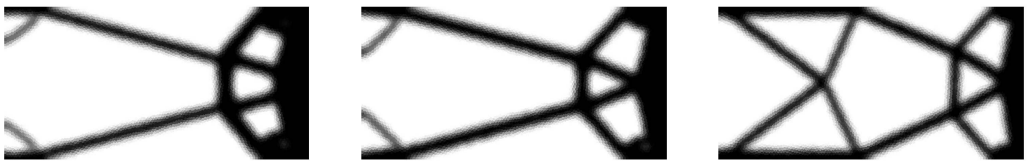

(a) gPC RTO design

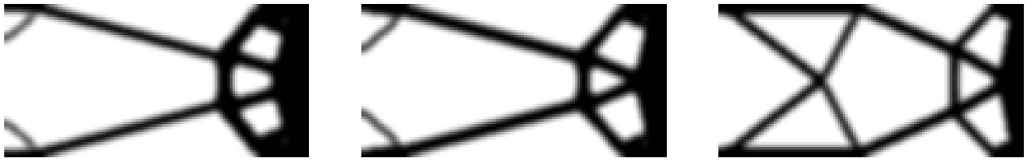

(b) MC RTO design

Figure 6.2: Optimized topologies for the cantilever beam using gPC RTO and MC RTO designs, for uniform distributions over the intervals $[F_{min}, F_{max}] = [0.95, 1.05]$ (left), $[F_{min}, F_{max}] = [0.9, 1.1]$ (center) and $[F_{min}, F_{max}] = [0.8, 1.2]$ (right).

In Figure 6.2 the reader can see the optimum topologies obtained by gPC RTO (top) and MC RTO (bottom), for different support of the random variable F. The topologies shown in Figure 6.2 are different from the deterministic counterparts in Figure 6.1(b) – some extra members can be observed on the left side of the structure – for different levels of uncertainties (length of $\texttt{Supp}\, F$). As the level of uncertainty increases, more members appear in the final topology. Finally, the robust designs using MC simulation present equivalent topologies and statistical measures, which demonstrates the accuracy of the proposed gPC RTO approach.

Table 6.1 compares statistical estimates for the compliance expected value μ_C and standard deviation σ_C, in the cases of robust and non-robust design. Remember that, in this context, non-robust design means first optimizing the topology via classical (deterministic) TO and then using MC simulation to propagate the loading uncertainties through the mechanical system. A good agreement between robust strategies based on gPC and MC is noted, as well as that the statistical measures for the non-robust design tend to approach infinity, since there is no connection between the left and right sides of the domain.It is also worth noting that, while the MC RTO needs 10^4 eval-

uations of the compliance function, the gPC RTO only needs 36 evaluations. This difference of three orders of magnitude demonstrates the efficiency of the gPC RTO implementation.

Table 6.1: Low-order statistics of cantilever beam compliance for robust and non-robust TO strategies.

Supp F	gPC RTO		MC RTO		Non-robust TO	
	μ_C	σ_C	μ_C	σ_C	μ_C	σ_C
$[0.95, 1.05]$	21.4	1.2	21.4	1.2	5.7 E7	6.7 E7
$[0.90, 1.10]$	23.5	2.9	23.4	2.8	2.3 E8	2.7 E8
$[0.80, 1.20]$	29.4	7.7	29.4	7.6	9.1 E8	1.1 E9

6.2 Michell type structure

In this second example RTO is applied on a simple Michell type structure considering three loads, with uncertain directions, applied at the bottom edge of the two dimensional system, as illustrated in Figure 6.3(a).

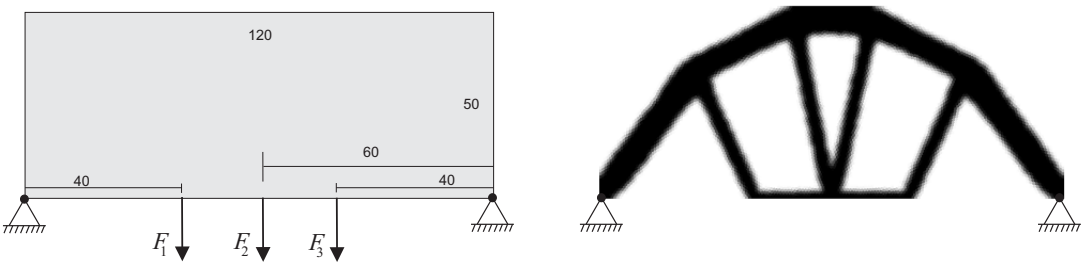

Figure 6.3: Michell type structure: (a) original configuration, (b) non-robust TO design.

The length and height of the structure are equal to 120 and 50 units, respectively. The design domain is discretized with a polygonal mesh with $N = 12,000$ finite elements, and all other parameters are the same as in the first example. For the deterministic case, magnitudes and directions of the three forces are defined as $F_1 = 1$, $F_2 = 2$, $F_3 = 1$, and $\alpha_1 = \alpha_2 = \alpha_3 = -90°$, respectively.

Meanwhile, on the stochastic case, the forces directions are modeled as the independent and identically distributed random variables $\omega \in \Omega \mapsto A_1(w) \in \mathbb{R}$, $\omega \in \Omega \mapsto A_2(\omega) \in \mathbb{R}$ and $\omega \in \Omega \mapsto A_3(\omega) \in \mathbb{R}$. Three scenarios

of probabilistic distribution are analyzed: (i) Normal, (ii) Uniform, and (iii) Gumbel. For the Normal and Gumbel distributions, mean values are assumed to be equal to the nominal values of α_1, α_2 and α_3, with all the standard deviations equal to 10°. In the Uniform case, the three supports are defined by the interval $[A_{min}, A_{max}] = [-100°, -80°]$. The probability density functions of these distributions are illustrated in Figure 6.4.

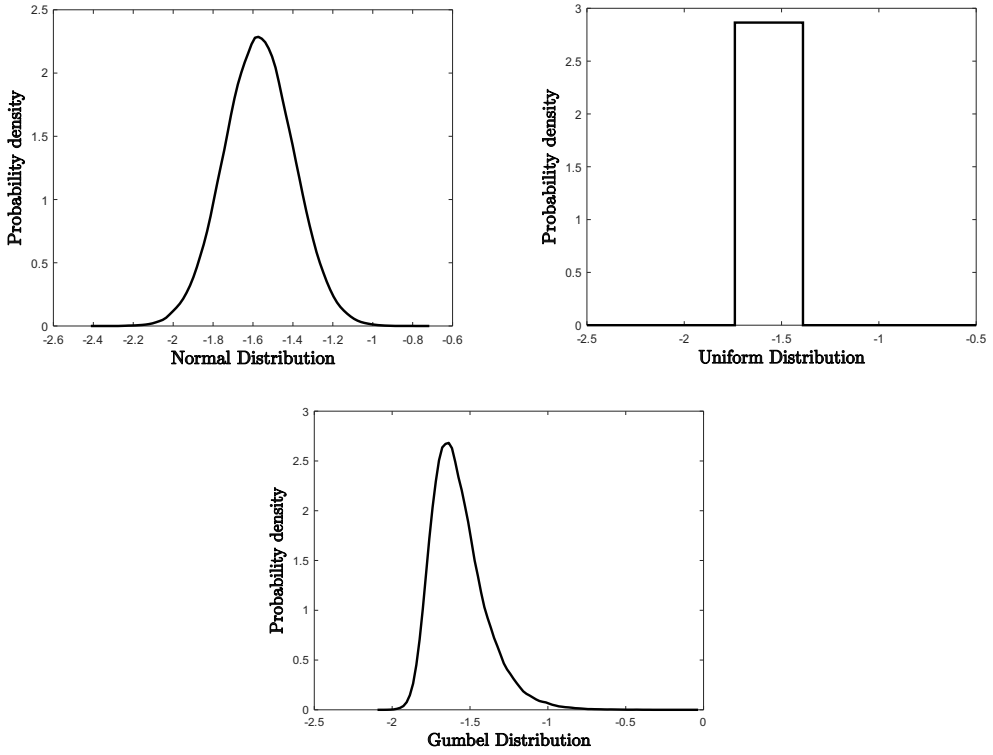

Figure 6.4: Probability distributions for the loads angles: normal (left), uniform (right) and Gumbel (bellow).

Now the random variable is defined as $\boldsymbol{\xi} = (A_1, A_2, A_3)$, thus $\nu_{rv} = 3$, and the family of orthogonal polynomials (basis) is chosen according to the random variable support. For simplicity, Hermite polynomials are used in the case of Gaussian or Gumbel parameters, while Legendre polynomials are the option when the random variable is uniform distributed. Employing gPC RTO with an expansion of order $p_{pc} = 5$ (thus $1 + \nu_{pc} = 56$) total number of $\nu_{gq} = 216$ collocation points and and weight factor value $\mathsf{k} = 1$, one obtains the robust designs shown in Figure 6.5, where connections at fixed points are created to balance the horizontal components of non-vertical forces. Note that the non-robust design in Figure 6.5(b) only presents four bars connected at the forces application points, no connection at the joints can be seen. This occurs because the forces are always vertical. However, when gPC RTO design is used, there are connections at the joints, because the angle variability induces horizontal

force components.

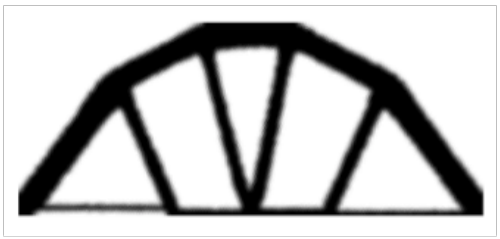

6.5(a): Normal

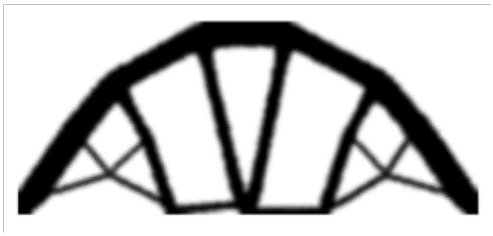

6.5(b): Uniform

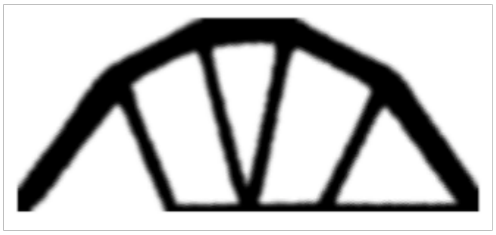

6.5(c): Gumbel

Figure 6.5: Optimized topologies for the Michell type structure using gPC RTO design, with different probability distributions for load angle: (a) Normal, (b) Uniform and (c) Gumbel.

The statistical results of the robust design compared with the non-robust counterpart can be appreciated in Figures 6.6, 6.7 and Table 6.2, which show the compliance probability densities and their low order statistics, respectively, for the different distributions considered in the force angle.

One can observe from these simulation results that the range variability of compliance is reduced, which implies that the robust design is less sensitive to loading uncertainties than its non-robust counterpart. As shown in Figure 6.5, the final topologies are symmetric for the normal and uniform distributions but is asymmetric for the Gumbel distribution.

Table 6.2: Low-order statistics of the compliance for the Michell type structure using robust and non-robust TO strategies.

distribution	gPC RTO		Non-robust TO	
	μ_C	σ_C	μ_C	σ_C
Normal	251.6	6.0	314.2	113.3
Uniform	253.3	5.7	262.7	33.3
Gumbel	249.1	6.7	312.5	128.9

In the second analysis for this example, the influence of the weighting factor in the robust optimization process is addressed. The aim is to minimize

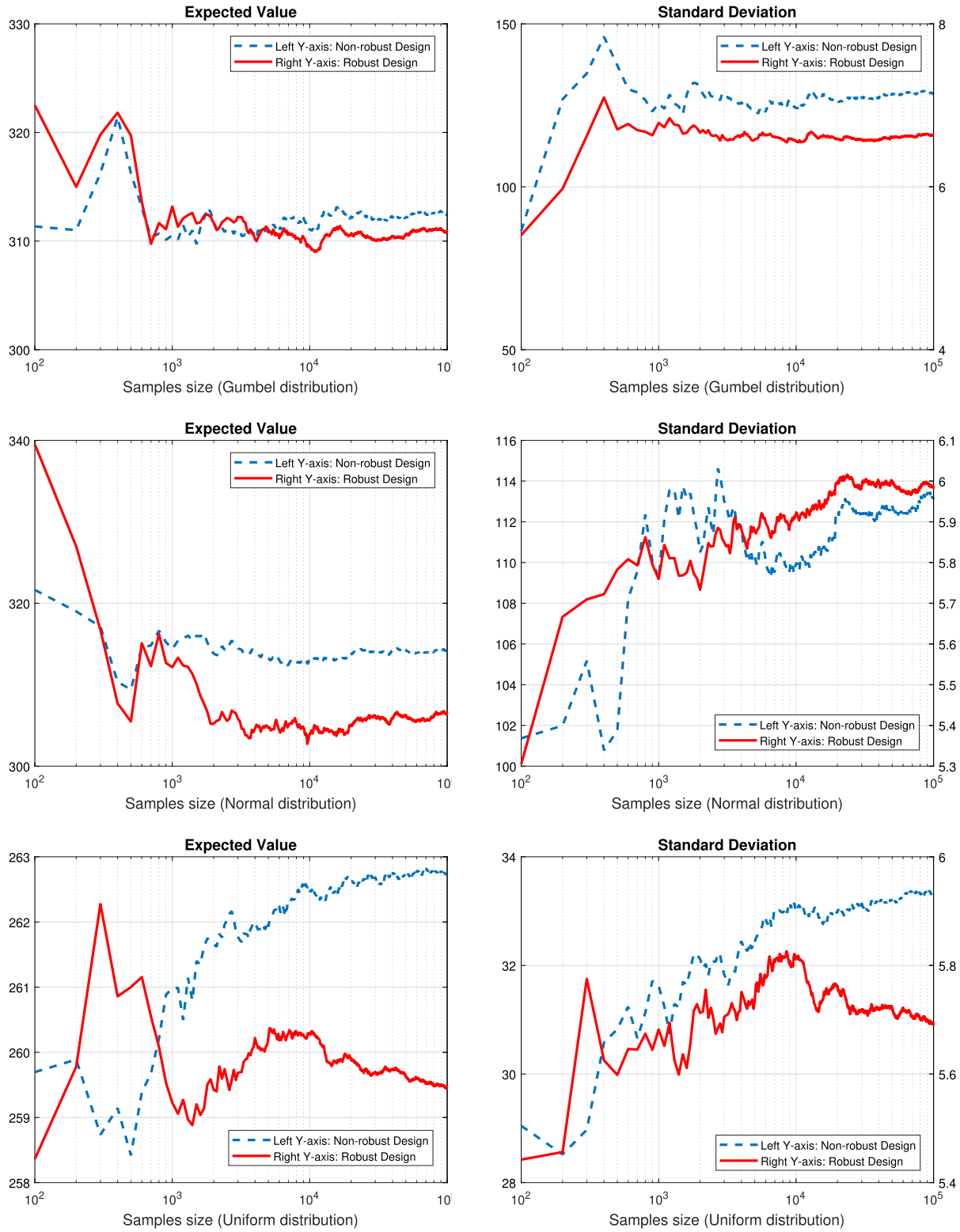

Figure 6.6: Estimation of the mean and standard deviation value of the robust and non-robust design using Monte Carlo simulation.

the variability by increasing the value of k, because this factor is directly related to the standard deviation term on the objective function.

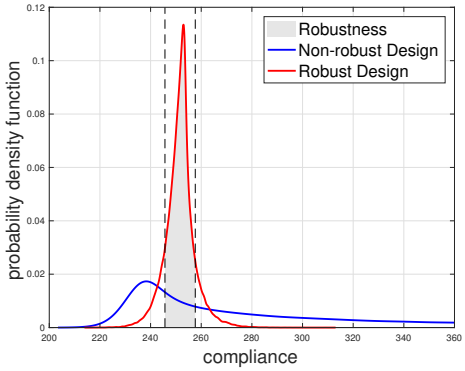

6.7(a): Normal

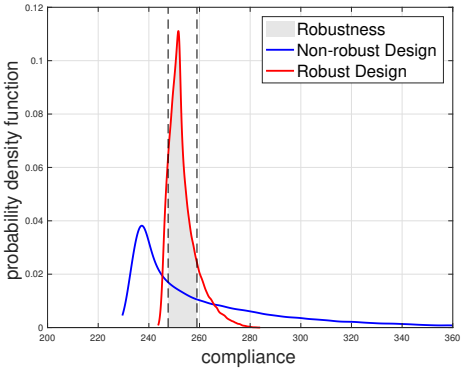

6.7(b): Uniform

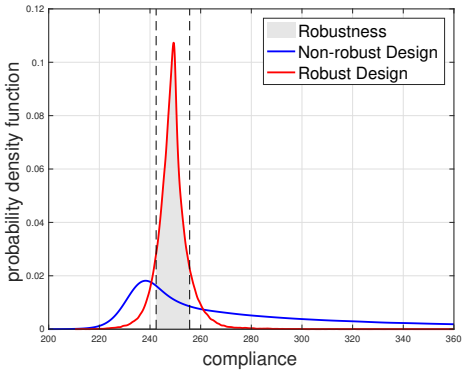

6.7(c): Gumbel

Figure 6.7: Probability density function of the compliance for the Michell type structure using non-robust and gPC RTO robust design, with different probability distributions for load angle: (a) Normal, (b) Uniform and (c) Gumbel.

Three different uniform distributions are considered for the random angle of the force and their supports are respectively defined by the intervals $[A_{min}, A_{max}] = [-95°, -85°]$, $[A_{min}, A_{max}] = [-100°, -80°]$ and $[A_{min}, A_{max}] = [-110°, -70°]$. The gPC RTO design strategy is employed for $\mathsf{k} \in \{0, 1, 2, 3\}$, generating the optimal topologies shown in Figure 6.8.

According to Table 6.3, all the designs shown in Figure 6.8 present significant lower expected compliance and standard deviation values when compared to the non-robust solution. The highest values of standard deviation are obtained using $\mathsf{k} = 0$, since we are minimizing only the expected compliance.

For $\mathsf{k} > 0$, both expected compliance and its standard deviation contribute to the objective function and we can observe that as the value of k increases, the standard deviation decreases. Based on the numerical experiments presented in Table 6.3, we recommend the value $\mathsf{k} = 3$, for practical use, because it leads to the best values of standard deviation with only a slight change in the expected compliance values.

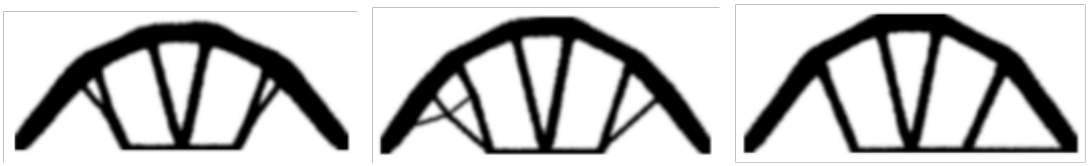

6.8(a): $\mathsf{k} = 0$

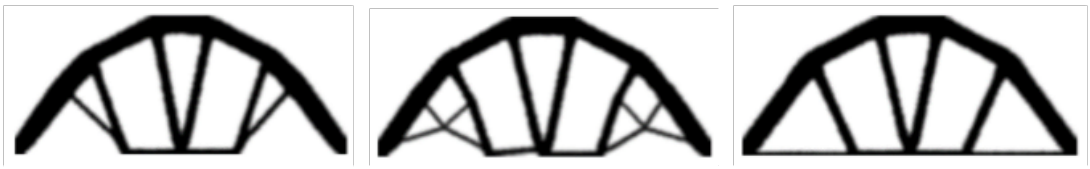

6.8(b): $\mathsf{k} = 1$

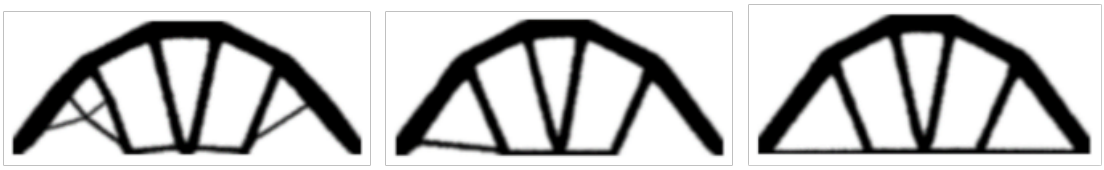

6.8(c): $\mathsf{k} = 2$

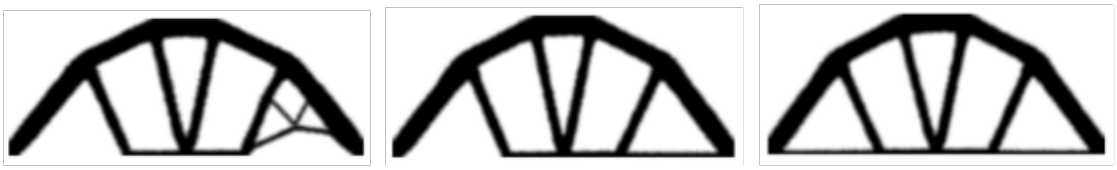

6.8(d): $\mathsf{k} = 3$

Figure 6.8: Optimized topologies for the Michell type structure using gPC RTO strategy, for different values of weight k and different uniform distributions for the angle: $[-95°, -85°]$ (left), $[-100°, -80°]$ (middle) and $[-110°, -70°]$ (right).

Table 6.3: Low-order statistics of the compliance for the Michell type structure using gPC RTO, with different force angles distributions and different weight factors.

		Supp A					
		$[-95°, -85°]$		$[-100°, -80°]$		$[-110°, -70°]$	
	k	μ_C	σ_C	μ_C	σ_C	μ_C	σ_C
gPC RTO	0	241.8	5.2	256.0	10.6	249.0	10.2
gPC RTO	1	247.2	4.3	253.3	5.7	249.2	6.4
gPC RTO	2	253.0	3.1	249.7	4.0	250.0	6.0
gPC RTO	3	248.9	2.4	247.0	2.9	250.1	5.6
Non-robust TO	-	364.4	14.2	366.1	28.4	373.0	56.9

6.3 2D bridge structure

This example corresponds to a simple bridge structure subjected to an uncertain distributed loading at the top edge, as illustrated in Figure 6.9(a).

The nominal load is uniform throughout the structure, with magnitude per unit of length equal to $F = 1$.

For the stochastic case, the load magnitude per unit of length in each point is assumed to be a Gaussian random field $(x, \omega) \in [0, l] \times \Omega \mapsto F(x, \omega) \in \mathbb{R}$ with correlation function

$$C_{FF}(x, x') = \sigma_F \tag{6-1}$$

such that the loads at any pair of points x, x' are fully correlated. The mean and standard deviation of the random field $F(x, \omega)$ are assumed as $\mu_F = 1$ and $\sigma_F = 0.3$, respectively.

For the optimization process, the prescribed volume fraction of material is set as 0.3, the filter radius is set as 3, the penalization factor 3, and the design domain is discretized with a polygonal mesh with $N = 10,000$ finite elements. The non-robust TO of the 2D bridge, performed using `PolyTop` with MMA optimizer, is shown in Figure 6.9(b). Furthermore, the first two rows of finite elements on the top of structure are fixed during the optimization process, to ensure that the bridge remains attached to the loading conditions. Allowing the final results to be more realistic. It is observed in Figure 6.9(b) that the non-robust design leads to a final topology which is similar to the classical case of a 2D bridge under an uniformly distributed load.

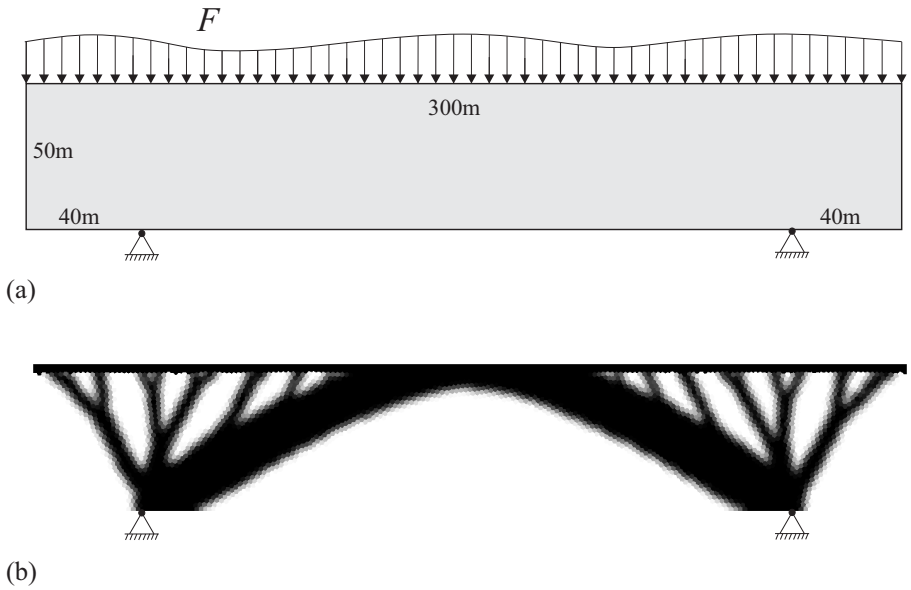

Figure 6.9: 2D Bridge structure: (a) original configuration, (b) non-robust RO design.

For the purpose of numerical computation, the random field $F(x, \omega)$ is discretized by means of $\boldsymbol{\xi} = (F_1)$, a single Gaussian random variable for which low-order statistics are the same as for the random field. The gPC RTO design is obtained using an expansion of order $p_{pc} = 5$ (with $1 + \nu_{pc} = 6$) and a total

number of $\nu_{gq} = 6$ collocation points for Hermite orthogonal polynomials, and weight factor values $\mathsf{k} \in \{0, 1, 2, 3\}$.

The final results are shown in Figure 6.10, where one can observe that some bars connected at the bottom of the bridge are different from those of the non-robust case in Figure 6.9(b). Moreover, as the value of k increases, the structure presents a more robust physical form, which represents a consistent result, because the standard deviation of the compliance is being forced to be smaller. The corresponding mean value and standard deviation of the compliance function, for the different values of k employed, are given in Table 6.4.

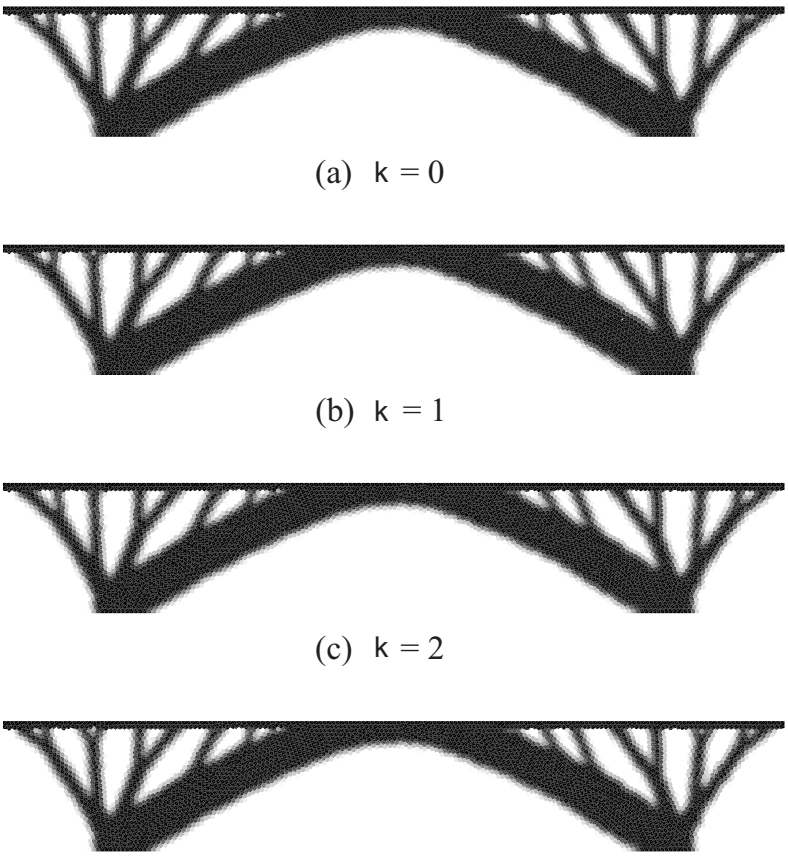

Figure 6.10: Robust design for the 2D bridge structure with fully correlated distributed load, for different values of weight k.

As a second analysis, the random load $F(x, \omega)$ is assumed to have the same low-order statistics as before, but an exponentially decaying correlation function

$$C_{FF}(x, x') = \sigma_F \exp\left(-\frac{|x - x'|}{l_{corr}}\right), \tag{6-2}$$

where l_{corr} is a correlation length for the random field. Note that, by this assumption, the loads at any two points x, x' in the 2D bridge are partially correlated. If the correlation length is increased, a strong correlation is obtained

Table 6.4: Low-order statistics of the compliance for a 2D bridge using gPC RTO and different weight factors.

κ	μ_C	σ_C
0	5.4443 E5	3.0666 E5
1	5.4481 E5	3.0657 E5
2	5.4462 E5	3.0646 E5
3	5.4455 E5	3.0642 E5

between the points x, x', so that $l_{corr} = \infty$ implies a perfectly correlated random field — the previous case where the field depends on a single random variable. On the other hand, when $l_{corr} = 0$, the random field is completely uncorrelated — many independent random variables are necessary for an accurate computational representation. In order to avoid the two limit cases, $l_{corr} = 120$ is chosen.

In terms of computational representation for numerical calculations, the random field $F(x, \omega)$ is discretized with the aid of Karhunen-Loève expansion described in section 3.6. The number of terms in this expansion is chosen in a heuristic way, seeking to satisfy the criterion presented in (3-62). A good compromise between accuracy and computational efficiency is obtained with $\nu_{kl} = 7$. Therefore, the random variable is $\boldsymbol{\xi} = (F_1, F_2, \cdots, F_{\nu_{rv}})$, a set of $\nu_{rv} = 7$ independent Gaussian random variables for which low-order statistics are the same as for the random field. Then, for this case we use a total number of $\nu_{gq} = 279936$ collocation points.

A comparison between non-robust and gPC RTO design, for $\mathsf{k} = 1$ and the different types of distributed load considered, are shown in Figure 6.11. The difference between the three obtained topologies is very clear, and can also be appreciated in Table 6.5, which shows the low-order statistics of the compliance in all cases analyzed.

Table 6.5: Low-order statistics of the compliance for a 2D bridge considering different design scenarios.

Non-robust TO		RTO full corr		RTO partial corr	
μ_C	σ_C	μ_C	σ_C	μ_C	σ_C
5.449 E5	3.076 E5	5.448 E5	3.066 E5	2.361 E5	9.708 E4

This example clearly shows that the nature of the distributed load has a significant effect on the RTO. Also from Table 6.5, it is possible to see that the compliance low-order statistics for a 2D bridge under a distributed load,

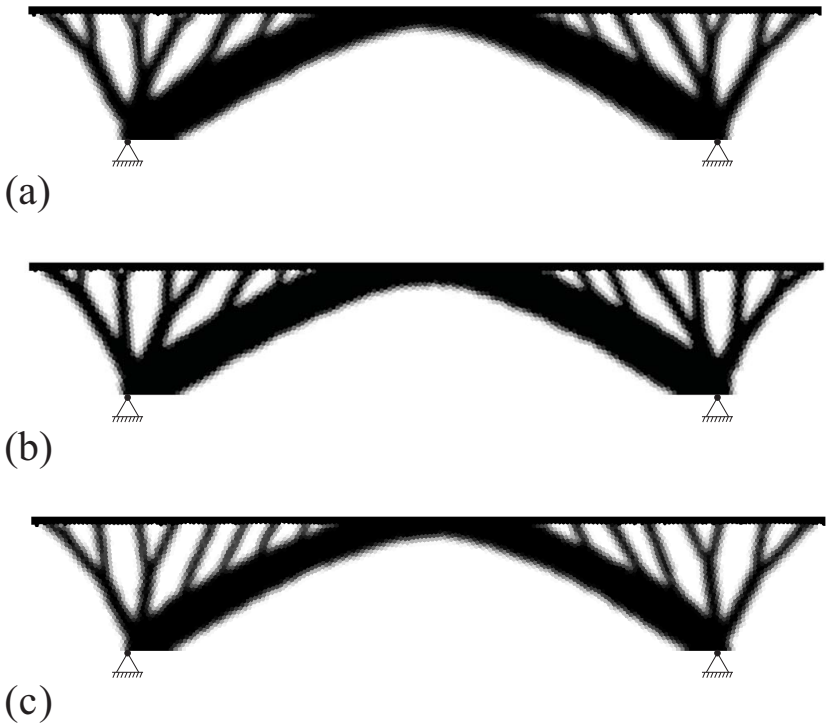

Figure 6.11: Optimized topologies for the 2D bridge structure: (a) non-robust TO with fully correlated load, (b) gPC RTO with fully correlated load, (c) gPC RTO with partially correlated load.

emulated by a partially correlated random field, are smaller than those for a fully correlated field.

6.4 Cantilever beam

This example considers a simple 2D Cantilever beam subjected to a vertical point load P applied in the middle right end. The design domain geometry is defined as L long, $5L/8$ height and $L/40$ thickness as illustrated in Figure 6.12(a). The topology optimization of cantilever for a deterministic configuration adopt a structure with isotropic material and a constraint of compliance $C = (4000P)/EL$, where E is the Young's modulus considered for all elements. The structure is discretized using 136 by 85 polygonal element mesh, a minimum allowable filter radius equal to $0.0185L$, and the penalization factor equal to 3. The values of P, L and E are defined as 1, 40 and 100 respectively. Therefore, we obtain the topology optimization for the deterministic case a minimum volume equal to 0.233, and is showed in Figure 6.12(b).

For the robust design, we consider material uncertainty, specifically being the Young's modulus of each polygonal element. Commonly, several works

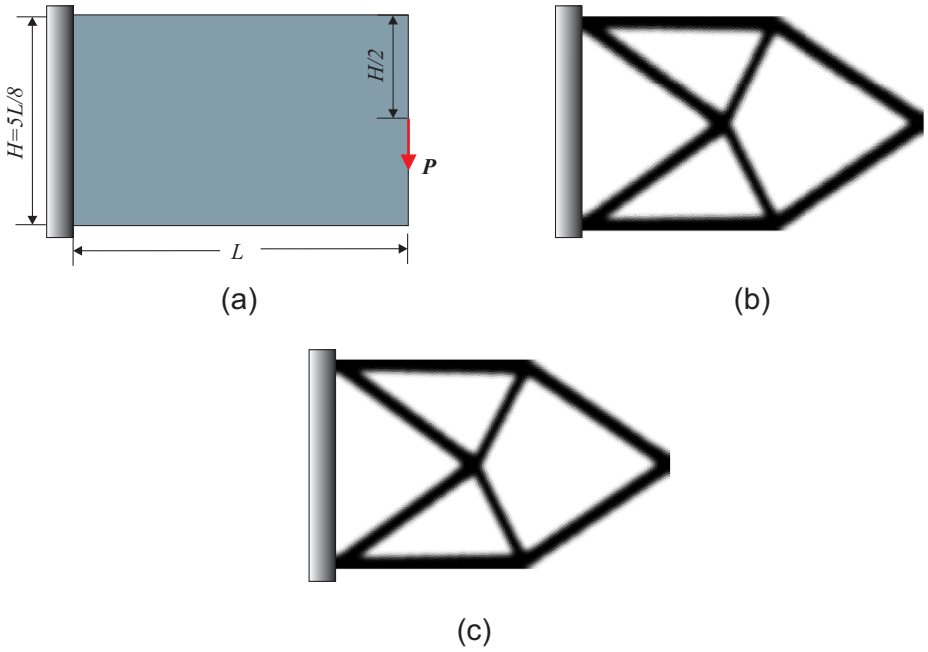

Figure 6.12: 2D Cantilever Beam. (a) Design domaind geometry. (b) Minimum volume under determinitics conditions. (c) Minimum volume under uncertainty conditions

choose to use Gaussian fields to represent the Young's modulus due to their simplicity and well-established properties. For reasons of comparison, the Cantilever beam example was take from [59], where an Log-normal Gaussian field was used for representing the variability of the material uncertainty and its propagtion was intrusively.

In this example, we represent a spatial variability through a 2D Gaussian and Non-Gaussian Homogeneous field with expected E and standard deviation value equal to $0.25E$. Therefore, for discretizing Gaussian fields, we use the K-L expansion presented in 3.6 with a correlation length $L/2$, $H/2$. Using $\nu_{kl} = 7$ uncorrelated random variables, we obtain a good approximation of Gaussian field. In Figure 6.13, are showed the eigenvalues and variance error with a Energy equal to 0.8987.

We test the formulation proposed using a Log-normal Gaussian field with equal conditions to the example from [59]. The constraint presented in Eq.(5-14) using a $\mathsf{k} = 0$ is estimated through the PCE of order 3. Thus, we obtain a minimum volume equal to 0.247. The result of optimization is showed in Figure 6.12(c).

From these results, we can see that the topologies obtained in the deterministic or stochastic case are similar. But the main idea is to know which topology is more robust to the variability caused by the uncertain material. Then, using the topology of structure obtained in deterministic

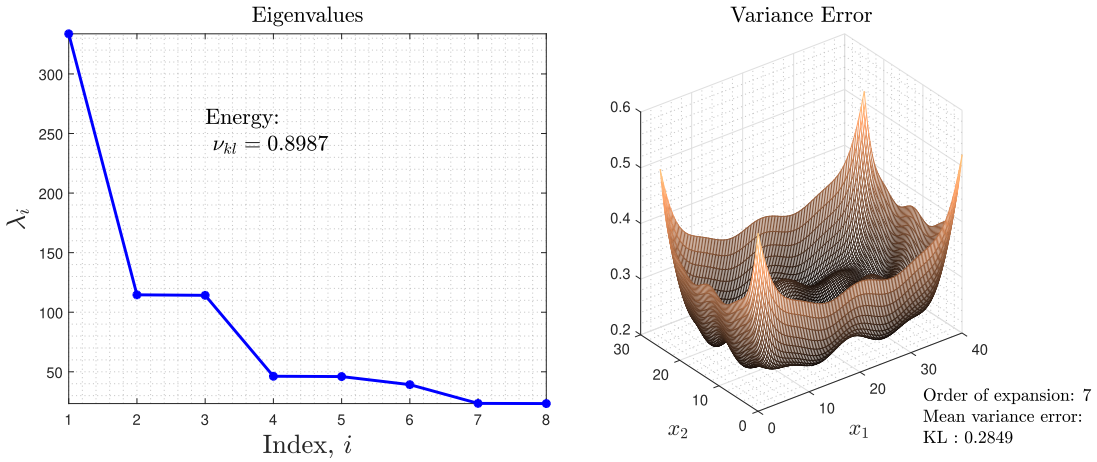

Figure 6.13: Approximation by truncated K-L expanson with 7 terms .

case, we calculate the expected value and standard deviation of volume using the ensembles of random field being the values obtained 0.281 and 0.181 respectively.

In Table 6.6, the fisrt column shows the results obtained from [59] and the second column shows the results using our algorithm both for diferent values of k. The main differences of between two formulation highlights in the use of polygon elements and the non-intrusive strategy for estimating the expected and standard deviation of compliance. Therefore, from Table 6.6 can be seen that the values are very similar.

Table 6.6: Comparison of Intrusive and Non-Intrusive Methods using Log-normal Gaussian field.

	[59]		Formulation proposed		
k	μ_C	σ_C	μ_C	σ_C	Vol
0	1.000	0.131	1.000	0.135	0.249
1	0.885	0.115	0.881	0.118	0.273
2	0.793	0.103	0.787	0.106	0.298
3	0.719	0.094	0.712	0.096	0.320
4	0.658	0.086	0.649	0.087	0.350
5	0.606	0.079	0.597	0.081	0.375

From a Gaussian Field with autocovariance function presented in Eq.(5-19). we obtain a Non-Gaussian field through of a non-linear transformation using a marginal uniform distribution as shown in Figure 6.14.

To visualize the influence of the spatial variability using Non-Gaussian field, we increase the standard deviation to $0.35E$ with same correlation length. In Figure 6.15, the first two columns show the robust design for different values

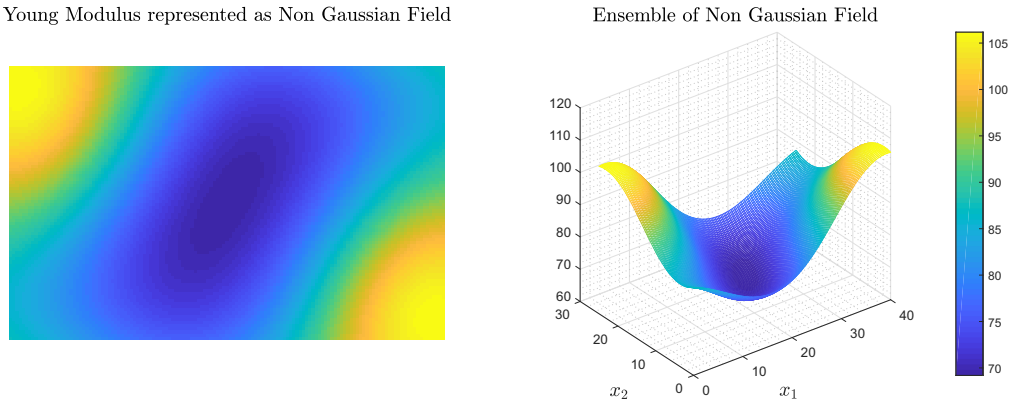

Figure 6.14: Ensemble of 2D Non-Gaussian field representing the Young's modulus.

of k. It may be noted that as the value of k increases the design becomes more robust and consequently the volume as well. The values obtained can be seen in the Table 6.7.

The varation of correlation length makes the random field more or less correlated and it influences in the discretization. We change the correlation length to $l_a = L/4$ and $l_b = H/4$ then, the robust design and variation of the results are shown in third column of Figure 6.15 and Table 6.7 respectively.

Table 6.7: Value of expected and standard deviation of compliance.

	$\sigma_{E^0} = 0.25E$ $l_a = L/2,\ l_b = H/2$			$\sigma_{E^0} = 0.35E$ $l_a = L/2,\ l_b = H/2$			$\sigma_{E^0} = 0.25E$ $l_a = L/4,\ l_b = H/4$		
k	μ_C	σ_C	Vol	μ_C	σ_C	Vol	μ_C	σ_C	Vol
0	1.000	0.148	0.249	1.000	0.229	0.259	1.000	0.105	0.247
1	0.870	0.129	0.276	0.813	0.186	0.304	0.904	0.095	0.265
2	0.771	0.114	0.302	0.684	0.157	0.349	0.826	0.086	0.284
3	0.691	0.102	0.324	0.591	0.136	0.393	0.762	0.079	0.300
4	0.627	0.093	0.354	0.521	0.119	0.441	0.704	0.073	0.315
5	0.574	0.085	0.385	0.466	0.106	0.494	0.656	0.068	0.339

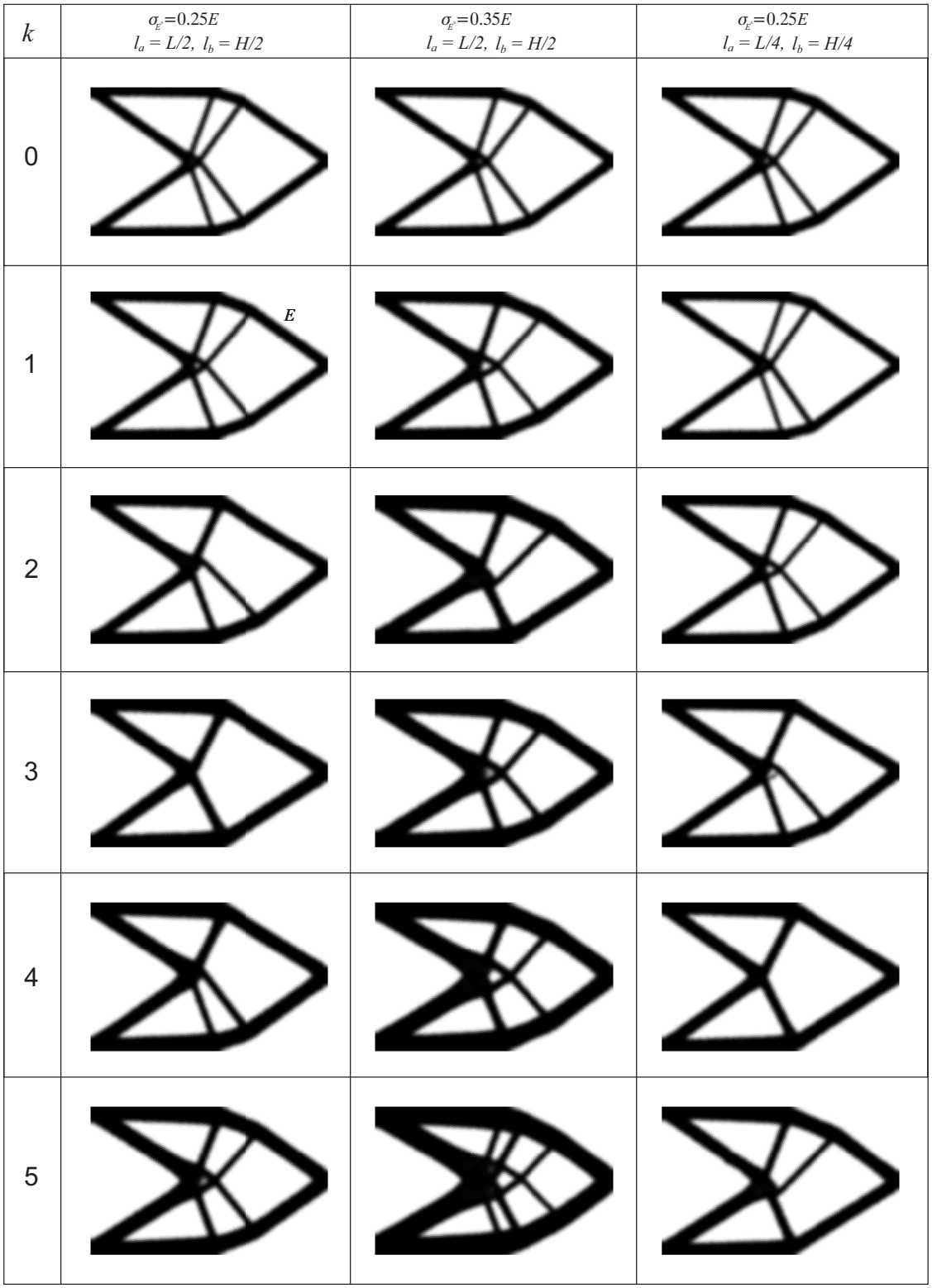

Figure 6.15: Robust design of 2D Cantilever beam problem.

7
Concluding Remarks

The aim of this work was to provide a general framework for robust topology optimization with the focus on mechanical structural where efficient algorithms were developed in order to identify, quantify and include uncertainties in the overall optimization procedure.

Therefore, this chapter recalls the themes addressed in the thesis, summarizes and highlights its main conclusions, contributions and suggest some paths for future works in the field of optimization under uncertainties.

7.1
Contributions and conclusions of the thesis

Firstly, In this thesis we presented the state-of-the-art techniques in uncertainties quantification using polynomial chaos expansions. Furthermore, we proposed a efficient approach for the topology optimization problem in presence of uncertainties.

The Robust Topology Optimization problem has been formulated and solved by means of an optimization procedure which integrates a classical TO algorithm with a stochastic spectral expansion based on gPC. This procedure compare their performance against the Monte Carlo simulation an established techniques, which is used to verify the accuracy and efficiency of the proposed methodology.

This approach is introduced to reduce the variability due to presence of uncertainties in loading and material properties applied to the mechanical structure of interest. The mathematical formulation of RTO problem was defined in two ways to show the performance of algorithm proposed.

First, the RTO minimize the weighted sum of the mean and standard deviation of the compliance subject to volume constraint where only loading uncertainties were considered. Their characteriztion was through of random

vectors and random field for the case of distributed loading. The Gaussian field is used for representing the fluctuation of the load module over its length and for this become computationally implementable the Karhunen-Loève expansion was implemented for discretizing the random field.

Second, the RTO minimize the volume subject to weighted sum of the mean and standard deviation of the compliance as constraint and where only uncertainties in material properties (Young's modulus) were considered. The spatial variability introduced in Young's modulus transform the optimization problem into multiples scenaries and consequently, the computational cost increases significantly with the dimension. Then, due to the spatial variability of the Young's modulus a Homogeneus Non-Gaussian field was used.

The simulation of second-order Non-Gaussian field was discussed in this study for representing the Young's modulus with upper and lower bounds. The uniform marginal distribution was chosen because to its flexibility in representing often distributions of data when upper and lower limits are given in practice. In addition, we also show how Non-Gaussian field can be introduced into topology optimization via the Translation of field and K-L expansion. The Log-normal field is also a very useful description of randomness but in this case for representing Young's modulus is debatable.

The computational cost for computing the coefficients of gPC increase as the stochastic dimension is defined with the number of random variables in the RTO and this problem is seen when random field are discretized in terms of countable uncorrelated random variables. The strategy for reducing the computational cost, was employing the sparse grid instead of the tensor product.

Furthermore, the gPC is compatible with RTO for computing the statistical measures of the compliance. The numerical examples presented here show a substantial benefit and exhibits topology changes within their design domains compared with their deterministic counterpart. The optimal topology configurations confirm that the uncertainty parameters might change the deterministically obtained optimal topologies.

The proposed methodology allows to obtain approximate outcomes with a much lower computational cost than that associated with Monte Carlo simulation, which makes it attractive, particularly in the context of structural topology optimization. Moreover, when using random load fields, the results show different topologies because the forces are correlated, i.e., each force depends on the other and therefore, their interactions with the structure have significant effects on the robust design. Also in this thesis, we compare the results obtained with Non-Gaussian field with similar examples found in the

literature where Gaussian field were considered.

Finally, a nice feature of these approach is that they can easily integrate several improvements at different levels when uncertainties are considered in various types of optimization problems.

7.2 Suggestions for future works

The limitation of the gPC can be observed when a large number of random variables is used to parametrize the stochastic model, since in this case a substantial number of terms is necessary to construct the expansion, and, consequently, the computational cost increases significantly with the dimension. This is often referred to as the curse of dimensionality, and it can be reduced using adaptive techniques such as the adaptive sparse grid.

The Adaptive Sparse Polynomial Chaos approximations is other technique based on the Least Angle Regresion (LAR) which was proposed for automatically detecting and retain progressively a small number of significant coefficients of the PC expansion [157]; [4].

Multifidelity Optimization is other approach to optimization under uncertainty that makes use of inexpensive, low-fidelity models to provide approximate information about the expensive, high-fidelity model. The multifidelity estimator is developed based on the control variate method to reduce the computational cost of achieving a specified mean square error in the statistic estimate [158]; [159].

Bibliography

[1] ODEN, J. T.; MOSER, R. ; GHATTAS, O.. **Computer predictions with quantified uncertainty, part ii**. SIAM News, 43(10):1–4, 2010.

[2] PATELLI, E.. **COSSAN: A Multidisciplinary Software Suite for Uncertainty Quantification and Risk Management**, p. 1909–1977. Springer International Publishing, Cham, 2017.

[3] SUDRET, B.. **Uncertainty propagation and sensitivity analysis in mechanical models–contributions to structural reliability and stochastic spectral methods**. Habilitationa diriger des recherches, Université Blaise Pascal, Clermont-Ferrand, France, 2007.

[4] BLATMAN, G.. **Adaptive sparse polynomial chaos expansions for uncertainty propagation and sensitivity analysis**. Tese de Doutorado, Clermont-Ferrand 2, 2009.

[5] LE MAÎTRE, O.; KNIO, O.. **Spectral Method for Uncertainty Quantification with applications to computational fluid dynamics**. Springer, USA, 2010.

[6] CHRISTENSEN, P.; KLARBRING, A.. **An Introduction to Structural Optimization**. Springer, New York, 2008.

[7] BENDSØE, M.; SIGMUND, O.. **Topology Optimization: Theory, Methods and Applications**. Springer-Verlag, New York, 2003.

[8] ZEGARD, T.; PAULINO, G.. **Toward GPU acceleratd topology optimization on unstructured meshes**. Struct. Multidisc Optim, 48:473–485, 2013.

[9] BENDSÃ¸E, M. P.; SIGMUND, O.. **Topology Optimization: Theory, Methods, and Applications**. Springer-Verlag Berlin Heidelberg, 2004.

[10] CHOI, H.-J.. **A robust design method for model and propagated uncertainty**. Tese de Doutorado, Georgia Institute of Technology, 2005.

[11] ISUKAPALLI, S.. **Uncertainty Analysis of Transport-Transformation Model**. Tese de Doutorado, Graduate Program in Chemical and Biochemical Engineering - New Brunswick, New Jersey, 1999.

[12] MICHELL M.C.E., A. G. M.. **Lviii. the limits of economy of material in frame-structures**. The London, Edinburgh, and Dublin Philosophical Magazine and Journal of Science, 8:589–597, 1904.

[13] TALISCHI, C.; PAULINO, G. H.; PEREIRA, A. ; MENEZES, I. F. M.. **Polygonal finite elements for topology optimization: A unifying paradigm**. International Journal for Numerical Methods in Engineering, 82:671–698, 2010.

[14] TALISCHI, C.; PAULINO, G. H.; PEREIRA, A. ; MENEZES, I. F. M.. **PolyTop: a Matlab implementation of a general topology optimization framework using unstructured polygonal finite element meshes**. Structural and Multidisciplinary Optimization, 45:329–357, 2012.

[15] ROMERO, J. S.; SILVA, E. C. N.. **A topology optimization approach applied to laminar flow machine rotor design**. Computer Methods in Applied Mechanics and Engineering, 279:268–300, 2014.

[16] QIZHI, Q.; KANG, Z. ; WANG, Y.. **A topology optimization method for geometrically nonlinear structures with meshless analysis and independent density field interpolation**. Computational Mechanics, 54:629–644, 2014.

[17] DAPOGNY, C.; FAURE, A.; MICHAILIDIS, G.; ALLAIRE, G.; COUVELAS, A. ; ESTEVEZ, R.. **Geometric constraints for shape and topology optimization in architectural design**. Computational Mechanics, 59:933–965, 2017.

[18] LUO, Y.; NIU, Y.; LI, M. ; KANG, Z.. **A multi-material topology optimization approach for wrinkle-free design of cable-suspended membrane structures**. Computational Mechanics, 59:967–980, 2017.

[19] XIA, L.; DA, D. ; YVONNET, J.. **Topology optimization for maximizing the fracture resistance of quasi-brittle composites**. Computer Methods in Applied Mechanics and Engineering, 332:234–254, 2018.

[20] ZHANG, X. S.; PAULINO, G. H. ; RAMOS, A. S.. **Multi-material topology optimization with multiple volume constraints: a general**

approach applied to ground structures with material nonlinearity. Structural and Multidisciplinary Optimization, 57:161–182, 2018.

[21] NANTHAKUMAR, S. S.; VALIZADEH, N.; PARK, H. S. ; RABCZUK, T.. **Surface effects on shape and topology optimization of nanostructures**. Computational Mechanics, 56:97–112, 2015.

[22] PEREIRA, A.; TALISCHI, C.; PAULINO, G. H.; MENEZES, I. F. M. ; CARVALHO, M. S.. **Fluid flow topology optimization in polytop: stability and computational implementation**. Structural and Multidisciplinary Optimization, 54:1345–1364, 2016.

[23] DUAN, X.-B.; LI, F.-F. ; QIN, X.-Q.. **Adaptive mesh method for topology optimization of fluid flow**. Applied Mathematics Letters, 44:40–44, 2015.

[24] ANDREASEN, C. S.; SIGMUND, O.. **Topology optimization of fluid?structure-interaction problems in poroelasticity**. Computer Methods in Applied Mechanics and Engineering, 258:55–62, 2013.

[25] PARK, J.; SUTRADHAR, A.; SHAH, J. J. ; PAULINO, G. H.. **Design of complex bone internal structure using topology optimization with perimeter control**. Computers in Biology and Medicine, p. –, 2018.

[26] SCHUELLER, G.; JENSEN, H.. **Computational methods in optimization considering uncertainties - an overview**. Comput. Method Appl Mech Engrg, 198:2–13, 2008.

[27] BOOPATHY, K.. **Uncertainty Quantification and Optimization unde Uncertainty usign Surrogate Model**. Dissertação de Mestrado, The School of Engineerinf of the University of Dayton, Ohio - USA, 2014.

[28] ARORA, J.. **Optimization of Structural and Mechanical Systems**. World Scientific Publishing Co. Pte. Ltd., USA, 2007.

[29] AGARWAL, H.. **Reliability Based Design Optimization: Formulation and Methodologies**. D.Sc. Thesis, University of Notre Dame, Indiana, 2004.

[30] PADMANABAN, D.. **Reliability-Based Design Optimization for Multidisciplinary System Design**. Tese de Doutorado, University of Notre Dame, Indiana, 2003.

[31] SAHINIDIS, N. V.. **Optimization under uncertainty: state-of-art and opportunities**. Computer and Chemical Engineering, 28:971–983, 2004.

[32] RASSOUL, F. A. N.. **Reliability-based robust design optimization: A general methodology using genetic algorithm**. Computers Industrial Engineering, 74:199–207, 2014.

[33] RATHOD, V.; YADAV, P.; RATHORE, A. ; JAIN, R.. **Reliability-based robust design optimization: A comparative study**. IEEM, 74:1558–1563, 2011.

[34] SHAHRAKI, A.; NOOROSSANA, R.. **A Combined Algorithm for solving Reliability-based robust design optimization problems**. Journal of Mathematics and Computer Science, 7:54–62, 2013.

[35] IKJIN, L.; CHOI, K.; DU, L. ; GORSICH, D.. **Dimension reduction method for Reliability-based robust design optimization**. Computer and Structures, 86:1550–1562, 2008.

[36] IKJIN, L.; CHOI, K.; DU, L. ; GORSICH, D.. **Reliability-based robust design optimization: A multi-objective framework using hybrid quality loss function**. Quality and Reliability Engineering International, 26:27–41, 2009.

[37] FORRESTER, A.; SOBESTER, A. ; KEANE, A.. **Engineering Design Via Surrogate Modelling: A practical guide**. John Wiley, UK, 2008.

[38] KOZIEL, S.; EIFSSON, L.. **Surrogate Based Modeling and Optimization: Applications in Engineering**. Springer, UK, 2013.

[39] QUEIPO, N.; HAFTKA, R.; SHYY, W. ; GOEL, T.. **Surrogate-based analysis and optimization**. Progress in Aerospace Sciencies, 41:1–28, 2005.

[40] BOOPATHY, K.. **Uncertainty quantification and optimization under uncertainty using surrogate models**. Dissertação de Mestrado, University of Dayton, Ohio, 2014.

[41] PICHLER, L.; PRADLAWARTER, H. ; SCHUELLER, G.. **A mode-based Meta-Model for frequency response functions of uncertain structural systems**. Comput. Struct., 85:332–341, 2009.

[42] SANZIDA, N.; NAGY, Z.. **Polynomial Chaos Expansion (PCE) Based Surrogate Modelling and Optimiztion for Batch Crystalization**. Computed Aided Chemical Engineering, 33:565–570, 2014.

[43] WU, J.; ZHANG, L. ; ZHANG, Y.. **A nes interval uncertain optimization method for structures using Chebyshev surrogate models**. Computers Structures, 146:185–196, 2015.

[44] JURECKA, F.. **Robust Design Optimization Based on Metamodeling Techniques**. Tese de Doutorado, Technische Universität MÃ$\frac{1}{4}$nchen, Germany, 2007.

[45] STOCKI, R.. **Metamodel-based approaches for solving robust design optimization problems - software development perspective**. Computer Methods in Mechanics, 2011.

[46] SUZUKI, S.; KUROIWA, D. ; LEE, G.. **Surrogate duality robust optimization**. European Journal of Operational Research, 231:257–262, 2013.

[47] CHEN, J.; TANG, Y. ; HUANG, X.. **Application of surrogate based particle swarm optimization to the relaibility based robust design of composite**. Acta Mechanica Solida Sinica, 26:480–490, 2013.

[48] GASPAR, B.; SOARES, A. T. C.. **Assessment of the efficiency of Kriging surrogate models for structural reliability analysis**. Probabilistic Engineering Mechanics, 37:24–34, 2014.

[49] ZHAO, L.. **Reliability Based Design Optimization using surrogate model with assessment of confidence level**. Tese de Doutorado, University of Iowa, USA, 2011.

[50] ZHANG, W.; KANG, Z.. **Robust shape and topology optimization considering geometric uncertainties with stochastic level set perturbation**. International Journal for Numerical Methods in Engineering, 110:31–56, 2017.

[51] KESHAVARZZADEH, V.; FERNANDEZ, F. ; TORTORELLI, D. A.. **Topology optimization under uncertainty via non-intrusive polynomial chaos expansion**. Computer Methods in Applied Mechanics and Engineering, 318:120–147, 2017.

[52] DA SILVA, G.; CARDOSO, E.. **Stress-based topology optimization of continuum structures under uncertainties**. Computer Methods in Applied Mechanics and Engineering, 313:647–672, 2017.

[53] ZHANG, X. S.; DE STURLER, E. ; PAULINO, G. H.. **Stochastic sampling for deterministic structural topology optimization with many load cases: Density-based and ground structure approaches**. Computer Methods in Applied Mechanics and Engineering, 325:463–487, 2017.

[54] PUTEK, P.; PULCH, R.; BARTEL, A.; TER MATEN, E. J. W.; GÜNTHER, M. ; GAWRYLCZYK, K. M.. **Shape and topology optimization of a permanent-magnet machine under uncertainties**. Journal of Mathematics in Industry, 6:11, 2016.

[55] RICHARDSON, J.; FILOMENO COELHO, R. ; ADRIAENSSENS, S.. **A unified stochastic framework for robust topology optimization of continuum and truss-like structures**. Engineering Optimization, 48:334–350, 2016.

[56] ZHAO, J.; WANG, C.. **Robust structural topology optimization under random field loading uncertainty**. Structural and Multidisciplinary Optimization, 50:517–522, 2014.

[57] DUNNING, P. D.; KIM, H. A.. **Robust topology optimization: Minimization of expected and variance of compliance**. AIAA Journal, 51:2656–2664, 2013.

[58] JALALPOUR, M.; GUEST, J. K. ; IGUSA, T.. **Reliability-based topology optimization of trusses with stochastic stiffness**. Structural Safety, 43:41–49, 2013.

[59] TOOTKABONI, M.; ASADPOURE, A. ; GUEST, J. K.. **Topology optimization of continuum structures under uncertainty ? A polynomial chaos approach**. Computer Methods in Applied Mechanics and Engineering, 201–204:263–275, 2012.

[60] ASADPOURE, A.; TOOTKABONIA, M. ; GUEST, J.. **Robust topology optimization of structures with uncertainties in stiffness - Application to truss structures**. Computers & Structures, 89:1031–1041, 2011.

[61] CHEN, S.; CHEN, W. ; LEE, S.. **Level set based robust shape and topology optimization under random field uncertainties**. Structural and Multidisciplinary Optimization, 41:507–524, 2010.

[62] GUEST, J. K.; IGUSA, T.. **Structural optimization under uncertain loads and nodal locations**. Computer Methods in Applied Mechanics and Engineering, 198:116–124, 2008.

[63] KIM, N. H.; WANG, H. ; QUEIPO, N. V.. **Efficient shape optimization under uncertainty using polynomial chaos expansions and local sensitivities**. AIAA Journal, 44:1112–1116, 2006.

[64] DUNNING, P.; KIM, A.. **Robust Topology Optimization: Minimization of Expected and Variance of Compliance**. AIAA Journal, 51:2656–2664, 2013.

[65] JANSEN, M.; LOMBAERT, G. ; SCHEVENELS, M.. **Robust Topology Optimization of structures with imperfect geometry based on geometric nonlinear analysis**. Computer Methods in Applied Mechanics and Engineering, 285:542–467, 2015.

[66] CAI, K.; QIN, Q.; LUO, Z. ; ZHANG, A.. **Robust Topology Optimization of bi-modulus structures**. Computer-Aided Design, 45:1159–1169, 2013.

[67] MOHR, D.; STEIN, I.; MATZIES, T. ; KNAPEK, C.. **Redundant Robust Topology Optimization of truss**. Optimization and Engineering - Springer, 14:945–972, 2014.

[68] ASADPOURE, A.; TOOTKABONI, M. ; GUEST, J.. **Robust Topology Optimization of structures with uncertainties in stiffness - application to truss structures**. Computer and Structures, 89:1131–1141, 2011.

[69] TOOTKABONI, M.; ASADPOURE, A. ; GUEST, J.. **Topology Optimization of continuum structures under uncertainty - A Polynomial Chaos approach**. Computer Method in Applied Mechanics and Engineering, 201-204:263–275, 2012.

[70] **Uqlab: The framework for uncertainty quantification**. `https://www.uqlab.com/`.

[71] **Dakota: Explore and predict with confidence**. `https://dakota.sandia.gov/`.

[72] **Openturns: An open source initiative for the treatment of uncertainties, risks statistics**. `http://www.openturns.org/#`.

[73] **Top3d: An efficient 3d topology optimization program**. https://top3dapp.com/.

[74] **Topy is a lightweight topology optimization framework for python**. https://github.com/williamhunter/topy.

[75] **Polytop: A matlab implementation of a general topology optimization framework using unstructured polygonal finite element meshes**. https://paulino.ce.gatech.edu/software.html.

[76] OF AERONAUTICS, A. I.; ASTRONAUTICS. **AIAA guide for the verification and validation of computational fluid dynamics simulations**. American Institute of aeronautics and astronautics, 1998.

[77] IACCARINO, G.. **Quantification of uncertainty in flow simulations using probabilistic methods**. Relatório Técnico, NATO RESEARCH AND TECHNOLOGY ORGANIZATION NEUILLY-SUR-SEINE (FRANCE), 2009.

[78] SUN, Y.-H.; CHEN, T.; WU, C. Q. ; SHAFAI, C.. **Comparison of four friction models: feature prediction**. Journal of Computational and Nonlinear Dynamics, 11(3):031009, 2016.

[79] HANNA, S. R.; CHANG, J. C. ; FERNAU, M. E.. **Monte carlo estimates of uncertainties in predictions by a photochemical grid model (uam-iv) due to uncertainties in input variables**. Atmospheric Environment, 32(21):3619–3628, 1998.

[80] SAX, T.; ISAKOV, V.. **A case study for assessing uncertainty in local-scale regulatory air quality modeling applications**. Atmospheric Environment, 37(25):3481–3489, 2003.

[81] CHU, B.; LEE, S. ; CHANG, D.. **Determination of design accidental fire load for offshore installations based on quantitative risk assessment with treatment of parametric uncertainty**. Journal of Loss Prevention in the Process Industries, 45:160–172, 2017.

[82] SOIZE, C.. **Stochastic models of uncertainties in computational mechanics**. American Society of Civil Engineers Reston, 2012.

[83] OLSSON, H.; ÅSTRÖM, K. J.; DE WIT, C. C.; GÄFVERT, M. ; LISCHINSKY, P.. **Friction models and friction compensation**. Eur. J. Control, 4(3):176–195, 1998.

[84] HALDAR, A.; MAHADEVAN, S.. **Reliability assessment using stochastic finite element analysis**. John Wiley & Sons, 2000.

[85] CHOI, S.-K.; GRANDHI, R. ; CANFIELD, R. A.. **Reliability-based structural design**. Springer Science & Business Media, 2006.

[86] STEFANOU, G.; PAPADRAKAKIS, M.. **Assessment of spectral representation and karhunen–loève expansion methods for the simulation of gaussian stochastic fields**. Computer methods in applied mechanics and engineering, 196(21-24):2465–2477, 2007.

[87] STEFANOU, G.. **The stochastic finite element method: Past, present and future**. Computer Methods in Applied Mechanics and Engineering, 198:1031–1051, 2009.

[88] GRIGORIU, M.. **Simulation of stationary non-gaussian translation processes**. Journal of engineering mechanics, 124(2):121–126, 1998.

[89] GRIGORIU, M.. **Applied non-Gaussian processes: Examples, theory, simulation, linear random vibration, and MATLAB solutions**. Prentice Hall, 1995.

[90] GRIGORIU, M.. **Stochastic systems: uncertainty quantification and propagation**. Springer Science & Business Media, 2012.

[91] FERRANTE, F.; ARWADE, S. ; GRAHAM-BRADY, L.. **A translation model for non-stationary, non-gaussian random processes**. Probabilistic engineering mechanics, 20(3):215–228, 2005.

[92] PARK, S.; WILLIAMS, M.; PRINJA, A. ; EATON, M.. **Modelling non-gaussian uncertainties and the karhunen–loéve expansion within the context of polynomial chaos**. Annals of Nuclear Energy, 76:146–165, 2015.

[93] MATTHIES, H. G.; BRENNER, C. E.; BUCHER, C. G. ; SOARES, C. G.. **Uncertainties in probabilistic numerical analysis of structures and solids-stochastic finite elements**. Structural safety, 19(3):283–336, 1997.

[94] ZHANG, J.; ELLINGWOOD, B.. **Orthogonal series expansions of random fields in reliability analysis**. Journal of Engineering Mechanics, 120(12):2660–2677, 1994.

[95] LI, C.-C.; DER KIUREGHIAN, A.. **Optimal discretization of random fields**. Journal of engineering mechanics, 119(6):1136–1154, 1993.

[96] VANMARCKE, E.. **Random fields: analysis and synthesis**. World scientific, 2010.

[97] KARRHUNEN, K.. **Über lineare methoden in der wahrscheinlichkeitsrechnung**. Annales Academiae Scientiarum Fennicae Ser. A I, 37:3–79, 1947.

[98] LOÈVE, M.. **Probability theory. 1977**. Springer-Verlag, New York, 1977.

[99] DE ROCQUIGNY, E.. **La maîtrise des incertitudes dans un contexte industriel-1ère partie: une approche méthodologique globale basée sur des exemples**. Journal de la Société française de statistique, 147(3):33–71, 2006.

[100] DE ROCQUIGNY, É.. **La maîtrise des incertitudes dans un contexte industriel. 2nde partie: revue des méthodes de modélisation statistique physique et numérique**. Journal de la société française de statistique, 147(3):73–106, 2006.

[101] SOBOL, I. M.. **A primer for the Monte Carlo method**. CRC press, 1994.

[102] MCKAY, M. D.; BECKMAN, R. J. ; CONOVER, W. J.. **Comparison of three methods for selecting values of input variables in the analysis of output from a computer code**. Technometrics, 21(2):239–245, 1979.

[103] WIENER, N.. **The homogeneous chaos**. Amer J. Math, 60:897–936, 1938.

[104] GHANEM, R.; SPANOS, P.. **Stochastic finite elements: A spectral approach**. Springer, New York, 1991.

[105] CAMERON, R.; MARTIN, W.. **The orthogonal development of non-linear Functionals in Series of Fourier Hermite Functionals**. Annals of Mathematics, Second Series, 48:385–392, 1947.

[106] XIU, D.. **Generalized (Wiener-Askey) Polynomial Chaos**. Tese de Doutorado, Department of Applied Mathematics at Brown University, USA, 2004.

[107] ERNST, O.; MUGLER, A.; STARKLOFF, H. ; ULLMANN, E.. **On the Convergence of Generalized Polynomial Chaos Expansions**. ESAIM: Mathematical Modelling and Numerical Analysis, 46:317–339, 1999.

[108] XIU, D.; KARNIADAKIS, G.. **Modeling uncertainty in steady state diffusion problems with random inputs**. Computer Methods in Applied Mechanics and Engineering, 191:4927–4948, 2002.

[109] XIU, D.; KARNIADAKIS, G.. **The Wiener-Askey polynomial chaos for stochastic differential equation**. SIAM J Sci Computing, 24:619–644, 2002.

[110] ASKEY, R.; WILSON, J.. **Some basic hypergeometric polynomial that generalize Jacobi polynomials**. Mem Am Math, 54:1–55, 1985.

[111] STOER, J.; BULIRSCH, R.. **Introduction to Numerical Analysis**. Springer-Verlag, Berlin, 2 edition, 1993.

[112] PETTERSSON, M.; IACCARINO, G. ; NORDSTRÖN, J.. **Polynomial Chaos Method Hyperbolic Partial Differential Equations - Numerical techniques for fluid dynamics problems in the presence of uncertainties**. Springer-Verlag, New York, 2015.

[113] SHIRYAEV, A.. **Probability**. Springer - Berlin, Ger, 1996.

[114] STOYANOV, J.. **Couunterexamples in Probability**. John Wiley & Sons, New York, 1997.

[115] DEVROYE, L.. **Non-Uniform Random Variable Generation**. Spring-Verialag, New York, 1986.

[116] XIU, D.. **Numerical methods for stochastic computations: a spectral method approach**. Princeton university press, 2010.

[117] SMOLYAK, S.. **Quadrature and interpolation formulas for tensor products of certain classes of functions**. In: SOVIET MATH. DOKL., volumen 4, p. 240–243, 1963.

[118] GERSTNER, T.; GRIEBEL, M.. **Numerical integration using sparse grids**. Numerical algorithms, 18(3-4):209, 1998.

[119] GHANEM, R. G.; SPANOS, P. D.. **Stochastic Finite Elements: A Spectral Approach**. Dover Publications, 2nd edition, 2003.

[120] XIU, D.. **Numerical Methods for Stochastic Computations: A Spectral Method Approach**. Princeton University Press, 2010.

[121] MAÎTRE, O. P. L.; KNIO, O. M.. **Spectral Methods for Uncertainty Quantification: With Applications to Computational Fluid Dynamics**. Springer Netherlands, 2010.

[122] PETTERSSON, M. P.; IACCARINO, G. ; NORDSTRÖM, J.. **Polynomial Chaos Methods for Hyperbolic Partial Differential Equations: Numerical Techniques for Fluid Dynamics Problems in the Presence of Uncertainties**. Springer International Publishing, 2015.

[123] GHANEM, R.; RED-HORSE, J.. **Polynomial Chaos: Modeling, Estimation, and Approximation**, p. 521–551. Springer International Publishing, 2017.

[124] KUNDU, A.; ADHIKARI, S. ; FRISWELL, M.. **Stochastic finite elements of discretely parameterized random systems on domains with boundary uncertainty**. International Journal for Numerical Methods in Engineering, 100(3):183–221, 2014.

[125] SOIZE, C.; GHANEM, R.. **Physical systems with random uncertainties: Chaos representations with arbitrary probability measure**. SIAM Journal on Scientific Computing, 26:395–410, 2004.

[126] SOIZE, C.; DESCELIERS, C.. **Computational aspects for constructing realizations of polynomial chaos in high dimension**. SIAM Journal on Scientific Computing, 32:2820–2831, 2010.

[127] SOIZE, C.. **Polynomial chaos expansion of a multimodal random vector**. SIAM/ASA Journal on Uncertainty Quantification, 3:34–60, 2015.

[128] SOIZE, C.; GHANEM, R.. **Polynomial chaos representation of databases on manifolds**. Journal of Computational Physics, 335:201–221, 2017.

[129] KUNDU, A.; MATTHIES, H. ; FRISWELL, M.. **Probabilistic optimization of engineering system with prescribed target design in a reduced parameter space**. Computer Methods in Applied Mechanics and Engineering, 337:281–304, 2018.

[130] SOIZE, C.. **Uncertainty Quantification: An Accelerated Course with Advanced Applications in Computational Engineering**. Springer International Publishing, 2017.

[131] J MERCER, B.. **Xvi. functions of positive and negative type, and their connection the theory of integral equations**. Phil. Trans. R. Soc. Lond. A, 209(441-458):415–446, 1909.

[132] CIARLET, P. G.. **Linear and Nonlinear Functional Analysis with Applications**. SIAM, 2013.

[133] SUDRET, B.; DER KIUREGHIAN, A.. **Stochastic finite element methods and reliability: A state-of-the-art report**. Relatório Técnico, Technical Report UCB/SEMM, Department of Civil & Environmental Engineering,University of California, Berkeley, 2000.

[134] ATKINSON, K. E.. **The Numerical Solution of Integral Equations of the Second Kind**. Cambridge University Press, reissue edition, 2009.

[135] BETZ, W.; PAPAIOANNOU, I. ; STRAUB, D.. **Numerical methods for the discretization of random fields by means of the Karhunen?Loève expansion**. Computer Methods in Applied Mechanics and Engineering, 271:109–129, 2014.

[136] BELLIZZI, S.; SAMPAIO, R.. **Smooth decomposition of random fields**. Journal of Sound and Vibration, 331:3509–3520, 2012.

[137] PERRIN, G.; SOIZE, C.; DUHAMEL, D. ; FUNFSCHILLING, C.. **Karhunen?Loève expansion revisited for vector-valued random fields: Scaling, errors and optimal basis**. Journal of Computational Physics, 242:607–622, 2013.

[138] GORDON, J.. **Structure or Why Thing Don't Fall Down**. Penguin, Baltimore, 1978.

[139] SIGMUND, O.; PETERSSON, J.. **Numerical instabilities in topology optimization: A survey on procedures dealing with checkerboards, mesh-dependencies and local minima**. Structural Optimization, 16:68–75, 1998.

[140] BRUGGI, M.. **On the solution of the checkerboard problem in mixed-FEM topology optimization**. Computers & Structures, 86:1819–1829, 2008.

[141] BENDSÃ¸E, M. P.; KIKUCHI, N.. **Generating optimal topologies in structural design using a homogenization method**. Computer Methods in Applied Mechanics and Engineering, 71:197–224, 1988.

[142] SVANBERG, K.. **The method of moving asymptotes?a new method for structural optimization**. International Journal for Numerical Methods in Engineering, 24:359–373, 1987.

[143] SWILER, L. P.; WOJTKIEWICZ JR, S. F.; ELDRED, M. S.; GIUNTA, A. A. ; TRUCANO, T. G.. **Perspectives on optimization under uncertainty: Algorithms and applications.** Relatório Técnico, Sandia National Laboratories, 2005.

[144] BEYER, H.; SENDHOFF, B.. **Robust optimization - A comprehensive survey**. Computers Method in Applied Mechanics and Engineering, 196:3190–3218, 2007.

[145] SHIN, S.; SAMANLIOGLU, F. ; CHO, B.. **Cmputing trade-offs in robust desing: Perspective of the mean squared error**. Computers and Industrial Engineering, 60:248–255, 2011.

[146] TAGUCHI, G.. **Taguchi on robust technology devopment: Bringing quality engineering upstream**. ASME Press, New York, 1992.

[147] TAGUCHI, G.. **Introduction to quality engineering designing quality into products and process**. Quality Resources, White Plains, USA, 1986.

[148] PHADKE, M.. **Quality engineering using robust design**. Pretince Hall Englewood Cliffs, USA, 1989.

[149] CHEN, W.; ALLEN, J. K.; TSUI, K.-L. ; MISTREE, F.. **A procedure for robust design: minimizing variations caused by noise factors and control factors**. Journal of mechanical design, 118(4):478–485, 1996.

[150] BEYER, H. G.; SENDHOFF, B.. **Robust optimization ? A comprehensive survey**. Computer Methods in Applied Mechanics and Engineering, 196:3190–3218, 2007.

[151] BIRGE, J.; LOUVEAUX, F.. **Introduction to Stochastic Programming**. Springer-Verlag New York, 2011.

[152] DOLTSINIS, I.; KANG, Z.. **Robust design of structures using optimization methods**. Computer Methods in Applied Mechanics and Engineering, 193(23):2221–2237, 2004.

[153] SHIN, S.; SAMANLIOGLU, F.; CHO, B. R. ; WIECEK, M. M.. **Computing trade-offs in robust design: Perspectives of the mean squared error**. Computers & Industrial Engineering, 60:248 –255, 2011.

[154] KROESE, D. P.; TAIMRE, T. ; BOTEV, Z. I.. **Handbook of Monte Carlo Methods**. Wiley, 2011.

[155] RUBINSTEIN, R. Y.; KROESE, D. P.. **Simulation and the Monte Carlo Method**. Wiley, 3rd edition, 2016.

[156] WU, J.; GAO, J.; LUO, Z. ; BROWN, T.. **Robust topology optimization for structures under interval uncertainty**. Advances in Engineering Software, 99:36–48, 2016.

[157] BLATMAN, G.; SUDRET, B.. **Sparse polynomial chaos expansions and adaptive stochastic finite elements using a regression approach**. Comptes Rendus Mécanique, 336(6):518–523, 2008.

[158] NG, L. W.; WILLCOX, K. E.. **Multifidelity approaches for optimization under uncertainty**. International Journal for numerical methods in Engineering, 100(10):746–772, 2014.

[159] CHAUDHURI, A.; JASA, J.; MARTINS, J. ; WILLCOX, K. E.. **Multifidelity optimization under uncertainty for a tailless aircraft**. In: 2018 AIAA NON-DETERMINISTIC APPROACHES CONFERENCE, p. 1658, 2018.